Coordination Chemistry Reviews 424 (2020) 213506

Contents lists available at ScienceDirect

Coordination Chemistry Reviews

journal homepage: www.elsevier.com/locate/ccr

Analysis of extracellular vesicles as emerging theranostic nanoplatforms

Yanlong Xing [a], Ziyi Cheng [a], Rui Wang [a], Chuanzhu Lv [a,*], Tony D. James [b,*], Fabiao Yu [a,*]

[a] Key Laboratory of Emergency and Trauma, Ministry of Education, Key Laboratory of Hainan Trauma and Disaster Rescue, The First Affiliated Hospital of Hainan Medical University, Institute of Functional Materials and Molecular Imaging, College of Emergency and Trauma, Hainan Medical University, Haikou, 571199, China
[b] Department of Chemistry, University of Bath, Bath, UK

ARTICLE INFO

Article history:
Received 22 June 2020
Received in revised form 16 July 2020
Accepted 17 July 2020

Keywords:
Extracellular vesicle
Fluorescence analysis
Raman analysis
Microfluidics
Theranostic Nanoplatforms

ABSTRACT

Extracellular vesicles (EVs) are nanoscale lipid membrane–bound vesicles that are secreted by cells of both prokaryotes and eukaryotes and carry bioactive cargos including proteins, nucleic acid and lipids from source cells. Given their prominent ability in transporting bioactive components, EVs are regarded as promising biomarkers for disease diagnosis and emerging therapeutic nanoparticles. However, to exert their effect in clinical applications, effective isolation and sensitive analysis of EVs from complex biofluids is required. Recent advances in EV-related research has provided feasible approaches for developing emerging therapeutic nanoplatforms using EVs. With this review, we aim to provide a comprehensive and in-depth summary of recent advances in diverse assay methods for EVs including fluorescence, Raman/Surface-enhanced Raman Spectroscopy (SERS) analysis and other methods, as well as their clinical potential in constructing EV-based theranostic nanoplatforms towards various diseases. In particular, microfluidic-assisted analysis sytems, single EV detection and the main approaches of utilizing EVs for therapeutic purposes are highlighted. We anticipate this review will be inspirational for researchers in related fields and will provide a general introduction to scientists with various research backgrounds.

Contents

* Corresponding authors.
E-mail addresses: lyuchuanzhu@hainmc.edu.cn (C. Lv), T.D.James@bath.ac.uk (T.D. James), yufabiao@hainmc.edu.cn (F. Yu).

https://doi.org/10.1016/j.ccr.2020.213506
0010-8545/

1. Introduction

Extracellular vesicles (EVs) are lipid membrane-enclosed nanovesicles that are actively secreted by cells to the extracellular environment [1]. They have been isolated from most body fluids and significantly, the release of EVs is not just identified in mammalian cells but in lower eukaryotes and prokaryotes [2,3]. Initially being regarded as membrane debris, EVs have attracted increased research interest since their capability to stimulate adaptive immune responses was discovered [4]. Thereafter, EVs have been extensively investigated due to their function in transporting biological cargos e.g. proteins, lipids and nucleic acids, as well as mediating the intercellular communication between cells to regulate different biological processes locally or at a distance [5-7].

An increasing number of studies has confirmed that EVs play pivotal roles not only in the modulation of physiological function including immune response, stem cell maintenance and tissue repair etc. [1,5], but also in the pathological processes which induce a variety of diseases [8,9]. EVs shuttle bioactive molecules, and the lipid bilayer structure can protect the internal contents from degradation. Thus, they are recognized as promising biomarkers for liquid biopsies in the diagnosis of various diseases including tumours [10]. Compared to the tissue biopsy method, EV-based liquid biopsy offers significant advantages in cancer monitoring owing to the non-invasiveness, abundant tumour molecular information of EVs in biofluids and ability to surmount biological barriers [11]. Therefore, tumour cell-derived vesicles can be employed as effective biomarkers for cancer diagnosis, treatment and prognosis monitoring [12,13]. In addition, in view of their important biological functions, EVs are exploited as a unique nanoplatform for potential therapeutic agents, as well as drug delivery vehicles [14-16]. Nanoscale EVs exist in many body fluids yet many challenges exist for the translation of EVs into clinical applications, including effective isolation and rapid characterisation. As a result, increasing research has been directed towards overcoming these challenges with the development of improved EV-based enrichment and assay systems [17].

Herein, we will present a comprehensive overview on the recent advances in EV-based research, covering the composition and function, isolation and characterization, diverse analytic approaches, and the clinical potential toward different kinds of diseases (Fig. 1). In particular, we will focus on the recent advances in EV analysis based on fluorescence and Surface-enhanced Raman spectroscopy (SERS) methods, especially in combination with microfluidic platforms. We will also highlight the nanotechnological progresses in the development of EV-based theranostic nanoplatforms, as well as their applications for disease diagnosis and therapy.

2. Classification, biogenesis, and biological function

2.1. Classification and biogenesis of EVs

EVs are cell-released lipid vesicles from various origins with sizes in the range of 30 to 2,000 nm. Based on their different biogenesis, EVs are classified into three main groups: exosomes, microvesicles and apoptotic bodies [18]. Exosomes are derived from the inward invagination of the endolysosomal pathway, where they are formed intracellularly within multivesicular endosomes (or multivesicular bodies, MVB) and subsequently secreted in an exocytotic manner [1,19,20]. By contrast, microvesicles are generated through outward budding of the plasma membrane [18]. Both types of vesicles contain common contents including cytoplasmic proteins, some lipid raft-interacting proteins and nucleic acids, however, exosomes carry additional cargos than microvesicles due to their different biogenesis (Fig. 2) [2]. The abundant endosomal proteins in exosomes can be attributed to specific endosomal sorting mechanisms. Currently, the extensively recognized biogenesis mechanism for formation of MVBs and their intraluminal vesicles (ILVs) is endosomal sorting complex required for transport (ESCRT) which is composed of four complexes (ESCRT 0, I, II and III) and plays differing roles in delivering ubiquitinated transmembrane proteins, cargo sorting and vesicle generation [18]. In addition, it has been demonstrated that MVBs and ILVs can be formed by an ESCRT-independent mechanism, which is closely related to the sorted endosomal cargos. Therefore, regarding the biogenesis of exosomes, on one hand, they can be generated in an ESCRT-dependent manner owing to the contents of TSG101 and ALIX proteins from the ESCRT system; while on the other hand, exosome biogenesis can occur via an ESCRT-independent pathway due to the existence of tetraspanin proteins and sphingomyelinase etc. that are involved in endosomal vesicle trafficking [18].

Recently, not only the heterogeneity of EVs, but that of exosomes has gathered much research interest [21,22]. In a recent study, two exosome subpopulations have been identified using an asymmetric flow field-flow fractionation (AF4) approach. The large and small exosome vesicles that are named Exo-L and Exo-S exhibited different biophysical properties and organ biodistribution patterns [23]. To date, there is still a lack of specific

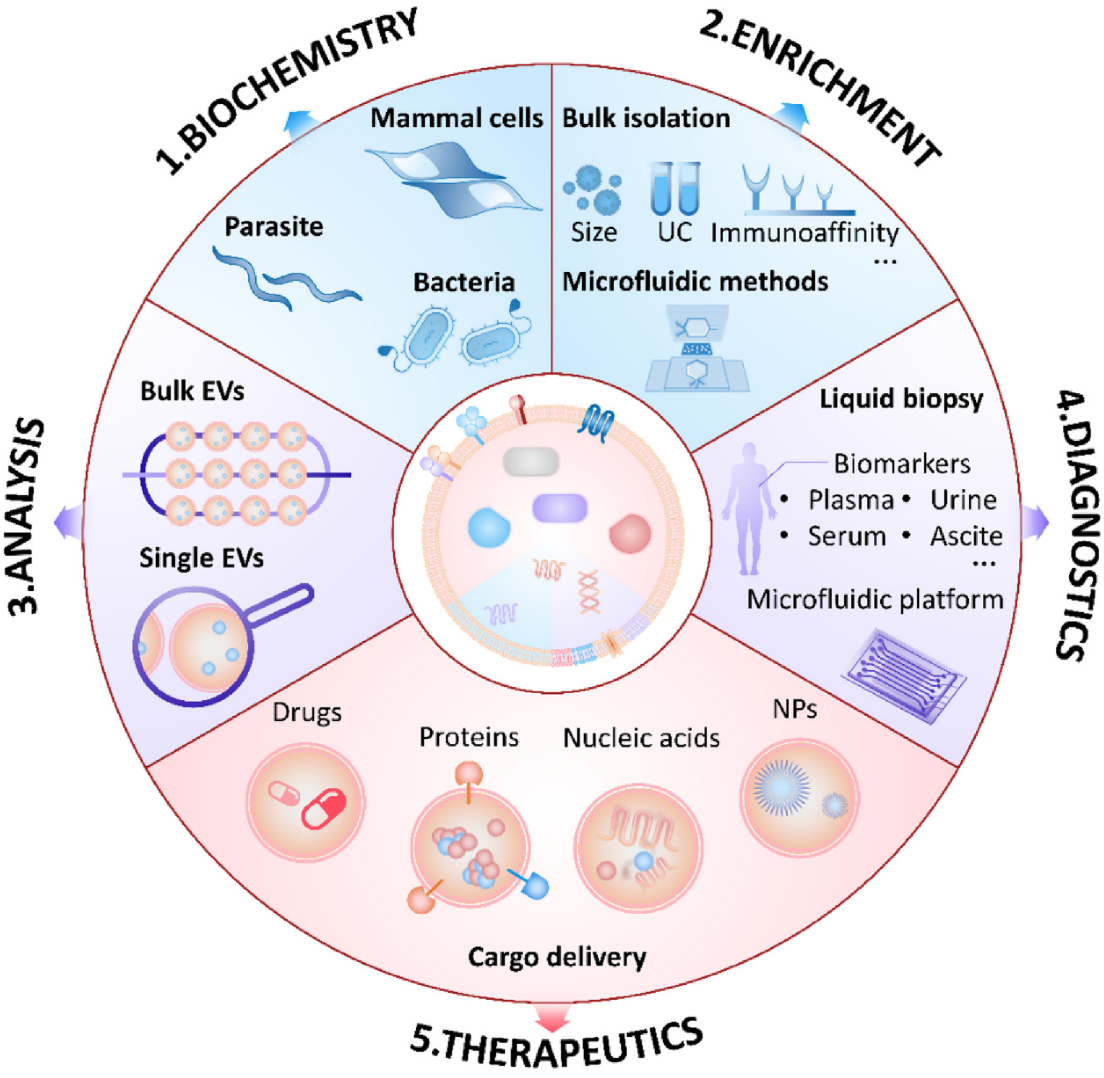

Fig. 1. Schematic illustration of analysis of extracellular vesicle for emerging theranostic platforms.

biomarkers which can separate exosomes from nanosized microvesicles [24], therefore, in this review, we cover both exosomes and microvesicles and the term 'extracellular vesicle' is used to refer to both types of vesicles (Table 1).

2.2. Physiological and pathological function of extracellular vesicles in eukaryotes and prokaryotes

EVs perform a vital function in the intercellular communication of physiological and pathological processes [9]. They can deliver active bio cargos including proteins, lipids and RNAs and other infectious particles to adjacent or distant cells and then regulate the target cell's behaviour [2]. This regulation occurs in a pleiotropic way: EVs can activate specific surface receptors on cells by proteins or bioactive lipid ligands, or fusing their membrane with the plasma membrane of recipient cells and transferring the delivered bioactive cargos into the recipient cells. EVs can be engulfed by various cells, such as macrophages and endothelial cells [10]. Therefore, they are considered as signalosomes with different cellular and biological functions [25,26]. For instance, in the immune system, EVs secreted from the immature dendritic cells can transfer major histocompatibility complex (MHC) peptide molecules to other dendritic cells to activate the immune response [27]. In addition, adaptive immune responses or suppressed inflammation can be triggered by EVs depending on the status of specific immune cells [26,28]. The key roles of EVs have also been studied in epithelia cells, as well as in the nervous system. Previous research has indicated that EVs secreted from intestinal epithelial cells can be involved in the antigen presentation of inflammatory conditions, and these EVs may regulate the capability of static epithelial cells to function at a distance [29]. In the nervous system, EVs are involved in neurite outgrowth and neuronal survival [30,31], as well as the communication of neurons via the transfer of neurotransmitter receptors and therefore contribute to neurobiological functions [32]. EVs have also been reported to facilitate stem cell maintenance and plasticity, which may be used to aid tissue regeneration after injury [33].

Apart from the regulation of biological function, EVs also participate in the pathogenesis of several diseases including tumours, neurodegenerative diseases and infectious diseases etc. Clear evidence indicates that tumour cell secreted EVs can transfer cargos, which results in the development of a pre-metastatic tumour niche, promoting angiogenesis and tumour cell migration in metastases, finally inducing tumour progression [34-38]. These tumour-derived vesicles that carry immunosuppressive molecules can suppress the immune responses and promote immune escape by modulating T cell activity [39,40]. In addition to tumour cells, tumour-related macrophages and tumour microenvironment can

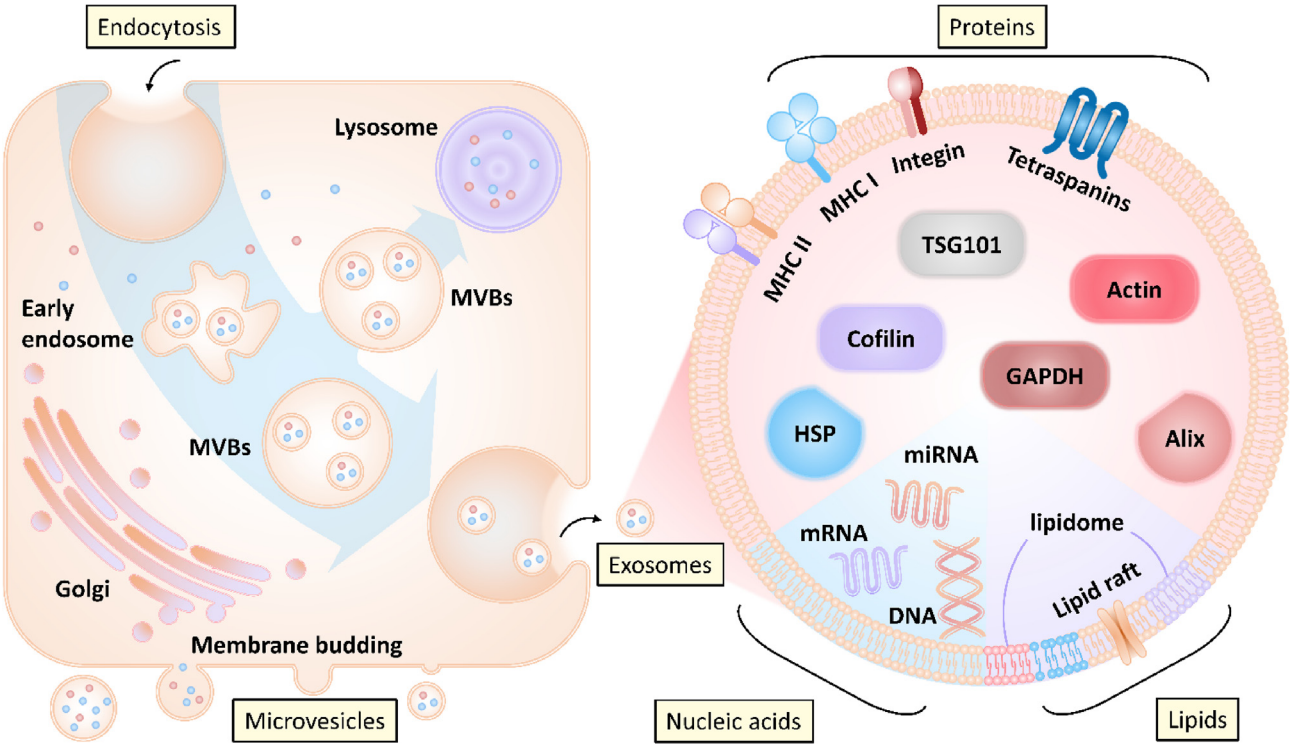

Fig. 2. Extracellular vesicle formation and release (left). Overall composition of exosomes (right).

Table 1
Classification of extracellular particles.

Vesicle types	Subset	Size	Origin	Markers
Exosomes	Exo-S Exo-L	60–80 nm 90–120 nm	Endolysosomal pathway	Tetraspanins, ESCRT components, PDCDIP, TSG101, flotillin, MFGE8
Microvesicles		150–1000 nm	Plasma membrane	Integrins, selectins, CD40 ligand
Apoptotic bodies		500–2000 nm	Plasma membrane, endoplasmc reticulum	Phosphatidyl serine, genomic DNA

also secrete EVs that accelerate the local invasion of cancer cells [41-43]. Within the nervous system, EVs derived from cells transfer pathogenic proteins to recipient cells to induce central nervous system diseases [44], such as neurodegenerative Alzheimer's disease and Parkinson's disease [44-46]. Additionally, EVs have also been involved in the spread of diverse pathogens such as HIV-1 and prions, resulting in the spread of infectious diseases [47,48].

The biology of EVs from eukaryotes e.g. mamalian cells have been extensively investigated. In comparison, EV research of prokaryotes including parasites and bacteria is only in its infancy. Due to the widespread diseases induced by parasites (mainly helminths, protozoa and ectoparasites) globally, understanding the mechanism of survival and persistence of parasites within their hosts are of critical importance. Recent research has indicated that parasites can release EVs which facilitate the cell–cell communication in the parasite-host interaction. Various parasites are able to generate EVs using different mechanisms and transfer bioactive cargos including proteins, lipids, glycans, RNA, and DNA through EVs to form infective niches upon internalization and modulate the immune system of the host, which then induce diseases [49-51]. Parasite derived EVs can transfer virulence factors, differentiation factors and drug-resistance genes between parasites. They can also mediate environmental adaptation under temperature and pH changes [52]. These findings provide valuable knowledge into parasite-host interactions and facilitate the understanding of the role played by EVs in parasite pathogenesis. However, there is still much to be understood including the nature of the cell machinery for the release and uptake of EVs, mode of EVs transport to the target, and whether blocking parasitic-EV secretion can influence disease progression etc. [53].

Bacteria can also secret membrane vesicles that affect different biological processes, including virulence, phage infection, export of cellular metabolites and intercellular communication [54]. Lee et al. reported on the mechanisms by which EVs released from gram-positive bacteria S. aureus could induce inflammasome activation. They also demonstrated that EVs could serve as a novel secretory pathway for *S. aureus* to transport protected cargos in a concentrated form to host cells during infections to modulate cellular functions [55]. It has been reported that bacteria released EVs could also affect the environment since they are abundant in sea water, indicating the important role of these EVs for carbon cycling in the marine ecosystem [56]. EVs also exist in microbial biofilms at a high level, where they serve as an essential component of the biofilm matrix and can shield cells existing in biofilms from antibiotics. In addition, microbial EVs exhibit immunomodulatory activities and as such are used as vaccines, which display excellent potential for applications in drug development and nanotechnology fields. Therefore, understanding the origin, the composition and content is of great importance for understanding bacterial induced infection. Furthermore, many bacterial vesicle functions, such as DNA transfer, cell detoxification and signal molecule release remain to be studied and represent valuable areas for future research [57].

2.3. Visualizing the in vivo events of EVs

Given the important biological and pathological roles of EVs, it is of importance to visualize these *in vivo* events to provide direct evidence of the function of EVs [58]. However, tracking and understanding the *in vivo* aspects of these nanosized vesicles is hindered by the lack of efficient labelling techniques, high resolution imaging techniques and appropriate animal models [59]. Wang et al. have used an aggregation-induced emission luminogen, DPA-SCP to tag mesenchymal stromal cells (MSC)-derived EVs and track their behaviour in a liver disease mouse model. The fluorescence imaging indicated that the DPA-SCP-labelled EVs were enriched in the liver and were stable for several days [60]. In another study, Liu et al. developed a phospholipid-based bioorthogonal labelling strategy to introduce optical probes into exosomes without influencing their native biological functions. The dynamic *in vivo* biodistribution and organotrophic uptake of multiple tumour exosomes in a single mouse were investigated (Fig. 3a) and indicated that the exosomes derived from different cell lines exhibited specific organotrophic uptake [61]. In order to evaluate the practicability of visualizing EVs within tumour tissue using multiphoton intravital microscopy, Breakefield et al. implanted mouse thymoma cell line EL4 which was expressed with PalmGFP into the dorsal skinfold chambers to form solid tumours. They observed green fluorescent punctate all over the tumour cells, with varied densities representing the different classes of tumour-released vesicles throughout the tumour. In addition, large EVs (around 1 μm diameter) were found to be tethered to tumour cells over a long period of time (Fig. 3b). However, limited by the sensitivity and imaging resolution of the technique used in the 3D environment of tumours *in vivo*, the behaviour of small EVs was difficult to be visualized [62].

While the above research provides bulk information on EV distribution *in vivo*, the live visualization of EV secretion and uptake to understand the exact function of EVs in physiology and pathology are still difficult to realize in mouse models. As such, in order to visualize EVs clearly at single molecule level, high resolution imaging and appropriate animal models are required. Studies have indicated that zebrafish embryos can be used as animal models due to many advantages including rapid growth, low cost, amenability to genetic modification, vascular networks and natural transparency that allow non-invasive imaging [63,64]. Based on the combination of high-resolution microscopy and zebrafish embryos, *in vivo* imaging at high spatiotemporal resolution was able to study how EVs diffused around secreting cells, cross biological barriers, and eventually circulate before disseminating throughout the body [64].

Niel et al. expressed a fluorescent CD63-pHluorin as a reporter in zebrafish embryos to form an integrated model for the investigation of EV secretion, transfer, and function *in vivo*. Using this model system, individual endogenous EVs could be visualized in live embryo of zebrafish using a combination of electron and fluorescence microscopy. They found that an EV subpopulation with exosome features were released into the blood circulation from the yolk syncnytial layer (YSL) in a syntenin-dependent manner. The uptake of YSL exosomes by endothelial cells and macrophages in the caudal vein plexus (CVP) were also visualized using fluorescence imaging (Fig. 3c) [65]. The biogenesis of exosome was interfered with syntenin, and the growth of CVP was affected, indicating the possibility of manipulating endogenous biogenesis of exosomes. While *in vivo* imaging of EVs provided a promising method for tracking circulating tumour EVs in zebrafish embryos. Using a multi-colour membrane dye MemBright [66], Goetz et al. demonstrated that circulating tumour EVs could be rapidly taken up and stored in degradative compartments by endothelial cells and blood patrolling macrophages. Additionally, tumour EVs activated macrophages and promoted metastatic outgrowth (Fig. 3d) [58]. Therefore, zebrafish embryos offer an ideal model to track normal endogenous EVs and tumour derived EVs in order to evaluate their inter-organ communication *in vivo* with high spatiotemporal resolution.

3. Isolation and characterization of EVs

EVs are important biomarkers for disease diagnosis, prognosis, and promising nanoparticles (NPs) for disease treatment. Therefore, there is high demand for efficient, and affordable techniques to isolate these nanosized vesicles [67,68]. However, isolating intact exosomes remains a challenge due to their small size and complex living environment, which limits disease-targeting applications of EV. Based on the physical and chemical properties of EVs, a variety of strategies have been reported [69]. Despite excellent recent developments, there are still significant hurdles to overcome, for example, medical applications are limited since the separation method which is not standardised results in low yield and poor stability [70]. In this section, we will discuss recent advances in the isolation of EVs, placing an emphasis on microfluidic-based approaches, together with the challenges and prospects. In addition, the characterization of EVs will be discussed.

3.1. Bulk method for the isolation of EVs

EV-based clinical application requires standard and effective EV isolation techniques as a prerequisite. Conventional EV isolation methods include ultracentrifugation, density gradient flotation, precipitation, size-based isolation, immunoaffinity capture etc. [22,67,70]. According to a recent report, ultracentrifugation continues to be the most used isolation method (81%) of worldwide EV research owing to the effectiveness in obtaining abundant EVs. Immunoaffinity capturing methods are still regarded as the most effective technique to isolate the desired exosomes with structural and compositional integrity [71]. Different isolation strategies can influence the EV populations' glycosylation profile and lead to diverse glycosylated EV populations. Thus, it is important to apply suitable EV cell culture conditions and isolation protocols in order to ascertain the functional and structural complexity of the EV glycoconjugates [72]. The principles of different bulk isolation methods, as well as their individual advantages and limitations are listed in Table 2. Some representative and emerging EV isolation techniques are exemplified.

By utilizing the AF4 technique, extracellular NPs could be fractionated based on their hydrodynamic size. This approach demonstrated a unique ability to separate NPs using two perpendicular flows (channel flow and crossflow) inside a thin, flat channel with a semi-permissive bottom wall membrane. The AF4 separation method offered a number of advantages over other isolation methods for EV analysis, including gentle, label-free, rapid (<1h), good reproducibility and with high recovery of analytes. More importantly, when compared to other available techniques, AF4 can provide a large dynamic range of size-based separation of EVs at high resolution (1 nm) [80]. Since the lipid bilayer of exosomes were rich with phosphate groups, an isolation method using the specific interaction of the phosphate groups with TiO_2 was developed to isolate EVs directly from human serum. Due to the high affinity binding, model exosomes could be isolated reversibly with excellent recovery (93.4%) [97]. An origami-paper-based device for the successful isolation of biomarkers resulting in fewer steps and less damage was developed. The multi-folded device using the ion concentration polarization technique a Nano electrokinetic phenomenon that enriched charged biomolecules, enabled the preconcentration of EVs on specific layers (~5-fold) Subsequently,

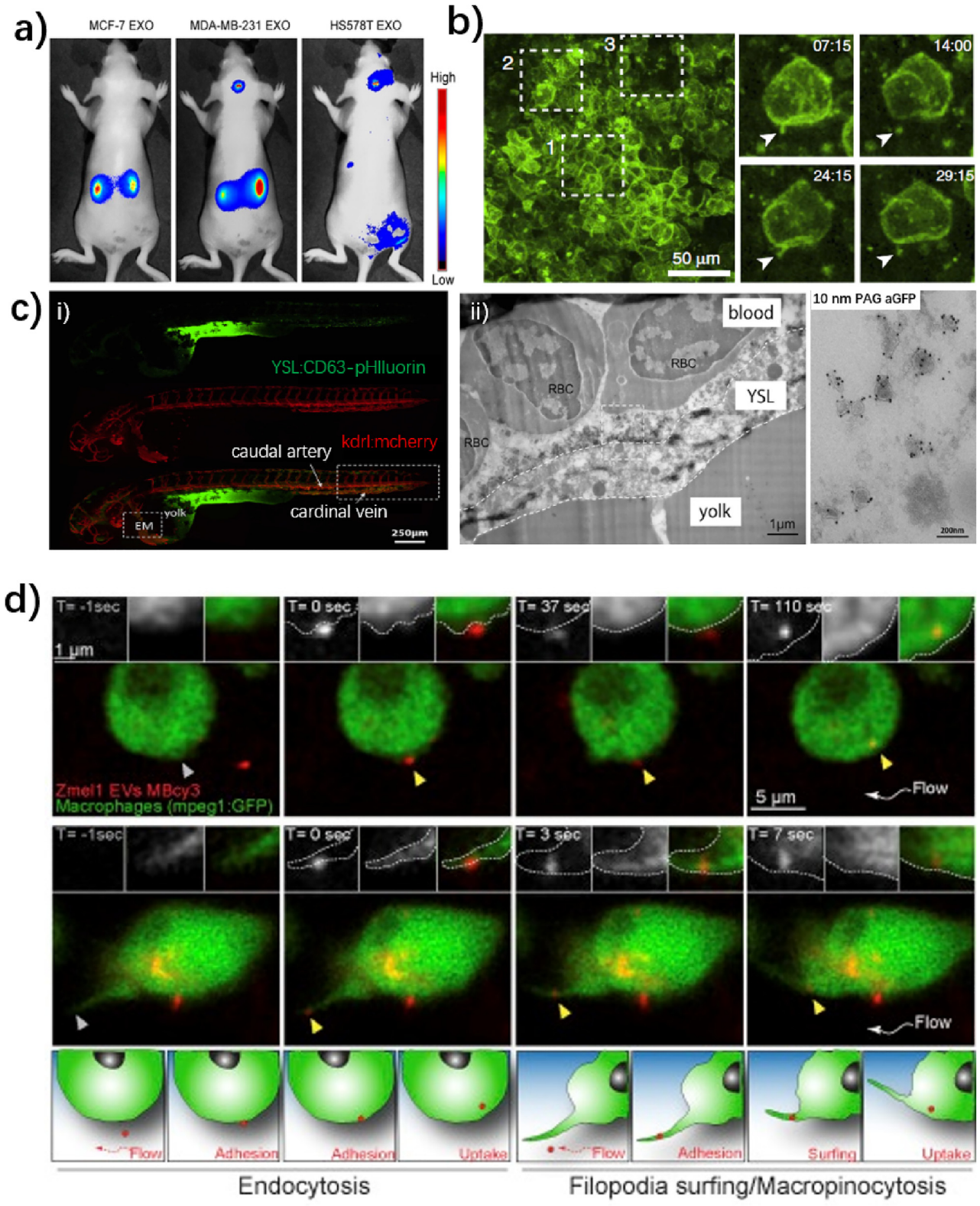

Fig. 3. a) *In vivo* tracking of breast-cancer-cell-derived exosomes in mice given intravenous injections of fluorescently labelled MCF-7-, MDA-MB-231-, and HS578T-secreted exosomes. Adapted with permission from ref [61]. Copyright 2018 American Chemical Society. b) Left: Intravital image of the central region of EL4 tumour. The white squares represent regions with the absence (1), low (2) and intermediate density (3) of detectable PalmGFPt vesicles. Right: Time-lapse recordings (min:s) highlighting a tethered vesicle. Adapted with permission from ref [62]. Copyright 2015 Nature Publishing Group. c) i) Fluorescence imaging of a 3 dpf Tg(kdrl:Hsa.HRAS-mCherry) embryo treated with ubi:CD63-pHluorin in the YSL. Box [EM] shows the region for EM analysis, indicated in (ii). Adapted with permission from ref [65]. Copyright 2019 Cell Press. d) Confocal imaging of Tg(mpeg1:GFP) embryos showing: (top) the attachment and uptake of EVs by endocytosis and (bottom) the sliding of EVs on the macrophage protrusion and its fast internalization. Adapted with permission from ref [58]. Copyright 2019 Cell Press.

Table 2
Comparison of diverse EV isolation techniques.

Isolation techniques		Principle of enrichment	Advantages	Disadvantages	Refs.
Bulk method	Ultracentrifugation	Multiple centrifugal steps to remove debris, cells, large vesicles, precipitate and isolation of EVs based on size and density	Lowered cost and risks of contamination, Big sample capacity and results in large amounts of exosomes	Large equipment cost, extended run time, and labour intensive with low portability	[67,71,73,74]
	Density gradient flotation	Size, shape, and density of the EV	Current gold standard; high purity	Time (>4h); large sample volume; low recovery; requires ultracentrifuge;	[22,71]
	Precipitation	Changing the solubility or dispersibility or EVs using water-excluding polymers Surface charge	Simple to use, no specialized equipment, large and scalable sample capacity	Co-precipitation of contaminants; Long run time, Requires pre-and post-cleanup	[70,75]
	Size-based isolation	Uses size-exclusion chromatography (SEC) and ultrafiltration (UF); based on size and molecular weight	SEC: high-purity, integrity and biological activity of EVs, reproducibility. UF: rapid, no special equipment, good portability, direct RNA extraction	SEC: dedicated equipment, scale up nontrivial, extended run time. UF: moderate purity, deterioration, low recovery	[76]
	Affinity-based capture	Immunoaffinity and lipid layer affinity Specific binding between exosome membrane-bound antigens (receptors) and immobilized antibodies (ligands)	Specificity; high purity; subtyping possibility	High reagent cost, low capacity and low yields, cell-free samples	[77,78]
	Field flow fractionation	Size and molecular weight	Wide separation range; large variety of eluents; subpopulations	Extended duration; requires fractionation equipment	[79,80]
	Acoustic enrichment	Size and molecular weight	Label-free	Instrument requirement	[81]
	Ion concentration polarization technique	Ion concentration and polarization on origami paper-based platform	Facial operation; no damage to vesicles	Low yield; nonregenerative	[82]
Microfluidic-based method	Size-based sorting	Size and shape	Low sample consumption; Rapid sample processing; Portability; Low cost	Low throughput; Sample pre-treatment	[83-86]
	Viscoelasticity	Size, shape, and density of the EV			[87]
	Acoustofluidics	Size and molecular weight			[88]
	Immuno-based binding	Immunoaffinity			[89-96]

by unfolding the device these vesicles could be isolated from the rest of the sample [82].

3.2. Microfluidic-based approaches

With the rapid progress of nanomaterials and nanotechnology, a variety of new EV enrichment approaches have been established, especially in combination with microfluidic systems. Microfluidic platforms are ideal tools for exosome separation because they have excellent flow control, rapid mixing and precise processing of solutions, which are regarded as ideal systems to study nanosized vesicles [98,99]. Microfluidic-based isolation is built on the differences in EVs' physical or biochemical properties like size, density, and immunoaffinity. Additionally, by integrating acoustics, electrophoretic, and electromagnetic techniques, various advanced isolation approaches have been rapidly evolving. In one such aspect, using microfluidic devices, reagent consumption and separation time could be reduced. In another aspect, microfluidic technologies can meet the requirements of EV isolation from the perspective of cost-effectiveness, enhanced purity, and point-of-care measurement and diagnosis. Microfluidic-based isolation and enrichment techniques of EVs can be divided into three categories: size-based sorting, label-free enrichment which is based on viscoelasticity or acoustics and immunoaffinity methods [70,100].

3.2.1. Size-based sorting

By embedding nanofilters, nanopillars or porous membrane in the microdevice, EVs can be isolated based on their size [101-104]. For instance, by integrating two nanofilters into a lab-on-a-disc device, a label-free, rapid, and highly sensitive method for EV quantification and isolation was constructed (Fig. 4a). Using a tabletop-sized centrifugal microfluidic system, the biological sample could be transferred through the two nanofilters, facilitating the enrichment of EVs during the second round of filtration using a pore diameter of 20 nm with size range of 20 to 600 nm. The Exodisc was able to isolate intact EVs from raw biological samples e.g. cell-culture supernatant or clinical urine samples within 30 min with high recovery [83]. In another study, porous polymer monoliths were utilized as microfluidic filtration membranes and integrated with a microchip to isolate vesicles from whole blood samples. The combination of DC electrophoresis as an alternative driving force resulted on the transfer of particles through the filter in order to achieve an increased separation efficiency of vesicles from proteins [84]. Wunsch et al. have used deterministic lateral displacement (DLD) pillar arrays to isolate and enrich microscale particles. Manufacturable silicon procedures were used to form nanoscale DLD (nano-DLD) arrays with uniform gap sizes in the range of 25 to 235 nm. When the Péclet (Pe) numbers were low, with competing diffusion and deterministic displacement effect, nano-DLD arrays could realize the on-chip separation of EVs between 20 and 110 nm with high resolution [85]. In addition, a spatial separation of EV samples based on particle size was evaluated using Marangoni flow and the coffee-ring effect of microdroplets. Subsequent transfer of a drying droplet resulted in increased mean sizes of EVs in the sample using repeated subsampling during coffee-ring formation of a droplet. Importantly, the method facilitated size-based sorting, separation, and recovery of EVs for downstream analysis [86].

3.2.2. Contact-free isolation

Contact-free isolation techniques that combine viscoelasticity or acoustics have been developed recently. Viscoelastic microfluidics can be used for particle manipulation based on particle movement produced due to size-dependent elastic lift forces in a

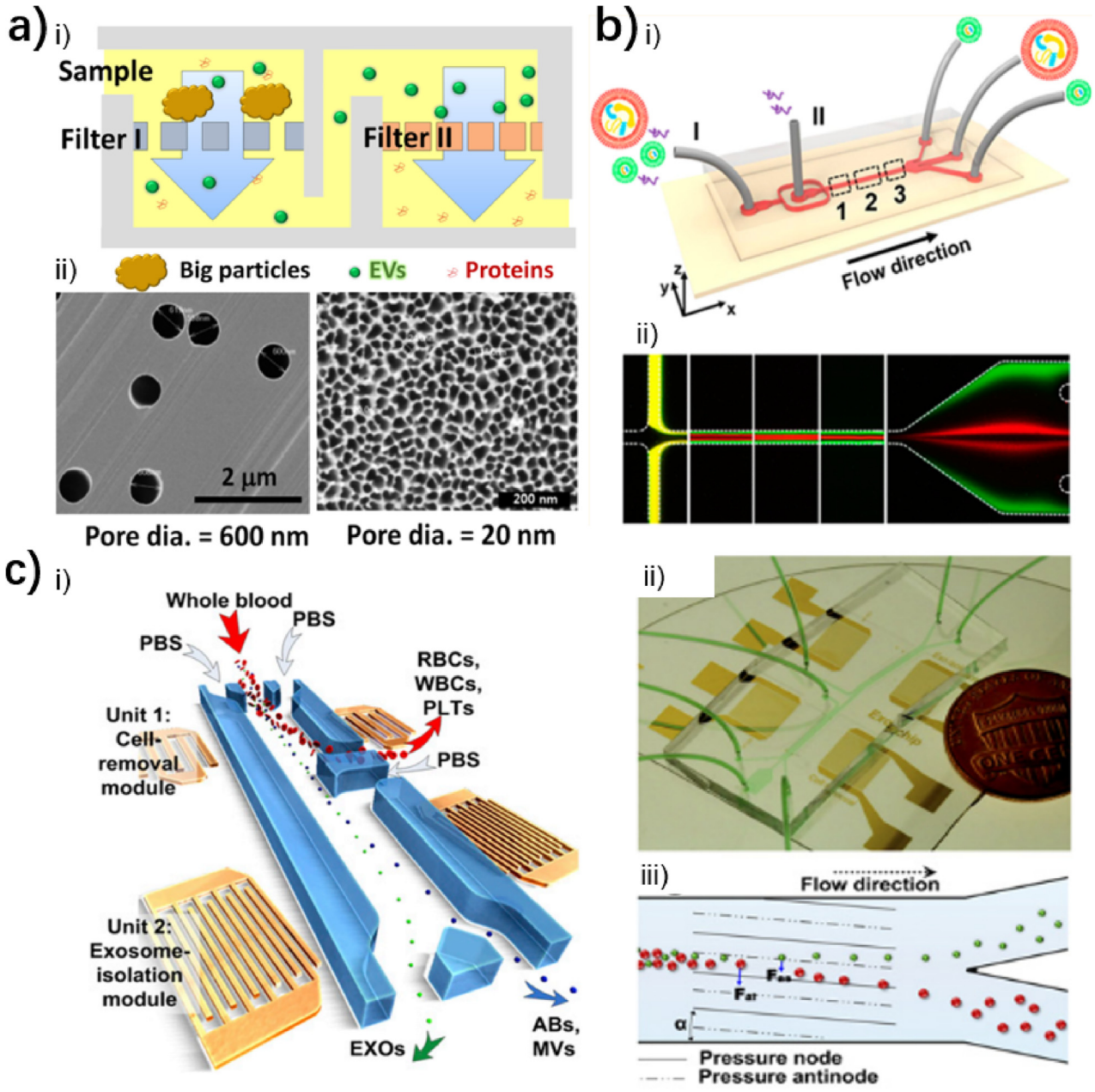

Fig. 4. a) i) Cross-sectional view of the filters in the microdevice, indicating fluidics for the size-based isolation of EVs. ii) SEM images of the two filters I (pore diameter = 600 nm) and II (pore diameter = 20 nm). Adapted with permission from ref [83]. Copyright 2017 American Chemical Society. b) i) Schematic illustration showing the microfluidic chip for exosome separation from large EVs. ii) Fluorescent image showing separation of the binary mixture of 100 nm (green) and 500 nm (red) polystyrene particles. Adapted with permission from ref [87]. Copyright 2017 American Chemical Society. c) Schematic illustration of the integrated acoustofluidic device for isolating exosomes. i) Red blood cells (RBCs), white blood cells (WBCs), and platelets (PLTs) are firstly removed by the cell-removal module, and then exosomes (EXOs) are separated from other subgroups of EVs by the exosome-isolation module. ii) An optical image of the integrated acoustofluidic device. iii) Schematic illustration of the mechanism of size-based separation. Adapted with permission from ref [88]. Copyright 2017 National Academy of Sciences.

viscoelastic environment. Sun et al. directly separate exosomes from cell culture media or serum in a continuous, size-dependent manner using a viscoelastic based microfluidic system (Fig. 4b). By adding a biocompatible polymer poly-(oxyethylene) to control the viscoelastic forces, EVs were laterally driven and fractionated by size with a high separation purity (>90%) and recovery (>80%) [87]. As another label-free strategy, acoustic waves were used to isolate exosomes in a label-free and contact free manner directly from whole blood [105]. An acoustofluidic platform which involved the fusion of acoustics and microfluidics was fabricated to isolate exosomes directly from undiluted blood samples. The system consisted of two sequential surface-acoustic-wave (SAW) modules: exosome-isolation module and a cell-removal module. Each module relied on a tilted angle standing SAW field produced by one pair of interdigital transducers (Fig. 4c). First, the cell-removal module removed large blood components to acquire enriched EVs, then the exosome isolation module further purified the exosomes with high purity and yield [88].

3.2.3. Immuno-based isolation

Immunoaffinity-based capture of EVs represents the most promising technique for EV isolation. By targeting known surface

protein markers including the tetraspanin family (e.g., CD9, CD63, and CD81) and tumour related biomarkers (e.g. epidermal growth factor receptors, EGFR and epithelial cell adhesion molecule, EpCAM), EVs are captured by specific antibodies immobilized on solid surfaces. In addition, as a highly efficient capture method, immuno-based binding can be combined with microfluidic platforms for EV isolation [106,107]. Various microfluidic devices have been developed to isolate EVs, while individual microfluidic platforms exhibit unique characteristics. In general, there are two main types of devices, one is an antibody-functionalized surface in microchannels, the other is based on magnetic beads for capture [89,90]. In the first type of device, a microfluidic device with herringbone structure and a thermally responsive nanostructured substrate design (EVHB-Chip) was fabricated and used for isolation of EVs after modifying the surface with antibodies (Fig. 5a). The nanostructured substrate was composed of an ultra-thin (~150 nm) gelatin membrane which was modified with streptavidin-coated NPs. Combined with the chaotic mixing effect of the herringbone grooves, the interaction between EVs and the tumour specific antibody-coated surfaces could be maximized. Furthermore, using an optimized PEG linker to immobilize the antibodies enhanced the tumour specific EV capture. EVHB-Chip enabled the isolation of tumour-specific EV-RNA within 3 h and achieved 94% tumour-EV specificity and a limit of detection (LOD) of 100 EVs per μL, as well as efficient capture of tumour-derived EVs from plasma and serum of GBM patients [91]. While another chip design, used a covalently functionalized herringbone-grooved microfluidic device with antibodies towards exosome membrane biomarkers (CD9 and EpCAM) facilitating exosome isolation from small volumes of high-grade serous ovarian cancer (HGSOC) serum. Intact exosomes were released label-free after capture using a low pH buffer and neutralized immediately downstream to guarantee their stability [92]. In addition, nanomaterials, e.g. multiwall carbon nanotubes or silicon nanowires have been functionalized with specific recognition antibodies (e.g. anti-CD63 or anti-EpCAM) on micropillars to form 3D nanostructured microfluidic chips for capturing exosomes. Based on a combination of immunorecognition and the unique topography of these nanomaterials, exosomes could be purified efficiently [93,94].

In the second type of microdevice, magnetic beads conjugated with capture antibodies for EVs have been utilized to facilitate the isolation of EVs. He et al. reported a microfluidic approach for the integration of on-chip separation and analysis of EVs [95,96]. The microchip termed ExoSearch consisted of a Y-shaped injector, a serpentine fluidic mixer for on-chip mixing and magnetic bead-based exosome capture (Fig. 5b). The immunomagnetic beads could bind EVs as tight aggregates using magnetic forces for optical detection downstream. In addition, removing the magnet released the beads which could then collected from the chip to obtain purified and enriched EVs for variable benchtop measurements. The blood-based diagnosis of ovarian cancer was achieved using the ExoSearch chip using multiplexed measurement of three exosomal tumour markers (CA-125, EpCAM, CD24) using a training set of ovarian cancer patient plasma, the system exhibited an excellent diagnostic capability [96]. To facilitate point-of-care EV nucleic acid analysis, an integrated microfluidic platform for on chip extraction and detection of RNA in EVs by PCR was developed by Shao et al [108]. In this approach, the microfluidic platform termed immuno-magnetic exosome RNA (iMER) consisted of three operational compartments: enrichment of extracellular vesicles, RNA isolation and real-time RNA analysis on-chip (Fig. 5c). Firstly, specific antibody functionalized magnetic microbeads were used to separate the cancer exosomes. Then, the enriched vesicles were lysed, and passed through a glass-bead filter, so that the RNA was adsorbed onto glass beads by electrostatic interactions. The obtained RNA was eluted, reverse transcribed and analysed by quantitative polymerase chain reaction (qPCR). The whole procedure was accomplished on the same microchip, with integrated functional components. Using this approach, exosomal mRNA profiles of EVs derived from the blood of patients with glioblastoma multiforme (GBM) were evaluated, suggesting an effective method for predicting the treatment efficacy of GBM [108].

Apart from the widely used exosomal surface biomarker CD63, phosphatidylserine (PS) which is expressed on the outer surface of tumour-related EVs has been used as another biomarker for immunoaffinity-based EV isolation. Through conjugation with a PS-specific protein, cancer associated exosomes could be isolated from plasma, with 90% capture efficiency. Subsequently, the immobilized exosomes are easily released using Ca^{2+} chelation for further characterization [109]. Microdevices equipped with external driving forces, e.g. a current electrokinetic microarray chip device could be applied to isolate and recover glioblastoma exosomes from undiluted human plasma samples, based on the differences between the dielectric properties of the plasma and exosomes [110]. Given that microfluidic chip-based techniques possess many advantages in isolating EVs, the main challenges in translating microfluidic technology to a clinical platform are associated with how to improve their efficiency and yield for isolating EVs, as well as the reproducibility and consistency of enriched nanovesicles [70]. Over the last few years, research in EV isolation has grown rapidly, however, the poor standardization of isolation approaches is a significant obstacle for the development of this field. In brief, the need for a standard method for specimen handling, suitable controls, and isolation and analysis techniques to enable comparison of the results remain a challenge to the further development of EV-related applications [69,111].

3.3. Characterization of EVs

After isolation, the characterization of EVs is necessary to evaluate the quality of the obtained EVs. In general, EVs can be physically identified by the morphology and particle size distribution [70]. For morphology-based characterization, microscopic methods including scanning electron microscopy (SEM), transmission electron microscopy (TEM), cryo-electron microscopy (cryo-EM) and atomic force microscopy (AFM) have been widely employed. SEM provides the elemental composition and three-dimensional morphology of EVs [112]. With the assistance of SEM, EVs display uniform unimodal size distribution after being filtered using a 0.2 μm membrane [113]. Under high-resolution TEM, the morphology and structure of different sized EVs can be observed [114]. Cryo-EM can recognize the structure and morphology of EVs at low temperature avoiding the side effects induced by dehydration and chemical fixatives. Using cryo-EM the EVs exhibited round morphology and structure, which indicates that the cup-shaped structures of EVs observed by other EM techniques are most probably induced by dehydration of the vesicles [115]. Compared with the other microscopic methods, AFM has a unique advantage of providing the surface topography of these nanosized vesicles [116].

Dynamic light scattering (DLS) and nanoparticle tracking analysis (NTA) are the two main types of size-based characterization for EVs, which offer information on the size distribution of EVs. DLS provides the hydrodynamic diameter of EVs by measuring the scattered light emitting by these nanovesicles [79] and NTA is an optical particle tracking technique which can monitor the size distribution and concentration of vesicles in real time [117]. Unlike the bulk scattering of DLS, NTA can enable tracing of individual vesicles, offering unique advantages in single EV characterization [112].

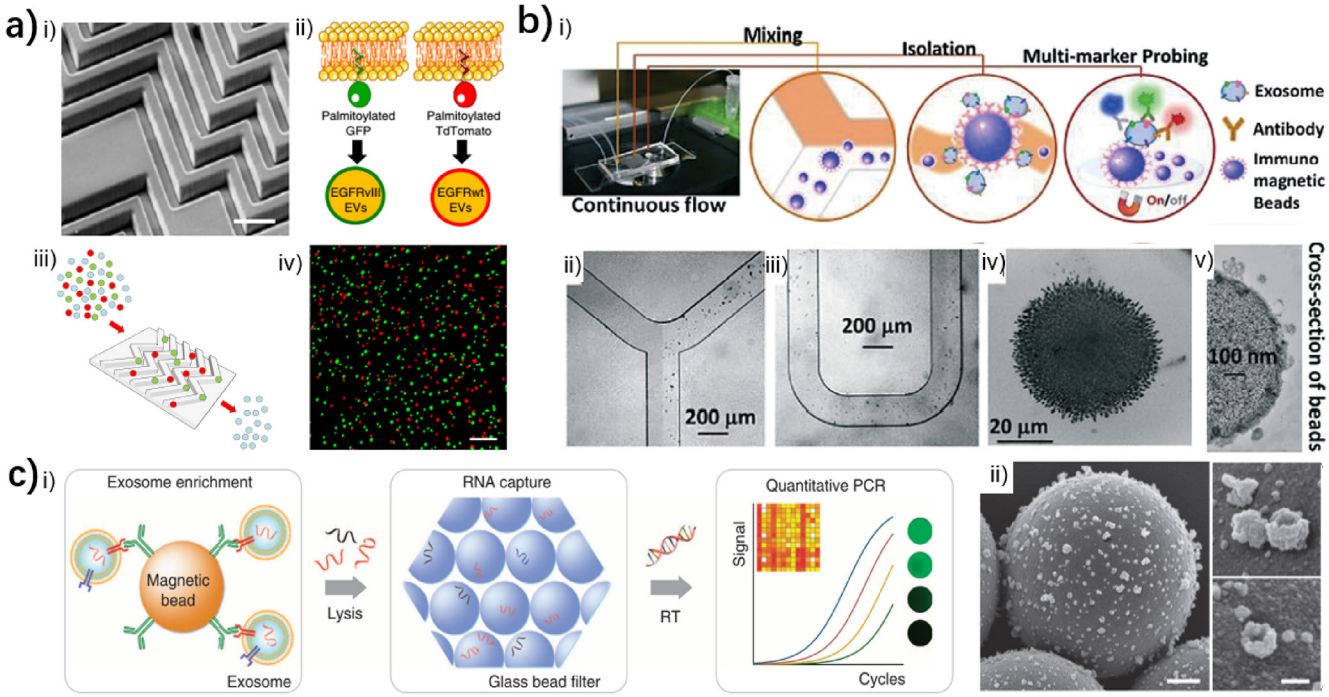

Fig. 5. a) i) SEM image of the 3D herringbone structure of the microfluidic device (scale bar 100 μm). ii) Cells were infected with PalmtdTomato (red) or PalmGFP (green) to produce fluorescently labelled EVs. iii) Schematic illustration of red and green fluorescent EVs running through the device to capture tumour EVs. iv) Image of digitally rendered signals of captured fluorescent EVs. (Scale bar 1 μm). Adapted with permission from ref [91]. Copyright 2018 Nature Publishing Group. b) i) Workflow of the ExoSearch chip for mixing, isolation and multi-marker probing of circulating exosomes. ii)-iii) Bright-field images of the microchannels showing the mixing and isolation of exosomes by magnetic beads. iv) Image of aggregated exosome-bound immunomagnetic beads. v) TEM image of cross-sectional view of an exosome-bound immunomagnetic bead. Adapted with permission from ref [96]. Copyright 2016 The Royal Society of Chemistry. c) i) Schematic illustration of the integrated immunomagnetic exosomal RNA (iMER) platform for exosome enrichment, RNA capture and real-time analyses. ii) SEM image of magnetic beads after immunoaffinity capture. Adapted with permission from ref [108]. Copyright 2015 Nature Publishing Group.

4. Analysis techniques for EVs

To better understand their composition and function, a variety of techniques have been used to identify EVs. The assay of EV contents is not only indicative of vesicle biogenesis but is also instructive for the liquid biopsy of various diseases which has attracted increasing research interest over the last few years. The growing demand for non-invasive liquid biopsy has led to the development of novel advanced methods for EV detection. However, establishing sensitive and reliable exosomes-based detection remains challenging due to their heterogeneity in size, the complexity of the biofluids and lack of standard characterization methods [118]. Increasing efforts have been directed towards developing new sensitive approaches for EV assays. These approaches depend on the analysis of the protein and nucleic acid which carries important cellular information from the parent cell. In this section, we will review advances in various analytical technologies for EV detection, that focus on the use of fluorescence and Raman-based assays.

4.1. Fluorescence approach

4.1.1. Protein analysis

Conventional protein analysis relies mainly on two bulk methods, Western blotting and enzyme-linked immunosorbent assay (ELISA) [111]. Cell derived EVs contain abundant transmembrane proteins such as EGFRs and adhesion proteins such as EpCAM. The nanosized exosomes are enriched with tetraspanins that are a superfamily of proteins with four transmembrane domains. Therefore, tetraspanins (e.g. CD9, CD63, CD81 and CD82) are utilized as specific surface proteins for exosome analysis with western blotting and ELISA. Intravesicular proteins of EVs including membrane transport proteins (Annexins, flotillin, GTPases), heat shock proteins (e.g. Hsp20, Hsp60 and Hsp70), proteins related to the formation of MVB (TSG101, Alix), phospholipases, lipid-associated membrane protein etc. can also be detected using conventional protein analysis [70].

Fluorescence based approaches are extensively applied as advanced detection methods for biomolecules, due to the advantages of high sensitivity, high selectivity and fast response etc. [119-123]. Therefore, various modern immuno-based protein analysis techniques have been developed, in combination with fluorescence-based methods, to enable facile, rapid and sensitive identification of EVs for clinical applications. For instance, Ochiya et al. reported on an approach using photosensitizer-beads termed Exoscreen to profile surface proteins of circulating EVs using an amplified luminescent proximity homogeneous assay without purification in serum (Fig. 6a). EVs from blood samples were captured by streptavidin-coated donor beads functionalized with a biotinylated antibody, which were detected using acceptor beads conjugated to a detection antibody (e.g. anti-CD9 and anti-63) that recognized the target EVs. Under an excitation laser of 680 nm, the donor beads could release singlet oxygen to excite the acceptor beads at a distance of<200 nm and generate a detectable fluorescence emission at 615 nm. Therefore, this approach was able to identify small EVs (diameter < 200 nm). Through the quantification of CD147 and CD9 on circulating EVs in serum from colorectal cancer patients, colorectal cancer could be diagnosed, suggesting that ExoScreen was suitable as an effective liquid biopsy technique [124]. In another study, to avoid the time-consuming pretreatment of EV samples, Takeuchi et al. used molecular imprinting to create exosome binding cavities on a gold substrate. After exceptional post-imprinting in-cavity modifications, exchangeable antibodies and fluorescent reporter molecules were aligned inside

exosome-binding cavities (Fig. 6b). Then by recording the quenched fluorescence and increasing amounts of exosomes, this platform facilitated the rapid and highly sensitive sensing of intact exosomes and indicated great potential for discriminating prostate cancer derived exosomes from normal controls [125]. Based on a similar molecular printing strategy, antibody-conjugated signalling nanocavities were developed to achieve the size recognition and non-invasive detection of EVs. Various concentrations of cell secreted EVs were quantified by measuring the fluorescent images on the chip using an automated procedure. The system was used to detect cancer related intact EVs in tears and differentiated between healthy donors and breast cancer patients, clearly indicating the potential of this technology for liquid biopsy and early cancer diagnosis [126]. Lu et al. have reported on the multiplexed profiling of EVs secreted by single cells using spatially patterned antibody barcodes on a microchamber array. They used two different antibodies to recognize two antigens on each vesicle to form a sandwich assembly, where captured EVs could be detected using fluorescence signals (Fig. 6c). The high-throughput profiling of EV secretion from human oral squamous carcinoma cells suggested that such antibody barcodes could be used for multiplexed EV detection [127].

Aptamers are single-stranded oligonucleotides that can bind to targets with high specificity and affinity. They are employed as substitutes for antibodies in immunoaffinity detection and applications involving antibodies [128,129]. Therefore, fluorescence-based aptasensors have been reported for EV detection through the targeted binding of specific surface proteins of EVs [103,130]. Sun et al. developed an approach for profiling EV surface proteins and the classification and early detection of cancers using a thermophoretic aptasensor for the enrichment of EVs conjugated with aptamers (CD63 and EpCAM aptamer). Diluted serum samples were incubated with Cy5-conjugated aptamers (0.1 μM) to bind to the target protein with high specificity and sensitivity on the EV surface. Then a diluted serum sample in a microchamber was heated using a 1,480 nm laser, which lead to enrichment of EVs at the laser spot. The aptamer bound EVs generated an amplified fluorescence signal after accumulation. Moreover, the size-

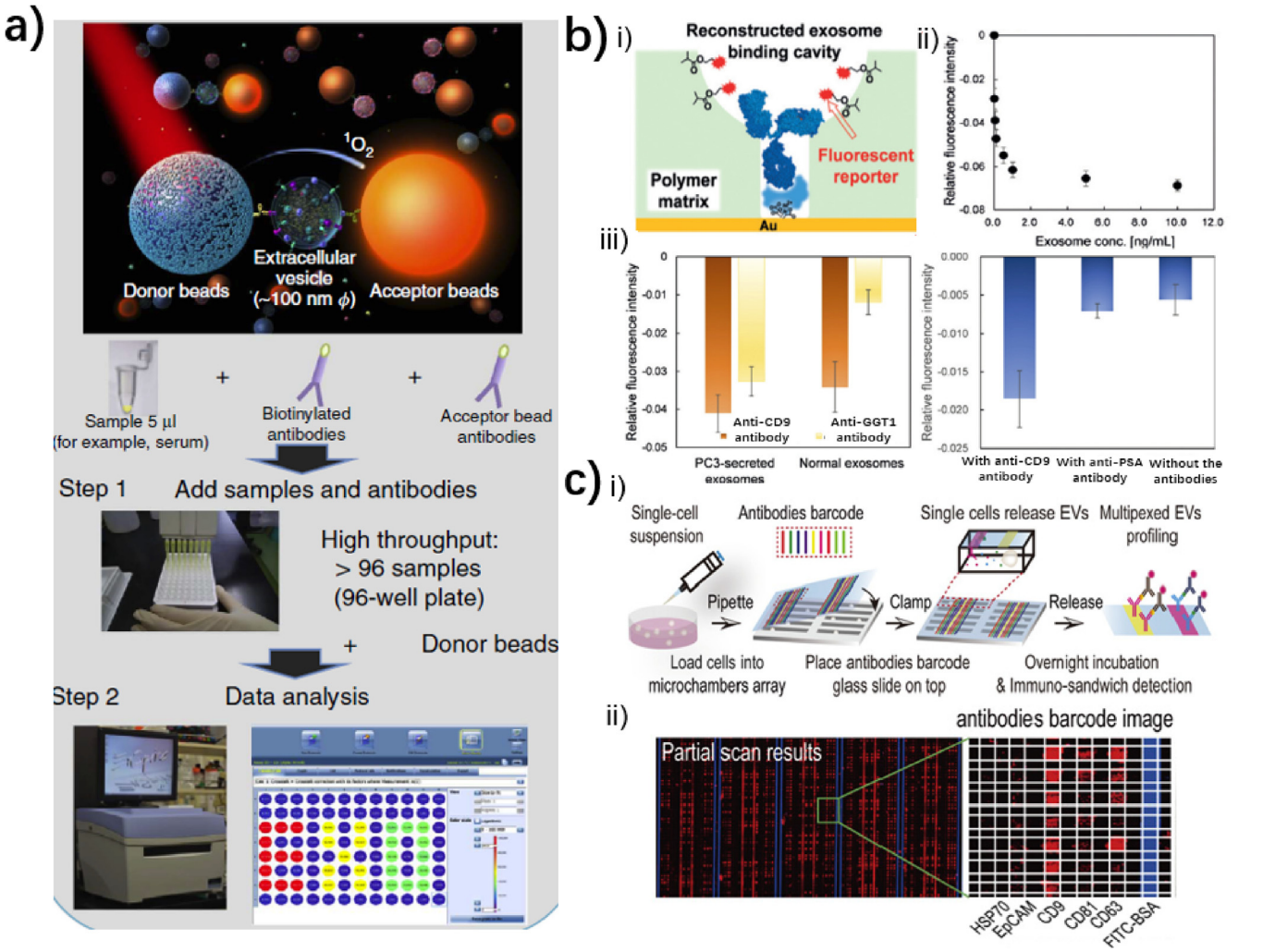

Fig. 6. a) Schematic illustration of the methods used for detecting circulating EVs. Adapted with permission from ref [124]. Copyright 2014 Nature Publishing Group. b) i) Schematic overview of the reconstruction of the exosome binding cavities and fluorescence-based sensing of intact exosomes. ii) Concentration-dependent signal of PC3-derived exosomes towards anti-CD9 antibody-functionalized binding cavities. iii) Response of exosomal CD9 and GGT1 on PC3-secreted and normal exosomes, and (Right) binding of tear exosomes to the cavities with the anti-CD9 antibody, anti-prostate specific antigen antibody, or control. Adapted with permission from ref [125]. Copyright 2019 John Wiley and Sons. c) i) Schematic of the workflow for multiplexed profiling of single cell EV secretion. ii) The raw data of multiplexed single-cell EV profiling showing fluorescence images. Right enlarged image indicates the fluorescent positive square spots intersecting CD63/CD81/CD9 antibody barcodes. Adapted with permission from ref [127]. Copyright 2019 National Academy of Sciences.

dependent accumulation of EVs induced by localized laser heating relied on the interplay of thermophoresis, diffusion and convection, while the thermophoretic effect on free aptamers or proteins due to their small size was negligible. The fluorescence intensity of concentrated aptamer bound EVs was associated with the level of expression for the EVs target surface protein. Combined with linear discriminant analysis, cancer detection and classification were possible using small serum volumes (<1 μL) [131]. Due to the high charge, aptamers have a strong thermophoretic effect, which can lower background signals and thus improves sensitivity [132]. Based on thermophoretic aptasensor strategy, Yang et al. also reported a Cy5 labelled PD-L1 (programmed death-ligand 1) aptamer to recognise the exosomal PD-L1 which is a key element in immunotherapy. Since the thermophoresis of the PD-L1 aptamer induced by infrared laser differs clearly from the exosome-aptamer complex as a result of binding-induced changes, the complex persists while free aptamer tends to be depleted in the hot spot. Compared to PD-L1 antibody, the newly developed PD-L1 aptamer, a short single strand DNA with smaller size, could avoid the hindrance of antigen glycosylation and exhibited enhanced binding to PD-L1 in cells (Fig. 7). Evaluation of the fluorescence intensity of the retained exosome-aptamer complexes and the depleted free aptamer at the laser hot spot, facilitated cancer diagnosis and prediction of the immunotherapy response [133].

Apart from bulk analysis, microfluidic platforms have been widely used for developing biosensing systems owing to their advantages of low sample consumption, integrated on-chip analysis, and rapid response etc. [134-136]. EV assay combined with functional nanostructures and microfluidic platforms can achieve rapid immunobinding of vesicles and sensitive detection. Zeng et al. developed a microfluidic chip with self-assembled 3D herringbone nanopatterns for the detection of exosomes. The microchip was constructed based on multiscale integration by designed self-assembly combining micropatterning and 3D nanostructured herringbone (nano-HB) mixer for flow manipulation and molecular recognition. This structure could effectively promote microscale mass transfer of bioparticles to improve binding speed and efficiency; and permit drainage of the boundary layer of fluid through the pores of the nanostructures. The nano-HB chip enabled low LOD of 10 exosomes per μL by staining EVs with fluorescent dye and quantitative detection of circulating exosomal markers to detect ovarian cancer using only 2 μL of plasma, indicating the potential for application in liquid biopsy-based cancer diagnosis [137]. For integrated microfluidic chips, after enrichment of EVs, the vesicles could be detected by subsequent functionalization, such as labelling with fluorescent dyes [138]. For instance, an immunomagnetic bead-based microfluidic platforms for exosome isolation could achieve on-chip detection of exosomes from human plasma using either chemi-luminescence detection following sandwich immunoassay [95] or multicolour fluorescence imaging after labelling the exosomes with a fluorescent dye in the microchamber for reliable cancer diagnosis [96]. Due to the high sensitivity, microfluidic-based analysis has significant advantages when translating from the lab-based environment into real world diagnostic applications [89].

4.1.2. Nucleic acid analysis

EVs carry proteins, as well as nucleic acids that are promising, minimally invasive diagnostic biomarkers for diseases. These nucleic acids include different forms of RNA and DNA, among which messenger RNAs (mRNAs) are a large family of coding RNA molecules that specify protein sequence information while microRNAs (miRNAs) are a class of small, noncoding RNAs [139,140]. Conventional analysis of nucleic acids is based on extraction procedures (e.g. precipitation), followed by amplification by polymerase chain reaction (PCR) and subsequent detection using endpoint electrophoresis or real-time fluorescence measurement based on a known target sequence of the exosome [111].

Studies have indicated that the level of exosomal miRNAs is correlated with disease development, owing to the intercellular communication roles mediated by EVs. It has been shown that specific EV encapsulated miRNAs are closely related to the phenotypes of certain types of cancer. These genetic materials are transferred by circulating exosomes to recipient cells and affect the cell microenvironment, which then stimulates cancer development [141]. Therefore, targeted, and sensitive detection of these miRNAs could not only contribute to a better understanding of the pathological roles of EVs, but in addition provide efficient tools for disease diagnosis [142]. Conventional quantitative reverse transcription PCR (qRT-PCR) has disadvantages including limited throughput, the requirement for a specific primer pair for each reaction and sophisticated pre-treatment [143]. Therefore, new approaches have been developed for the quantification of exosomal miRNAs. For instance, Chen et al. developed a ratiometric fluorescent bioprobe based on DNA-labelled carbon dots (DNA-CDs) and 5,7-dinitro-2-sulfo-acridone (DSA) for the detection of exosomal miRNA. The bioprobe was initially nonfluorescent due to the FRET effect between the carbon dots (CDs) and the DSA and exhibited strong fluorescence when bound to the target miRNA-21. Using the ratiometric fluorescence changes of CDs and DSA, it was possible to detect exosomal miRNA-21 [144]. Inspired by the infection mechanism of the virus, Zhang et al. developed a method for the *in situ* detection of exosomal miRNAs without any extraction procedure using virus-mimicking fusogenic vesicles (Vir-FV) (Fig. 8a). Fusogenic proteins on Vir-FVs could specifically target exosomes using the sialic-acid-containing receptors, which resulted in the efficient fusion of Vir-FVs and exosomes. The molecular beacons encapsulated in Vir-FVs specifically hybridized with the target miRNAs in the exosomes and generated a fluorescence signal. Using this approach to detect exosomal miR-21 it was possible to distinguish breast cancer patients from healthy controls, indicative of a potential diagnostic tool [145]. Lee et al. reported a fluorescence quenching-recovery-based molecular beacon sensor for the visualization of neurogenic exosomal miR-193a in cells. The fluorescent probe was constructed using a tightly bound quenched dye labelled peptide nucleic acid to the surface of graphene oxide. The subsequent recovery of the fluorescence upon addition of target miRNA was then used for miRNA sensing [146].

Based on a thermophoretic sensor in combination with nanoflares, a system for the highly sensitive *in situ* detection of exosomal miR-21 was developed, without complicated RNA extraction or target amplification [147]. A fluorescence signal was observed on DNA hybridization after transport of the incubated exosomes to the target miRNAs. With the assistance of the thermophoretic sensor for *in situ* detection of exosomal miRNAs, amplified fluorescence signals could be detected after the binding of exosomal miRNAs to nanoflares, which allowed the quantitative and direct measurement of exosomal miRNAs at as low as 0.36 fM in 0.5 μL serum samples. In addition, the selected exosomal biomarker miR-375 was also demonstrated to accurately differentiate estrogen receptor-(ER) positive breast cancer at an early stage (stages I, II) with a high accuracy (Fig. 8b) [147]. To date, a variety of fluorescent probes have been reported for the detection of exosomal surface proteins and miRNAs separately, while a combined assay of both specific biomarkers could provide disease information with high accuracy. Therefore, it is particularly important to develop an efficient method for the detection of multiple proteins and miRNAs in a single exosomal reaction. Using nano-sized molecular beacons and fluorescent dye-conjugated antibodies, exosomal miRNAs and surface proteins were simultaneously detected in captured exo-

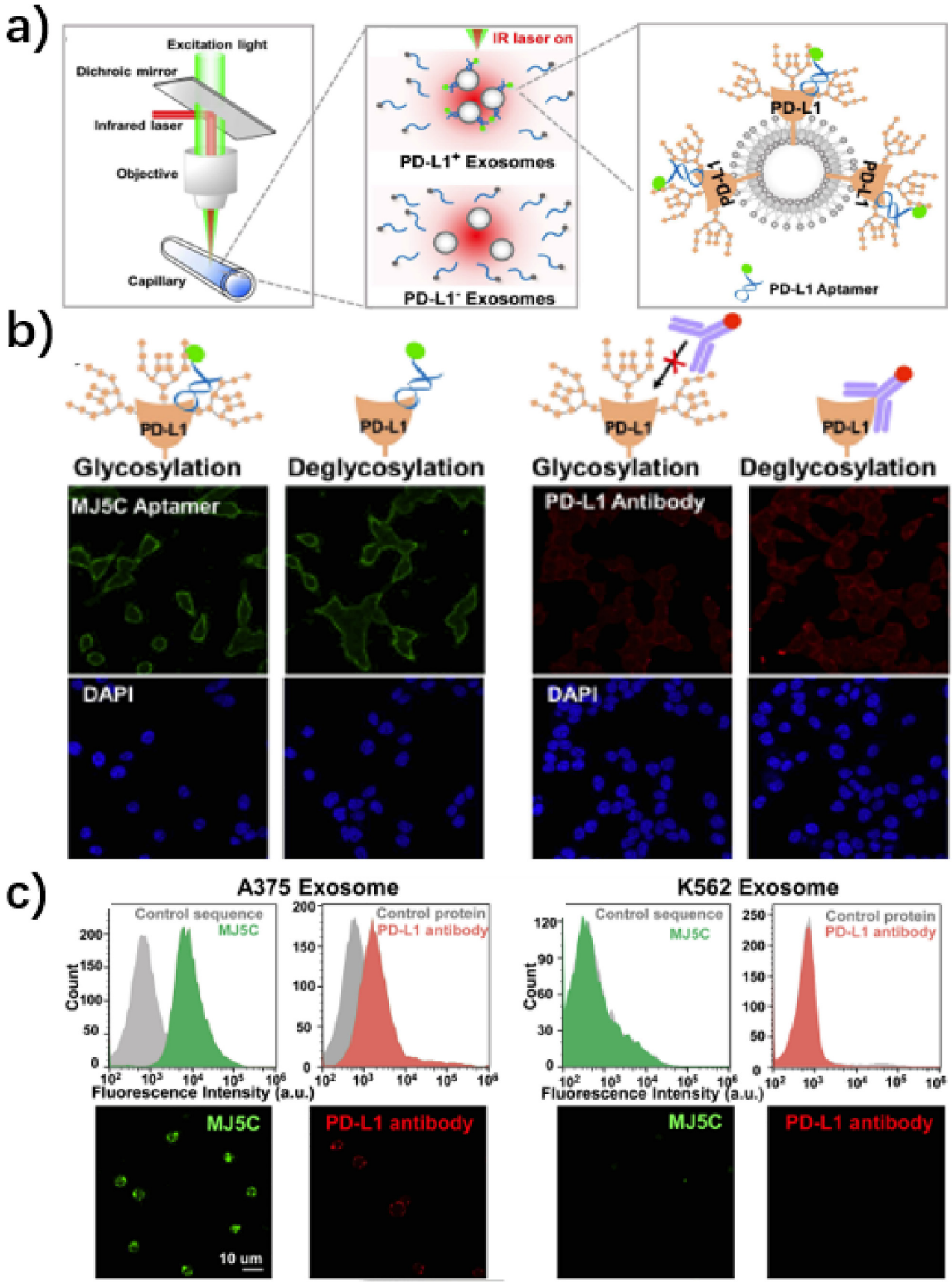

Fig. 7. a) Working mechanism of the exosomal PD-L1 quantification analysis. b) Fluorescence imaging of PD-L1 positive HCT116 cells treated with or without deglycosylation by PNGase F and stained with DAPI (blue), the MJ5C aptamer (green) or a PD-L1 antibody (red). c) Flow cytometry assay and confocal imaging of A375 Exosome and K562 Exosome, showing the binding outcome of the MJ5C aptamer and PD-L1 antibody to PD-L1 positive) and negative exosome conjugated beads, respectively. Adapted with permission from ref [133]. Copyright 2020 John Wiley and Sons.

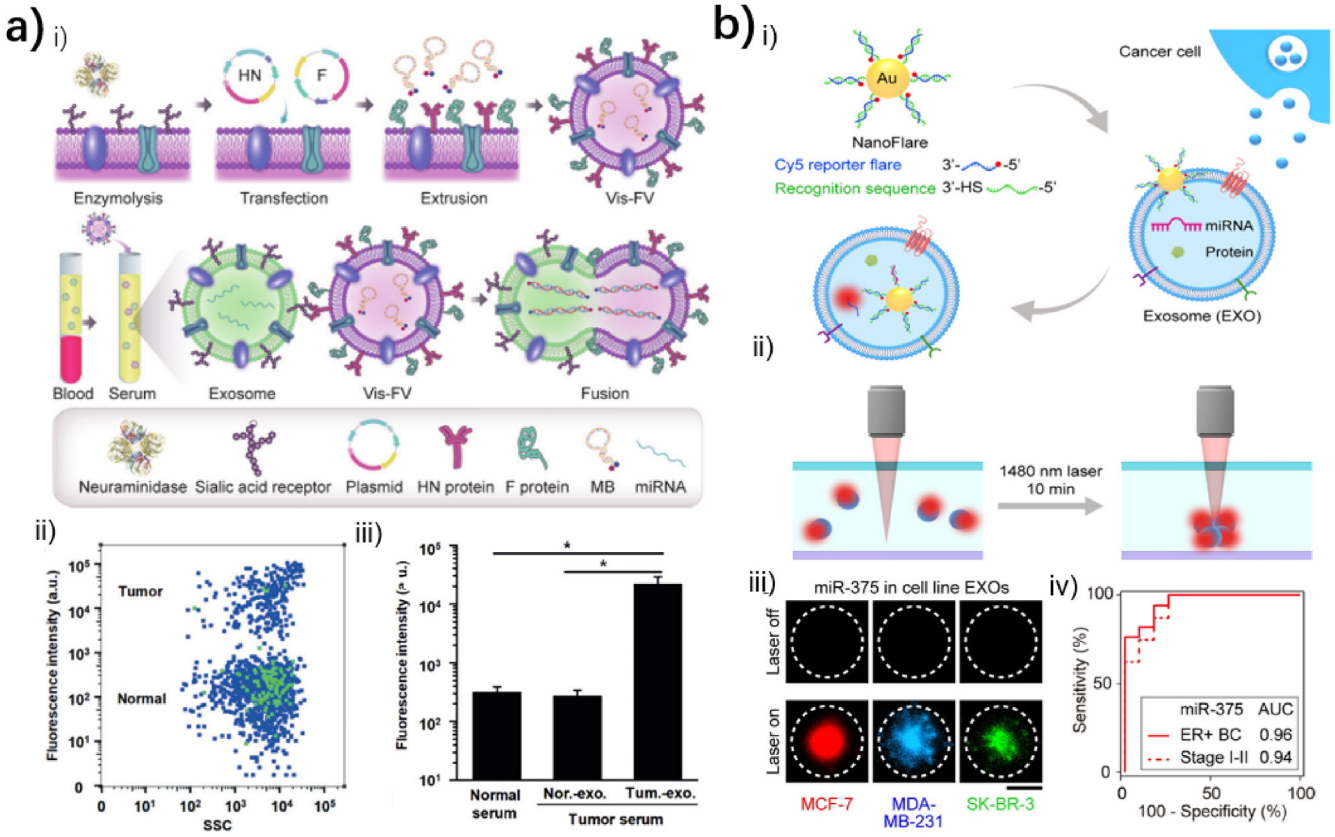

Fig. 8. a) Schematic illustration of the fusion between the Vir-FVs and exosomes induced by HN and F protein. ii) Representative bivariate dot-plots of Vir-FVs showing the difference between normal and tumour exosomes based on sensing of the tumour-associated miRNAs. iii) Fluorescence response of the fused vesicles from the serum of healthy control and cancer patients (both n = 5) after incubating with Vir-FVs. Adapted with permission from ref [145]. Copyright 2019 John Wiley and Sons. b) i) Schematic illustration of a thermophoretic sensor with nanoflares for *in situ* analysis of exosomal miRNAs. ii) Thermophoretic accumulation of nanoflare treated exosomes via localized laser heating to amplify the fluorescence response. iii) Fluorescence images of exosomes released by different breast cancer cell lines by thermophoretic sensor implemented with nanoflares. Scale bar, 50 μm. iv) Receiver operating characteristic analyses of exosomal miR-375 for differentiating ER + BC patients from HD, as well as for early detection of ER + BC (stages I, II). Adapted with permission from ref [147]. Copyright 2020 American Chemical Society.

somes with high specificity, which was shown to be an efficient liquid biopsy method for prostate cancer [148].

4.1.3. Lipid analysis

Lipids are essential molecular components of cells. The cell membrane bilayers contain a variety of lipid classes such as sphingolipids and phosphatidylcholine. Since EVs are derived from cells, they inherit the rich lipid contents from the paternal cells [149,150]. The biogenesis of EVs is related to the lipid content, however, EVs differ from the secreting cells in lipid composition. This may be caused by a process that allows for the sorting of specific lipid species into vesicles. Research has revealed that the lipid content of secreted vesicles changes after culturing tumour cells in an acidic environment, which mimics the deep core of tumours [151]. Therefore, it will become important in the future to be able to determine whether these changes reflect the changes in the type of EVs secreted, or rather in the intracellular targeting of the analysed components to these EVs [18]. Interest in the lipid composition and the function of lipids in EVs is rapidly growing as the role of lipids in vesicles is starting to become appreciated and understood [152].

For lipid detection of EVs, different kinds of approaches have been suggested to quantify the lipids in EVs, such as sulfovanilin assay, fluorescent dyes that incorporate into the membrane bilayers (e.g. dialkylcarbocyanins such as DiR), Fourier transform infrared spectroscopy or mass spectroscopy [153]. Although these methods can discriminate EVs with different protein/lipid ratio, they are not optimal for the quantification of the total amount of lipids in EVs, as their quantitative aspects are not well understood. For instance, the fluorescent dyes used to label lipid bilayers may give different signals depending on the membrane composition and lipid packing, and they may be distributed differently among cellular membranes [154]. Based on recent progress of using a Trp-BODIPY cyclic peptide to fluorescently label apoptotic vesicles [155], we expect that efficient EV lipid analysis techniques using various spectroscopic methods, imaging and other techniques will be developed over time, due to the increase in research activity towards the lipid composition of EVs.

4.2. Raman and SERS-based approaches

4.2.1. Label-free analysis of intact vesicles

Raman spectroscopy which analyzes the vibrational modes of analytes via measuring the nonelastic scattering effect upon laser irradiation has great potential in the optical analysis of EVs [156,157]. Based on the signals derived from EVs themselves, spontaneous Raman spectroscopy provides a label free and non-invasive approach to obtain the fingerprint vibrational spectra of target molecules. It enables the acquisition of the global chemical composition without employing an exogenous label and as such provides a facial method to assess EV purity and composition. In 2009 the first attempts to obtain the Raman spectrum of EVs was

reported, which provided the chemical composition of nano-sized vesicles derived from Dictyostelium cells [158]. Soon afterwards, spontaneous Raman spectroscopy was applied to the characterization, as well as the analysis of EVs for diagnosis. For example, the Raman signatures of urine derived EVs were obtained, which offered a potential development of a diagnostic tool for urinary system diseases [159]. The bulk characterization of EVs secreted by different subtypes of MSC were performed and compared. Raman spectroscopy can provide insight into the biochemical structure of EVs, and is capable of distinguishing nanovesicles of diverse origin, which facilitates the translation of EV research from the laboratory to a clinical environment [160,161]. With the understanding of EVs biofunction, disease cell derived EVs can be regarded as cancer biomarkers. For instance, a Raman optical tweezer was utilized to discriminate the EVs of prostate cancer cells from healthy donors using their different and specific signatures [162]. These studies illustrated the potential of using Raman spectroscopy to identify EVs as new biomarkers and achieve early stage diagnosis of diseases [163].

Apart from the unique characteristics of Raman spectroscopy in analysing EVs, it suffers from the limitation of weak signal intensity induced by the low Raman scattering efficiency (only one in 10^7 scattered photons). Alternatively, SERS has attracted widespread research interest for EVs analysis, owing to its ability to enhance the Raman responses of analytes by up to 10^{14}-10^{15} when in close proximity to plasmonic metallic (e.g. Au or Ag) nanostructures [157,164]. When used for analysing EVs, two main SERS strategies are used: the first one is termed label-free detection which is based on the use of plasmonic nanomaterials to obtain an enhanced Raman signal of EVs; while in the second method, uses additional specific Raman tag molecules which are bound to the EVs to generate enhanced Raman signals facilitating the indirect analysis of EVs [157]. From the initial study to obtain enhanced Raman signals of exosomes, Ag nanostructures were decorated on to a superhydrophobic surface, and the study provided useful information on the different contents of healthy and tumour cells [165]. After confirming the feasibility of label-free SERS analysis of EVs, various investigations using Ag as SERS substrate have been reported. For instance, a thin silver film-coated plasmonic nanobowl platform was fabricated to effectively capture exosomes derived from ovarian cancer cells for SERS measurement in order to provide biochemical data for both intact and ruptured exosomes (Fig. 9a) [166]. A subsequent investigation improved the specificity in capturing exosomes by utilizing an exosome specific peptide bound to Ag NPs. The targeted SERS approach resulted in the selective capture of exosomes and facilitated the recognition of specific spectra of captured exosomes [167]. In order to fabricate cost-effective SERS substrates that support point-of-care analysis, normal recordable disks (CD-R and DVD-R) were decorated with Ag and deployed in the label-free assay of exosomes [168].

In the SERS measurement of EVs, their heterogeneous nature can affect the analysis, generating different spectra and nonuniform data. Thus, the classification of heterogeneous Raman spectra by reading the specific assignments is tough. Instead of using the conventional method, principal component analysis (PCA) was used to analyse the whole SERS spectra of EVs, evaluating the common patterns of EVs from the same origin. Using a statistical pattern analysis, lung cancer cell secreted exosomes were clearly discriminated from normal cell originating exosomes with high sensitivity and specificity after the exosomes were deposited on to a substrate with gold NPs (Au NPs) (Fig. 9b) [169]. The combination of SERS and PCA was also used to demonstrate the correlation of non-small cell lung cancer (NSCLC) cell-derived exosomes with potential protein markers for cancer diagnosis. Typically, Choi et al. showed that the Raman patterns for cancerous exosomes were extracted by PCA and unique peaks were clarified through quantitative analysis of ratiometric mixtures of cancerous and normal exosomes. The Raman spectra of exosomal protein markers (CD9, CD81, EpCAM, and EGFR), displayed unique peaks that correlated well with dominant cancer markers verified by the highest similarity of the Raman band (Fig. 9c) [170]. In a recent study, the same group demonstrated an early-stage liquid biopsy of lung cancer by deep learning-integrated label-free SERS analysis of exosomes (Fig. 9d). The deep learning model was taught using the SERS signals of exosomes derived from normal and lung cancer cell lines resulting in a classification accuracy of 95%. In a group of 43 patients who displayed stage I and II cancer, 90.7% of patients using the deep learning model had higher similarity to lung cancer cell exosomes than for the healthy control [171]. Furthermore, principal component discriminant function analysis (PC-DFA) was used in combination with SERS to identify tumour-specific spectral signatures, which could be used to distinguish exosomes derived from pancreatic cancer or normal pancreatic epithelial cell lines with 90% accuracy. Using a cell line trained PC-DFA algorithm, the SERS spectra of exosomes isolated from pancreatic cancer patient serum samples were analysed and the exosome spectral signatures could be used for diagnosis [172]. Thus, label-free analysis of exosomes by Raman spectroscopy and SERS, in conjunction with advanced data processing algorithms have resulted in advantages for the discrimination of cancerous EVs from normal ones, which will contribute to the real-time early diagnosis of cancer.

4.2.2. SERS tag analysis

Recently, another methodology based on an indirect SERS approach has developed rapidly [173]. SERS tags are composed of noble metallic NPs decorated with specific Raman reporter molecules, such as fluorescent dyes (e.g. nile blue, R6G) or aromatic thiols/disulfides, which can generate amplified Raman signals [174,175] Then, by conjugating specific recognition units, mainly EV surface antibodies or aptamers, the SERS tags can be used to capture EVs and facilitate their indirect detection [157].

Many SERS tags have been reported to detect tumour derived EV providing the potential to develop sensitive liquid biopsy methods for cancer diagnosis. A SERS tag-based immunoassay has been reported to detect tumour-derived exosomes using magnetic nanobeads and SERS nanoprobes. The SERS nanoprobes are gold core–silver shell nanorods (Au@Ag NRs) coated with Raman reporter molecules and exosome-specific antibodies (anti-CD63 antibody). The fabrication of a magnetic nanobead requires the coating of Fe_3O_4 NPs with a silica shell and then conjugated with specific antibodies (anti-HER2). In the presence of target exosomes, the SERS nanoprobes and magnetic nanobeads can capture the exosomes through the formation of a sandwich-type immunocomplex, which can be precipitated using a magnet. Using this method, the SERS tag-labelled detection method for tumour-secreted exosomes was demonstrated [176]. An integrated capture and analysis system was developed using Fe_3O_4@TiO_2 NPs to enrich exosomes and anti-PD-L1 antibody modified Au@Ag@MBA SERS tags were added to tag the exosomal PD-L1 for quantification. This system could capture and analyse exosomes within 40 min with a detection limit of 1 PD-L1$^+$ exosome/μL. Using the personalized SERS signal analysis of NSCLC patients using a 4 μL clinical serum sample, was readily achieved [177].

In addition to bulk analysis, the SERS-tag immunoassay can be performed on miniaturized devices. For example, a small Au array device with 2-mm wells and printed antibodies was fabricated to capture exosomes (Fig. 10a). The detection of target proteins was achieved by using gold nanorods labelled with Raman reporter QSY21 as SERS tags, which displayed a LOD of 2000 exosomes/L. A complete analysis of different surface proteins indicated that exosomes derived from various breast cancer cells provided distinct

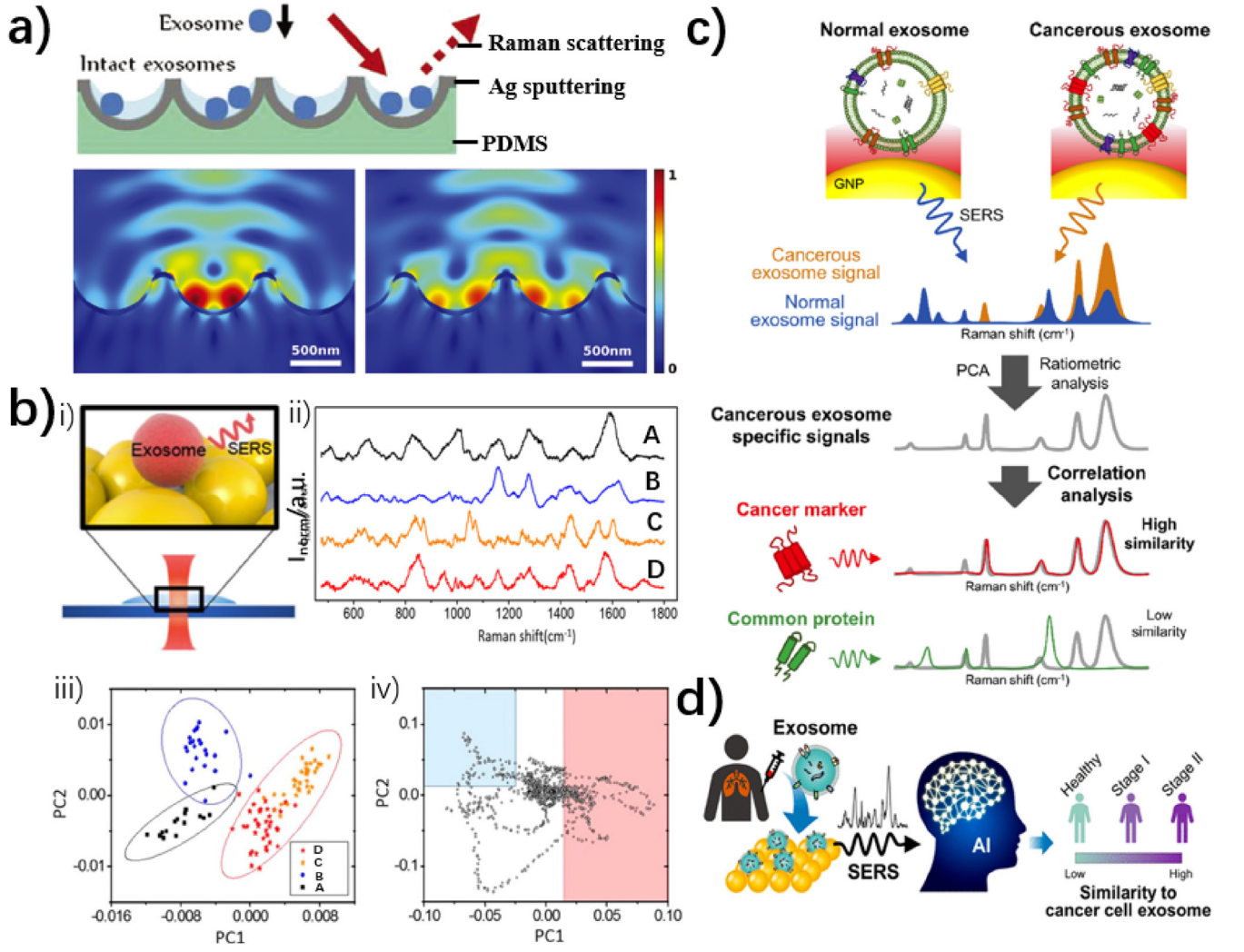

Fig. 9. a) Schematic diagram of the detection of exosomes using the nano bowl substrate and simulation of the electric field at different laser beam position. This simulation indicates that exosomes trapped inside the bowls are surrounded by uniform "hot-spots". Adapted with permission from ref [166]. Copyright 2015 The Royal Society of Chemistry. b) i) Schematic illustration of the detection of exosomes by SERS. ii) The SERS spectra obtained for cancer cell-derived exosomes (line B, Alveolar; line C, H522; line D, H1299) and normal controls (line A). iii) Principal component scatter plot with coloured clusters of control (A, black square), alveolar (B, blue circle), H522 (C, orange star), and H1299 (D, red star) derived exosomes, respectively. iv) Principal components of PCA result in panel iii). The red area shows the Raman shifts related to NSCLC-secreted exosomes, and the blue area suggests the Raman shifts associated with the alveolar cell secreted exosomes. Adapted with permission from ref [169]. Copyright 2017 American Chemical Society. c) Schematic of the Raman scattering profiles of lung cancer cell-derived exosomes and comparison to the profiles of their potential surface protein markers. Adapted with permission from ref [170]. Copyright 2018 American Chemical Society. d) Schematic illustration of the label-free SERS analysis of exosomes and the deep learning model for early diagnosis of cancer patients. Adapted with permission from ref [171]. Copyright 2020 American Chemical Society.

protein profiles compared to normal cells. Furthermore, exosomes extracted from the plasma of HER2-positive breast cancer patients exhibited high levels of specific surface proteins on exosomes e.g. HER2 and EpCAM, indicating the diagnostic application of these markers for breast cancer [178]. In another study, a polydopamine-modified immunocapture substrates and an ultra-thin polydopamine-encapsulated antibody-reporter-Ag(shell)–Au(core) multilayer (PEARL) SERS nano-tag was fabricated to enable the formation of a "chip-exosome-SERS tag" sandwich structure for the detection of pancreatic cancer-derived exosomes (Fig. 10b). In this assay, antibodies against various target surface proteins of exosomes were individually encapsulated into the SERS tag. With a typical spectral signal of the Raman reporter molecule, the quantitative analysis of exosomes was achieved with high sensitivity. Moreover, by applying the migration inhibitory factor (MIF) antibody-based SERS tag in a clinical serum sample, pancreatic cancer patients could be rapidly distinguished from healthy controls. In addition, metastasized tumours were discriminated from metastasis-free tumours with high sensitivity, apart from the different stages of tumour node metastasis (a discriminatory sensitivity of over 95% of P1-2 stages from the P3 stage). Thus, PEARL SERS immunoassays offer a potential means for the classification, early diagnosis, and metastasis monitoring of pancreatic cancer [179].

Numerous studies have proved the essential roles of miRNA in tumour progression, indicating the potential of using miRNAs as reliable cancer biomarkers [180]. MiRNAs in exosomes (exosomal miRNAs) are highly stabile in body fluids due to the protection of the exosomal lipid bilayer structure, and as such have been regarded as an excellent source of biomarkers for the early stage diagnosis and prognosis of cancer [181]. The previously reported SERS biosensors for targeting miRNA can be categorized into two main kinds: one is based on a SERS sandwich hybridization assay, which used Au/Ag nanostructures as SERS nanoprobes functionalized with probe nucleic acid in order to recognize target miRNA [182]; the other one was based on a SERS nanoprobe and duplex-specific nuclease (DSN) signal amplification strategy [183]. In the

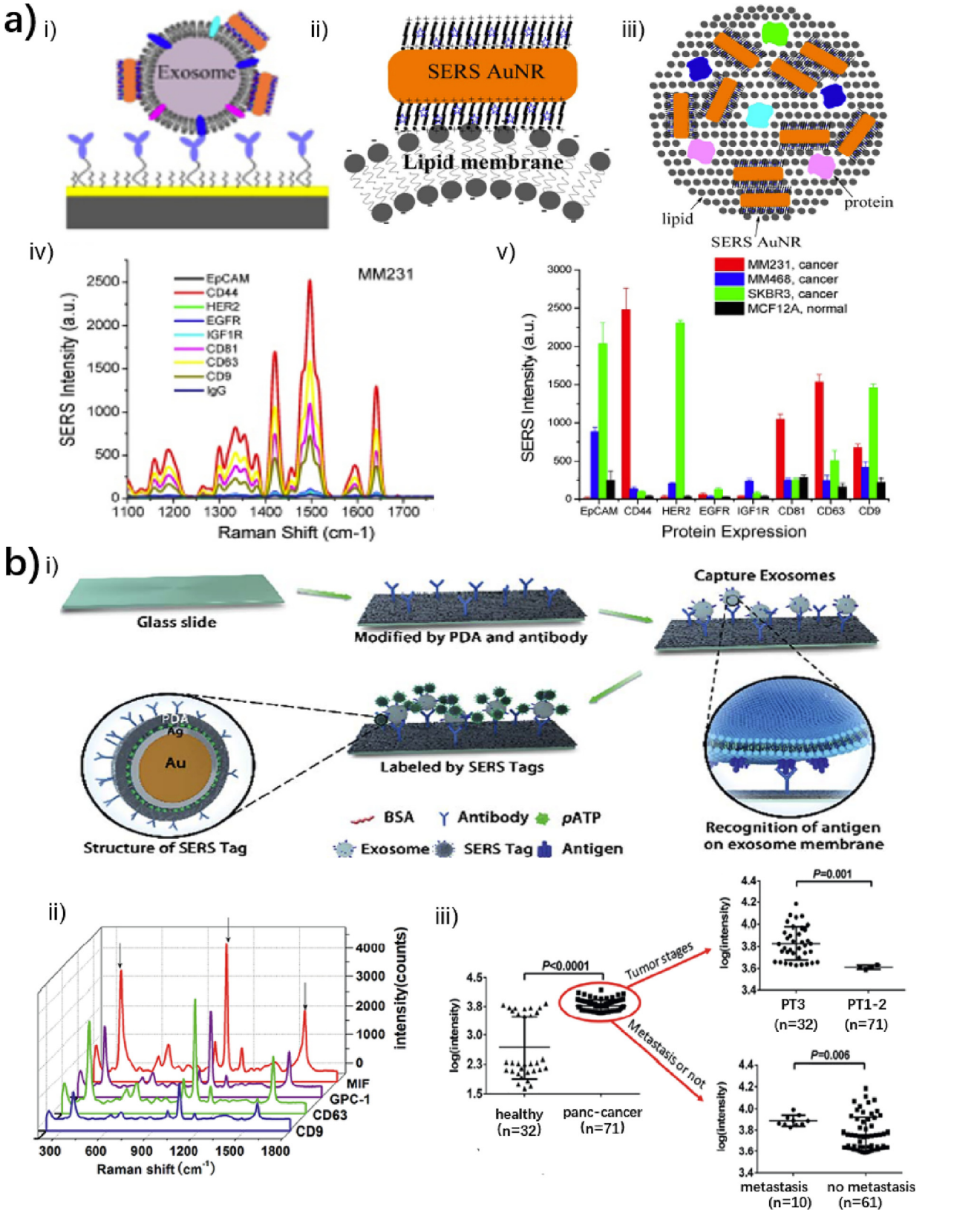

Fig. 10. a) i) Schematic overview of the Raman exosome assay. ii) and iii) are the side and top views of the interactions between exosome lipid membrane and SERS AuNR, respectively. iv) Protein profiling of exosomes derived from breast cancer cells MM231. Average SERS spectra (n = 3) of exosomes targeting different surface proteins, using IgG as the control. v) Comparison of protein profiles on normal and cancer cells. Data are shown as the mean intensity of the 1497 cm^{-1} peak with standard deviation (n = 3). Adapted with permission from ref [178]. Copyright 2018 Ivyspring International Publisher. b) i) A schematic overview of the PDA chip and PEARL SERS tag-based exosome sensors. ii) SERS spectra of the anti-CD9, CD63, MIF and GPC1 groups for PANC-01-secreted exosomes. iii) Shapiro–Wilk analysis plots of the SERS outcome of serum samples of pancreatic cancer patients (n = 71) and healthy controls (n = 32) using the anti-MIF platform. The ordinate represents log values of Raman intensity. Adapted with permission from ref [179]. Copyright 2018 The Royal Chemical Society.

former case, a uniform plasmonic gold nanopillar substrate was fabricated for the specific and ultrasensitive determination of exosomal miRNAs, using a sandwich hybridization strategy between the miRNAs and two short locked nucleic acid (LNA) probes (Fig. 11a) [184]. Upon exposure to analyte solution and air drying, the plasmonic gold nanopillars tilt towards each other due to capillary force creating numerous hotspots inside the substrate, thereby achieving the detection of target miRNAs which were hybridized to specific LNA probes with single-nucleotide specificity. The proposed SERS sensor displayed wide dynamic range (1 aM to 100 nM), ultralow detection limit, multiplex sensing capability and favourable miRNA recovery in serum. In addition, this sensor allowed for the reliable observation of exosomal miRNA expression patterns from breast cancer cell lines, and in addition the discrimination of various cancer subtypes, which proved their utility for cancer diagnosis by measuring exosomal miRNAs in body fluids [184]. In the latter case of miRNA SERS probe, magnetic concentration was often applied to effectively enhance the signals generated by target miRNA. Due to the low abundance of miRNA, DSN which could preferentially cleave DNA in DNA/RNA heteroduplexes while being inactive toward single-stranded DNA or single-stranded RNA was used to achieve high sensitivity and signal amplification [181]. For instance, a SERS tag was constructed, which was composed of a signal reporter element Au@R6G@AgAu NPs (ARANPs), a recognition element (DNA capture probe targeting exosomal miRNA, CP), a separation element (silica microbead, SiMB) and a DSN to assist signal amplification. Upon binding of target miRNA, DNA in heteroduplexes can be specifically cleaved by DSN resulting in the release of ARANPs from the surface of the SiMB. However, the target miRNA remained intact and was then involved in the next round of target-recycling and amplification. Detection limits of 5 fM. were achieved by the combination of a stable SERS intensity and signal amplification. The system was used for detecting exosomal miRNAs from cancer patients and demonstrated the point-of-care evaluation potential for clinical analysis [181]. Another DSN-assisted dual-SERS biosensor based on a Fe_3O_4@Ag-DNA-Au@Ag@DTNB (SERS tag) conjugates was developed and applied for detecting exosomal miRNA-10b using a SERS quenching strategy (Fig. 11b). Fe_3O_4@Ag-DNA-SERS tags core-satellite assemblies can result in intense Raman signals using a dual-SERS enhancement by the combination of Au@Ag of the SERS tag and Ag shell of Fe_3O_4@Ag and particularly after magnetic concentration. In the presence of a target miRNA, it can hybridize with the complementary DNA probes. The incubation with DSN enzyme induces the selective cleavage of DNA from DNA/miRNA duplexes, therefore the SERS tag is separated from the Fe_3O_4@Ag substrate and triggers the SERS signal quenching. The liberated miRNA can then bind with additional DNA. With the proposed SERS tag, single-base recognition with a detection limit of 1 aM can be achieved in one step. Significantly, target microRNA in plasma-derived exosome and residual supernatant plasma of blood samples from pancreatic ductal adenocarcinoma (PDAC) could be directly quantified using the method, (Fig. 11b) [185].

4.3. SPR technique

In addition to the widely applied fluorescence and SERS approaches, surface plasmon resonance (SPR) approaches have been extensively investigated. SPR real-time sensing and label-free, technique which detects molecular interactions taking place close to certain metals (e.g. Au/Ag) surfaces by monitoring the changes in refractive index caused by molecules interacting with the surface [186]. Utilizing SPR in combination with antibody microarrays specific to exosomal membrane proteins, exosomes can be quantitatively detected for potential diagnosis applications [187]. The size of exosomes perfectly accommodates the surface plasmon wave depth, which allows the detection of multiple exosome subpopulations directly from blood. For instance, taking advantage of an antibody array on Au substrate, exosomes derived from neurons and oligodendrocytes were isolated and detected with high sensitivity. Furthermore, by applying a second antibody, the membrane components of exosomes on each subpopulation can be quantified by the SPR signal (Fig. 12a), which facilitates the determination of the abundance of exosomes from different cellular origin [188]. Instead of antibody, a sensitive SPR aptasensor has been developed for the detection of exosomes with dual AuNP-assisted signal amplification. The dual NP amplification was based on the controlled hybridization of AuNPs to the aptamer linked AuNPs, which were attached to the surface of the EVs stabilized on the Au film. The electronic coupling in these plasmonic nanostructures, as well as the coupling effects between the Au film and AuNPs greatly enhanced the observed SPR signal. This SPR aptasensor provided a low LOD of 5×10^3 exosomes/mL and could differentiate the exosomes derived from breast cancer cells from normal breast cells [189].

To facilitate label-free and high-throughput detection of tumour-derived exosomes without pre-treatment, Lee et al. developed a nano-plasmonic exosome (nPLEX) sensor equipped with periodic Au nanohole arrays on a microfluidic chip to achieve sensitive exosome protein analyses using SPR assay [190]. The system was based on optical transmission through periodic nanoholes rather than total internal reflection. Improved detection sensitivity was achieved since the depth of probing (<200 nm) matched the size of the exosome. In the microchip, each Au nanoarray was functionalized with antibodies to enable profiling of exosomal proteins on the surface and in lysates. This approach not only offered improved sensitivity over earlier methods, but also enabled improved portability when combined with miniaturized optics. Using nPLEX to analyse ascites samples from ovarian cancer patients, it was shown that exosomes from ovarian cancer cells can be detected by their expression of CD24 and EpCAM, indicating the potential for disease diagnostics using exosomes [190]. Apart from Au/Ag, titanium nitride (TiN) is an alternative plasmonic support material, which exhibited tuneable plasmonic properties in the visible and near-infrared region. A biotinylated antibody-functionalized TiN (BAF-TiN) based biosensor was developed for the quantitative detection of exosomes isolated from human glioma cell line through the binding of exosomal surface proteins. This biosensor exhibited good biocompatibility, high stability and favourable label-free sensing of exosomes [191].

4.4. Electrochemical techniques

Electrochemical sensing is regarded as an effective technique that has great applicability in clinical settings due to fast response times and high sensitivity via signal amplification with redox-active reporters. Combined with magnetic beads, an integrated magneto-electrochemical compact sensor device (iMEX) was developed. EVs were captured by magnetic beads from plasma of a patient, then labelled with HPR enzyme and then detected using an electrochemical readout (Fig. 12b). The device consists of eight channels which permitted parallel and high-throughput measurements, resulting in a high sensitivity of $< 10^5$ vesicles from 10 μL samples within 1 h. In addition, this miniaturized portable sensor device exhibited excellent clinical potential through the analysis of EVs of ovarian cancer patients [192]. Based on similar capture, labelling and detection methods, an EV-based diagnostic platform (integrated kidney exosome assay, iKEA) was developed for the non-invasive urine-based analysis to evaluate kidney transplant rejection [196].

In addition, electrochemical aptamer-based exosome assays have been developed, to take advantage of aptamers in bioassays [197]. Exposed CD63 proteins on the surface of exosomes could

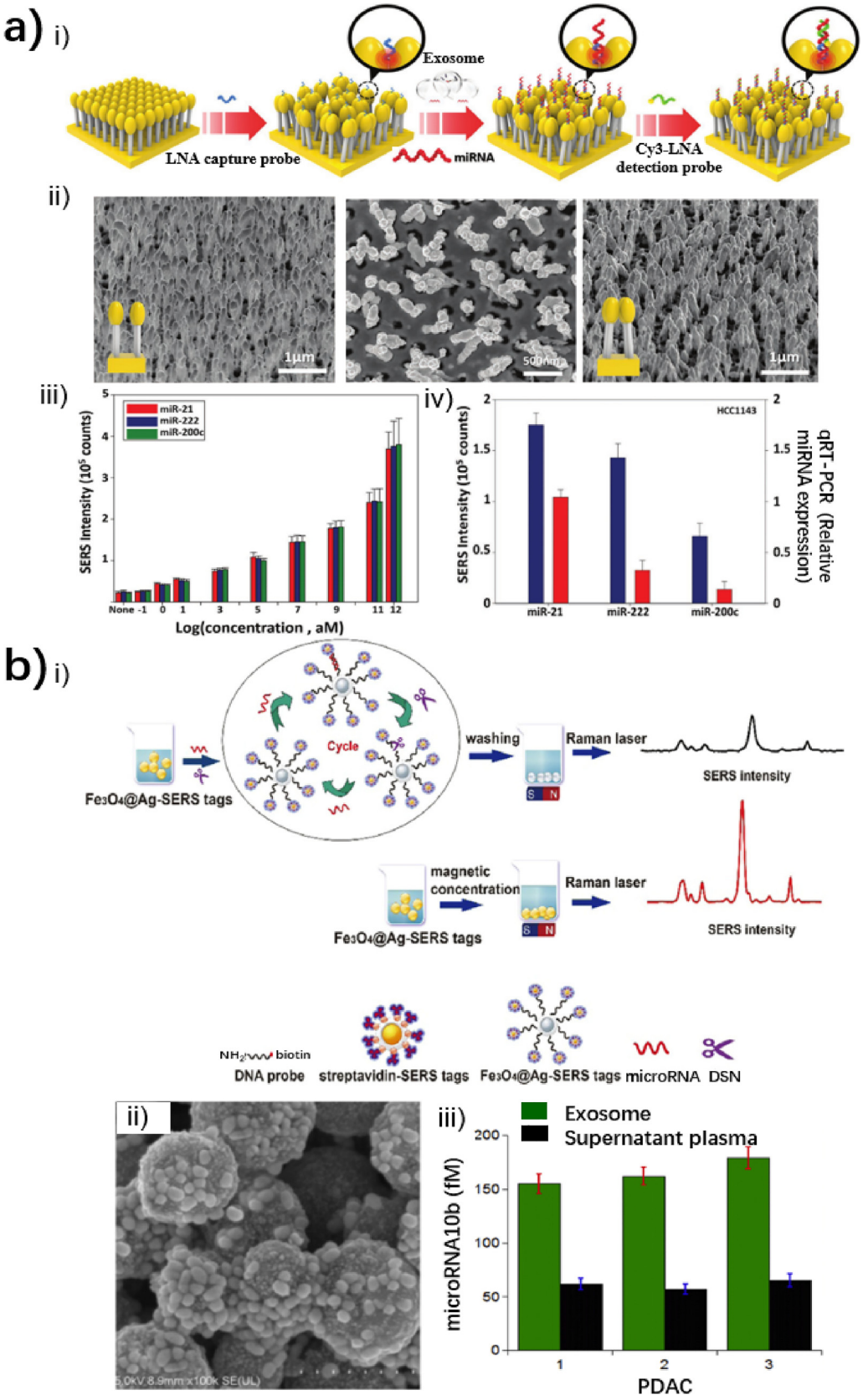

Fig. 11. a) i) Schematic overview of exosomal miRNA detection using a SERS sensor. ii) From left to right, SEM images indicating upright plasmonic gold nanopillar SERS substrates, the top and side view of the plasmonic head-flocked gold nanopillar SERS substrates after solvent evaporation. iii) Cy3 intensity at 1150 cm^{-1} was plotted against the concentration of target miRNAs to show the sensitivity of the SERS sensor for detecting target miRNAs. iv) Levels of target exosomal miRNAs were detected by the SERS sensor (blue bars) and qRT-PCR (red bars) in breast cancer cells. Adapted with permission from ref [184]. Copyright 2019 John Wiley and Sons. b) i) Schematic illustration of DSN-assisted SERS detection of microRNA. ii) SEM image of Fe3O4@Ag-SERS tags core-satellite assemblies. (iii) Determination of microRNA-10b concentration in exosome and residual supernatant plasma from three patients with PDAC. Adapted with permission from ref [185]. Copyright 2019 Elsevier.

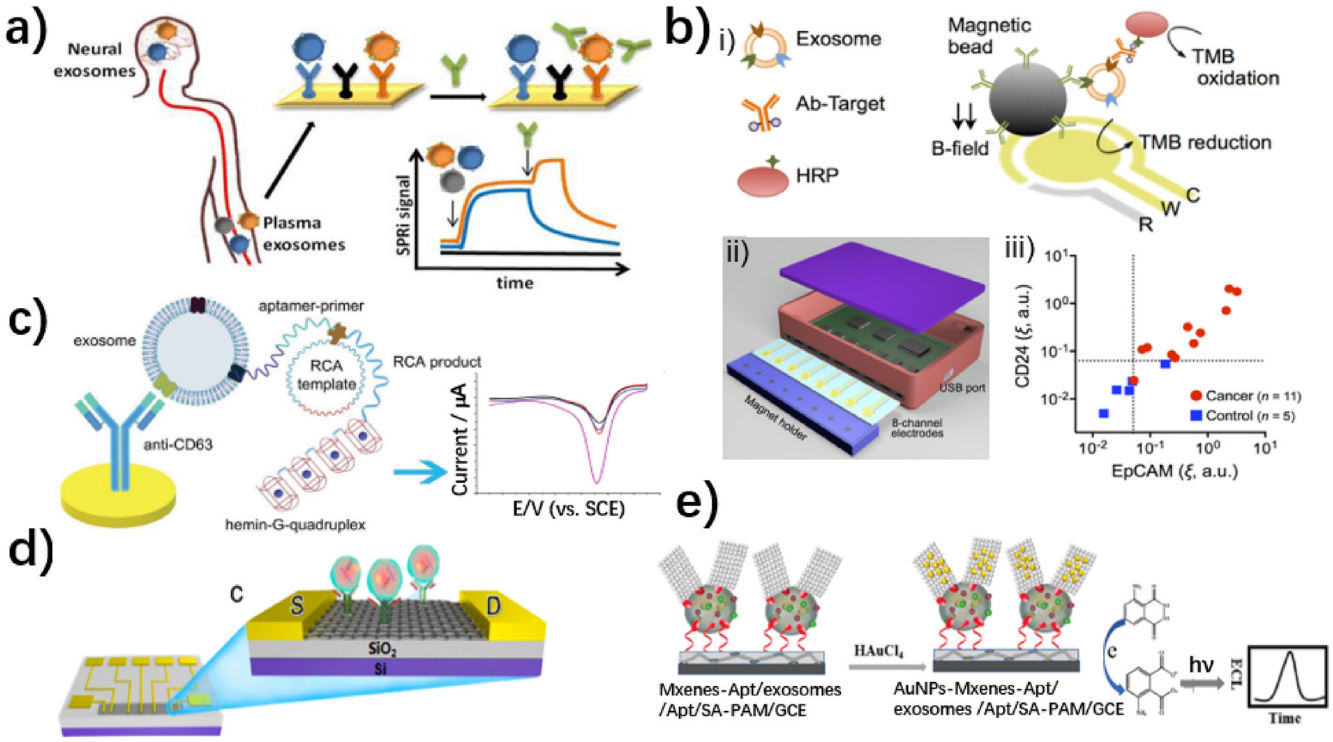

Fig. 12. a) Schematic illustration of detection of various brain-derived subpopulations of plasma exosomes by SPR imaging Adapted with permission from ref [188]. Copyright 2018 American Chemical Society. b) i) Schematic overview of iMEX assay. Exosomes are captured on magnetic beads directly in plasma and labelled with HRP enzyme for electrochemical detection. The magnetic beads are coated with antibodies against CD63, an enriched surface marker in exosomes. The working (W) and the counter (C) electrodes are made of gold (Au), and the reference electrode (R) is made of silver/silver chloride (Ag/AgCl). HRP, horseradish peroxidase; TMB, 3, 3′, 5, 5′-tetramethylbenzidine. ii) Sensor schematic. The sensor can simultaneously measure signals from eight electrodes. Small cylindrical magnets are located below the electrodes to concentrate immunomagnetically captured exosomes. iii) Plasma samples from ovarian cancer patients (n = 11) and healthy controls (n = 5) were analysed by the iMEX assay. The levels of EpCAM and CD24 were much higher in cancer patients. The expression levels of EpCAM and CD24 (ξEpCAM vs ξCD24) were highly correlated (R^2 = 0.870). Adapted with permission from ref [192]. Copyright 2016 American Chemical Society. c) Illustration of the label-free electrochemical aptasensor for highly sensitive detection of exosomes. Adapted with permission from ref [193]. Copyright 2019 John Wiley and Sons. d) Reduced graphene oxide (RGO) FET biosensor. After anti-CD63 functionalization in the sensing region, exosomes can be directly bound to the CD63 antibody functionalized RGO FET biosensor for electrical and label-free detection. Adapted with permission from ref [194]. Copyright 2019 American Chemical Society. e) Principle of the electrogenerated chemiluminescence (ECL) biosensor for exosomes detection based on *in situ* formation of AuNPs decorated Ti_3C_2 MXenes nanoprobes. Adapted with permission from ref [195]. Copyright 2020 American Chemical Society.

be caught by a CD63 aptamer functionalized substrate, e.g. electrode or immunomagnetic beads. Subsequently, different signal amplification strategies can be used to promote measurement e.g. reduction of H_2O_2 to generate an electrochemical signal [90]. For instance, Li et al reported a label free aptasensor to detect gastric cancer derived exosomes by combining a hemin/G-quadruplex system and rolling circle amplification. Firstly, gastric exosome specific aptamer was attached to a primer sequence that is complementary to a G-quadruplex circular template. Then, target exosomes were captured by anti-CD 63 antibodies modified on a gold electrode, which could trigger rolling circle amplification and produce multiple G-quadruplex units (Fig. 12c). This horseradish peroxidase mimicking DNAzyme could generate electrochemical signals by catalysing the reduction of H_2O_2 [193]. In another example, an electrochemical aptasensor has been developed for the ultrasensitive detection of tumour exosomes based on click chemistry and the DNA hybridization chain reaction for signal amplification. Alkynyl-4-ONE was used to modify exosomes, followed by conjugation with an azide-labelled DNA probe using a copper (I)-catalysed click reaction. Using the addition of auxiliary DNA, long self-assembled DNA concatemers were fashioned by hybridization chain reaction for signal amplification. Reduction of H_2O_2 by horseradish peroxidase could generate a current, which was used to quantify the exosomes [198]. In a catalytic molecular machine-driven biosensing method, target exosomes were enriched on anti-CD63-functionalized immunobeads and subsequently recognized by a DNA chain, which initiated a catalytic molecular machine that relied on cascade toehold-mediated strand displacement reaction (CTSDR). Afterwards, amplified electrochemical signals was generated and could be recorded for quantitative sensing of exosomes [199].

4.5. Other methods

In addition to widely deployed fluorescence, SERS, SPR and electrochemistry-based assay techniques, other approaches such as field effect transistor (FET) [194], colorimetric sensing [200], upconversion luminescence resonance energy transfer (LRET)-based sensing [201], MS-based sensing, giant magnetoresistance (GMR) biosensors [202] and electrogenerated chemiluminenscence biosensors [195] have been developed to detect EVs. FET based biosensors are regarded as promising label-free sensing tools for various biomolecules. After interaction between biomolecules and the sensing surface, microelectrical signals are generated, amplified and detected. A reduced graphene oxide (RGO) FET biosensor modified with CD63 in the sensing area was fabricated and used for the label-free quantification of exosomes (Fig. 12d). This method exhibited a LOD down to 33 particles/μL and the capability of differentiating exosomes derived from serum samples of healthy control and prostate cancer patients [194]. A paper supported aptasensor using LRET from upconversion NPs (UCNPs) to gold nanorods (Au NRs) was established for the detection of exosomes. In the presence of exosomes, the two parts of the aptamer can combine with the CD63 protein on the surface of the exosomes

and therefore reduce the distance between UCNPs and Au NRs, facilitating LRET and promoting luminescence quenching. The quenching of the luminescence of the UCNPs was linearly correlated to the concentration of exosomes and enabled detection and quantification, with a LOD of 1.1×10^3 particles/μL [201]. By analysing exosomal proteins using matrix-assisted laser desorption/ionization combined with Fourier-transform ion cyclotron resonance mass spectrometry, platelet factor 4 protein was found to be a new exosomal biomarker in the serum of patients with different liver diseases [203]. Magnetic responsive probes based on 2D MoS_2–Fe_3O_4 nanostructures were used to build an ultrasensitive giant magnetoresistance biosensor for exosome detection. When modified with an aptamer, the 2D magnetic hybrid nanostructures enable both multidentate targeting and multi-magnetic particle-based signal amplification, increasing the magnetic sensor performance, and thus affording high selectivity and excellent reproducibility with a detection limit of 100 exosomes per μL [202]. In a recent study, an ultrasensitive electrogenerated chemiluminescence (ECL) biosensor was reported for the detection of exosomes. The ECL biosensor was developed by *in situ* decoration of AuNPs on aptamer modified MXenes (AuNPs-MXenes-Apt) (Fig. 12e). Due to the large surface area of MXenes, this hybrid biosensor presented efficient recognition of exosomes and high ECL signal, resulting in high selectivity toward exosomes from different kinds of tumour cell lines, as well as human serum specimens [195].

5. Single EV analysis

5.1. Exosome heterogeneity

Increasing evidence has indicated that EVs are heterogeneous in origin, size, and molecular constituents. This intrinsic heterogeneity affects their *in vivo* function, and as such has attracted significant attention [22]. Currently available methods focus mainly on the bulk analysis of vesicles, which is not suitable for understanding the exosome-to-exosome phenotypic heterogeneity and their accurate quantification. Therefore, powerful single EV analysis technologies are required to understand the various EV types and subpopulations, as well as providing information on the heterogeneity of biomarker expression [204]. In this section we will review recent progress for the evaluation of single EVs, with the aim of unravelling the biogenesis, molecular composition, diversity, and future applications of EVs, including fluorescence-based flow cytometry, fluorescence imaging, Raman spectroscopy etc.

5.2. Fluorescence-based analysis

5.2.1. Flow cytometric analysis

Flow cytometry is a technique able to simultaneously quantify and qualify huge numbers of small vesicles. However, conventional flow cytometry cannot be employed to detect vesicles with sizes smaller than 300 nm, and the lack of reference materials hinders the validation of EV analysis protocols. Fortunately, high-resolution flow cytometry uses the bright fluorescent labelling of cell-derived vesicles and flow cytometric analysis of these vesicles, facilitates fluorescence-based detection of single nanosized particles with standardized quantification and multiparameter characterization. This method can be used in nanobiology to investigate the basic aspects of cell-derived vesicles. While many potential clinical applications exist including a comprehensive analysis of vesicle-based biomarkers in body fluids and quality control analysis of vesicles for use as therapeutic agents [205]. This technology has been used to detect the specific proteins on individual vesicles and resulted in the phenotyping of individual exosomes and identification of exosome subsets produced by dendritic cells undergoing different modes of activation [206].

Combined with imaging techniques, imaging flow cytometry (IFCM) is a multiparametric technique that enables visualization and direct quantification of images obtained. The method has been reported to sensitively detect blood-derived particles/vesicles with diameters above 200 nm, however, its potential for the detection of single EVs needs to be further explored. Using fluorescently labelled EVs (e.g. CD63eGFP EVs) as a biological reference material, the IFCM acquisition and analysis parameters could be optimized for the detection of single EVs [207]. In a detailed analysis, EVs are stained with a robust immunofluorescence protocol, and the unbound excessive antibodies are removed before IFCM analysis. The suitability of commercially available fluorophore-conjugated antibodies for single EVs detection has been validated using correlative light- and electronmicroscopy (CLEM). IFCM was used to analyse the tetraspanin (CD9, CD63, CD81) proteins on EVs from human and murine cell cultures as well as plasma samples. The results indicated that this technique could permit the detection and precise quantification of EV subpopulations secreted from malignant gliomas as well as other cancer types, suggesting a robust technique for future characterization and isolation of tumour specific EV populations, which are highly desired for clinically relevant applications [208]. Nano-flow cytometry provides high resolution below 100 nm, through a combined implementation of fluorescence triggering, narrow laser beam, sensitive detectors, and instrumental configuration. Therefore, it has been used to quantify the heterogeneous distribution of EV cargo across the entire secretome of cancer cells. In combination with structured illumination (SIM) and AFM, the architecture of EV populations can be reconstructed and the changes under the conditions of malignant transformation and targeted therapy-induced stress can be uncovered (Fig. 13a) [209].

5.2.2. Fluorescence imaging-based analysis

To achieve the *in situ* analysis of the contents of nanosized exosomes in clinical samples, recent progresses in fluorescent imaging e.g. fluorescence super-resolution microscopy, total internal reflection fluorescence (TIRF) microscopy has made these technologies suitable for observing single NPs, e.g. exosomes. The TIRF assay allows imaging of single NPs via monitoring the fluorescence of particles excited by total internal reflection and quantifying them using the fluorescence intensity [213]. Therefore, a TIRF-based single-vesicle imaging platform was applied for the *in situ* analysis of single exosomes. DNAzyme-based fluorescent probes were constructed due to their capability for signal amplification and flexibility in structure design. After penetrating exosomes, DNAzyme probes could specifically bind with target miRNAs and be detected by TIRF microscopy. With a penetration depth of about 100–300 nm, TIRF imaging assay could realize the direct quantification of exosomal miRNAs in serum samples. Therefore, it was possible to quantify the target miRNA content of whole exosomes at the single-vesicle level with a high signal-to-noise ratio and yield the precise stoichiometry of miRNAs and exosomes [214]. Most fluorescence microscopic strategies are greatly limited by the imaging channels due to the broad excitation and emission spectra of fluorophores. To tackle this problem, DNA points accumulation for imaging in nanoscale topography (DNA-PAINT) provides a facile approach to achieve successive detection of multiple targets through the transient interaction between two complementary DNA strands. The continuous fluorescence on and off in the focus plane induced by the binding events of DNA strands can be

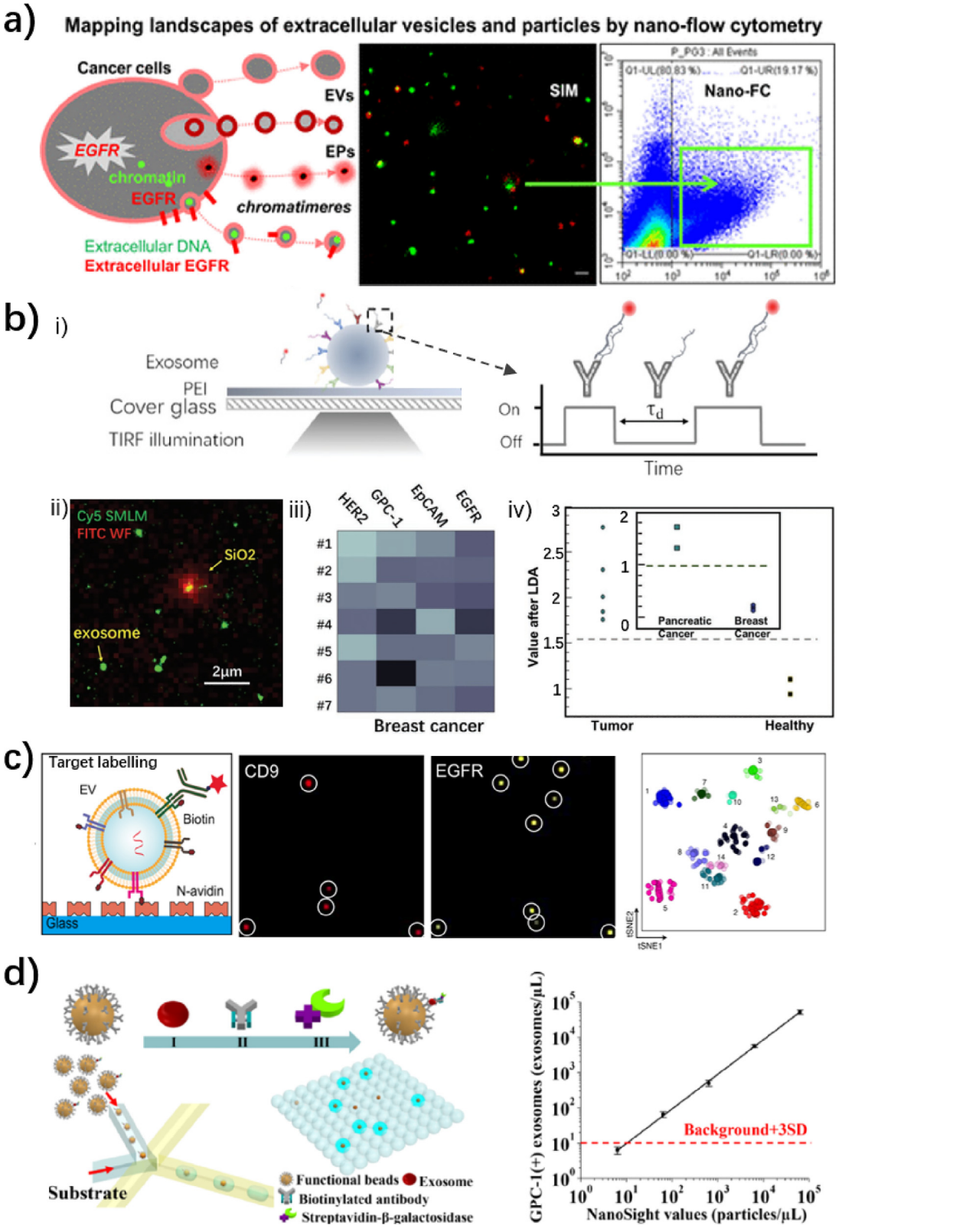

Fig. 13. a) Schematic illustration of mapping subpopulations of cancer cell-derived EVs and particles by nano-flow cytometry. Adapted with permission from ref [209]. Copyright 2019 American Chemical Society. b) i) Exosomes were immobilized on a chamber slide under TIRF illumination during imaging. (Right) The principle of qPAINT-based analysis for profiling surface biomarkers of exosomes. ii) The merged image of the Cy5 and FITC channels. iii) The g value of four biomarkers on exosomes derived from breast cancer blood samples. iv)The detection results of seven unknown samples with the proposed model. Insert is the determination of cancer patients. Adapted with permission from ref [210]. Copyright 2019 John Wiley and Sons. c) Left-right: Scheme of the captured EV stained by fluorescent antibodies before imaging; Individual EV were labelled with fluorescent antibodies against conventional EV markers (CD9) as well as tumour markers (EGFR); Two-dimensional tSNE mapping of the 11-dimensional data set with an optimized clustering solution of 14 unique clusters. Adapted with permission from ref [211]. Copyright 2018 American Chemical Society. d) Schematic showing the droplet digital ExoELISA for exosome quantification. (Right) Droplet digital ExoELISA calibration results showing the dynamic range of the captured exosomes spans 5 orders of magnitude. Adapted with permission from ref [212]. Copyright 2018 American Chemical Society.

detected by TIRF microscopy (Fig. 13b). A quantitative analysis platform was developed to facilitate sequential quantification analysis of multiple exosomal surface biomarkers at the single-exosome level using DNA-PAINT and a machine learning algorithm was used for analysis, in order to achieve multiplexed profiling of single exosomes. The profiling of four exosomal surface biomarkers (HER2, GPC-1, EpCAM, EGFR) were evaluated as part of a proof of concept study in order to identify exosomes from pancreatic cancer and breast cancer-derived blood samples with high accuracy (Fig. 13b) [210].

When used for single-EV analysis, microfluidic platforms provide many advantages including ultrasmall volume, small particle manipulation etc. For instance, Weissleder et al. immobilized EVs, on an integrated microfluidic platform for on-chip immunostaining and fluorescence imaging (Fig. 13c). Multiple rounds of imaging cycles were carried out for different target markers. Multidimensional data analysis was subsequently used to characterize groups of EV. This method permitted multiplexed protein profiling of individual vesicles and the successful analysis of heterogeneous biomarkers from EVs [211]. A droplet-based single-exosome-counting enzyme-linked immunoassay (droplet digital ExoELISA) approach for the digital qualification of single exosomes was developed by Zheng et al. The exosomes were immobilized on magnetic microbeads through sandwich ELISA complexes tagged with an enzymatic reporter. The as constructed beads were then isolated and encapsulated, while ensuring just a single bead was captured per droplet (Fig. 13d). With this approach, a LOD down to 10 enzyme-labelled exosome complexes per microliter ($\sim 10^{-17}$ M) was achieved. In addition, the quantitative detection of exosomes in plasma samples from breast cancer patients was demonstrated [212]. Furthermore, an aptamer and λ-DNA-mediated approach was reported for the simultaneous separation and analysis of individual EVs in a microfluidic system which was designed for viscoelastic-based size-selective separation of EVs [87]. In order to detect EV subpopulations, DiI-labelled EVs were incubated with Cy5-conjugated HER2 (human epidermal growth factor receptor 2) aptamer and FAM-conjugated EpCAM aptamer before sorting. Target EV surface proteins could be efficiently recognized using small aptamers (2–3 nm in size), facilitating aptamer-based single EV analysis with high signal-to-noise ratios [215].

5.3. Raman microspectroscopy and SERS

Raman spectroscopy is regarded as a promising non-destructive technique for exosome characterization owing to the high efficiency in obtaining the chemical composition of nanovesicles. For single EV analysis, laser trapping technology termed as laser tweezer Raman microscopy or Raman tweezers microspectroscopy (RTM) is suitable due to its capability to characterize single particles. The RTM strategy integrates laser trapping with Raman probing techniques. It uses the same laser radiation to achieve both optical trapping of the target particles and excitation for Raman probing of the content of the particles. Therefore, RTM is capable of trapping single vesicles at the laser's focal point using a tightly focused laser beam and providing the global chemical composition of single EVs without using any exogenous label [159]. The inability of RTM to characterize nanosized biomolecules was demonstrated using experiments on liposomes, exosomes derived from human urine and rat hepatocytes etc. Strong intra-sample biomolecular heterogeneity of the individual trapped EVs was provided directly from the Raman spectra, demonstrating the promising use of RTM for single EV research (Fig. 14a) [216]. Using this method, the Raman spectra of individual exosomes derived from several cell lines were analysed. Using PCA, it was possible to recognize the subpopulations of exosomes. Comparison of the spectral differences between various exosome subpopulations revealed that the main chemical differences between the various subpopulations was the membranes content of the EVs'. These results on the analysis of exosome variability at the single vesicle level are important to illuminate the role of exosome subtypes with respect to their phenotype and ultimate biological function [217]. Additionally, combined with a microfluidic platform, the immunocapture of EVs and the characterization at the single EV level in terms of size, distribution, and chemical fingerprint using multimodal analysis was achieved using multimodal characterization with Raman spectroscopy, SEM, and AFM [218].

To obtain enhanced Raman signals from single EVs, a surface functionalization strategy was used, which was based on the electrostatic adsorption of 4-dimethylaminopyridine (a cationic coating) and 10 nm AuNP on to the anionic surface of EVs in order to form an irregularly shaped nanoshell around the EVs. This nanocoating allows the production of an enhanced Raman signal whilst keeping a colloidal suspension of the individual vesicles (Fig. 14b). Combined with partial least squares discriminant analysis of the Raman spectra, EVs from different origin could be distinguished based on their SERS fingerprints [219]. Furthermore, by combing fluorescence and Raman spectroscopy, multispectral optical tweezers were developed to investigate single vesicles for molecular fingerprinting of EV subpopulations. This technique provided a tool for the sensitive measurement of Raman chemical composition, together with discrimination using antibody fluorescence labelling [221].

5.4. Other techniques

Apart from fluorescence and Raman spectroscopic-based techniques, other approaches such as interferometric plasmonic imaging and resonance-enhanced atomic force microscopic IR spectroscopy (AFM-IR) assays have been developed for single vesicle analysis. In this section we will describe some recent research developments. Interferometric plasmonic microscopy (iPM) is a label-free approach capable of imaging single exosomes. Therefore, the real-time adsorption of exosomes onto Au surfaces was monitored, and individual exosomes were easily distinguishable as bright spots. When integrated with fluorescent microscopy, the fluorescent images were recorded after decorating the lipid membrane of exosomes with DiIC18 dye, which corresponded well with the iPM images (Fig. 14c). Compared with conventional plasmonic assays that measure the light intensity induced by a large number of exosomes, iPM offers single-exosome sensitivity. Therefore, the dynamic interaction between exosomes and antibodies was monitored, together with the tracking of intermediate adsorption behaviour of exosomes on an antibody-coated surface (Fig. 14c). It was anticipated that this method could be used to explore exosome–antibody binding kinetics and contribute to potential clinical exosome analysis [220]. The AFM-IR approach is also a label-free technique which can be used to investigate the structural composition of single EVs with nanoscale resolution. EVs isolated from cell culture medium are incubated on a suitable substrate, then, nano-IR spectra and nano-IR images are collected by the AFM-IR instrument. This approach can uncover the heterogeneity across individual EVs, within the same population and between different populations, as well as detecting lipids, proteins and nucleic acids within individual EVs. It is anticipated that the improved understanding of EV composition and structure through AFM-IR will contribute to the understanding of EV biology [222]. A proximity dependent barcoding assay was used to evaluate the surface proteins of individual exosomes using next-generation sequencing and antibody DNA conjugates. Following the validation of the method using artificial streptavidin-oligonucleotide complexes, the variable composition of surface proteins on individual exosomes originating from human body fluids or cell culture media

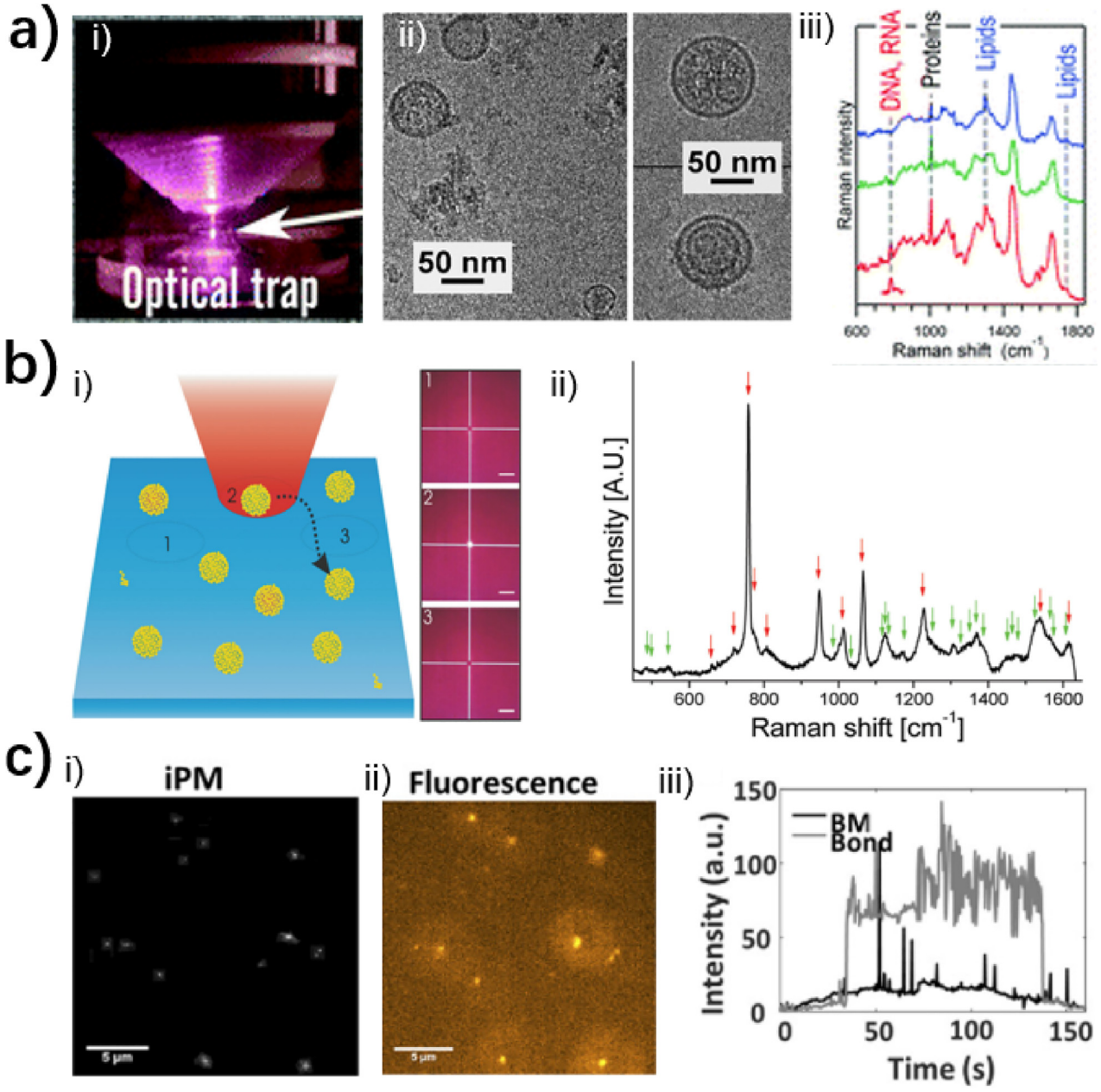

Fig. 14. a) i) Image of an optical trap applied in RTM. ii) Cryo-TEM images of exosomes from rat hepatocytes. iii) Raman spectra of three independent vesicle groups from the same sample of rat hepatocytes. Adapted with permission from ref [216]. Copyright 2019 The Royal Society of Chemistry. b) i) Schematic illustration of the SERS measurements of AuNP coated ELVs. Each spectrum is derived from another vesicle by moving the laser to a different spatial location (e.g., 1, 2, 3). The presence of a gold coated ELV was verified by a scattering signal (location 2). Scale bar = 10 μm. ii) SERS spectrum of RBC-released ELVs coated with AuNP. Red arrows illustrate peaks arising from the DMAP AuNP coating. Green arrows show presumed ELV related peaks. Adapted with permission from ref [219]. Copyright 2016 John Wiley and Sons. c). i) and ii) showed the iPM and fluorescent images of exosomes. iii) Real-time iPM signals of an exosome binding to antibodies or that underwent Brownian motion. Adapted with permission from ref [220]. Copyright 2018 National Academy of Sciences.

were determined. Exosomes derived from various sources were characterized by comparing specific combinations of surface proteins and their abundance, facilitating the independent quantification of exosomes in mixed samples as markers for tissue-specific disease development [223].

6. Application in diagnostics and therapeutics

EVs deliver cargos that reflect the physiological status of the cell and tissue, modulate pathophysiological processes, initiate diseases and affect their progression and response to treatment. Therefore, as a direct result the detailed investigation into EVs function has revealed their great potential as biomarkers for the diagnostics of various diseases [224]. Furthermore, it is becoming evident that these vesicles are involved in many pathological processes, providing opportunities for therapeutic applications, e.g. drug delivery [225].

6.1. Diagnosis and prognosis

EVs isolated from bodily fluid of patients differ from those of normal controls. Therefore, disease derived EVs have been evalu-

ated using various approaches to achieve early accurate diagnosis and improved prognosis of different diseases using their valuable contents including proteins, nucleic acids and lipids (Table 3). The protein and nucleic acid contents of EVs have been thoroughly evaluated as biomarkers for disease diagnosis and prognosis [226]. For instance, compared to control patients, unique protein species were detected in EVs obtained from urine samples of patients with kidney injury [227]. In addition, lipids have been associated with specific diseases [153]. Therefore, the lipid contents on EVs are regarded as effective biomarkers for liquid biopsy [68,228].

Cancer cell derived EVs contain different miRNAs and proteins that are absent in non-malignant cells, and such nanovesicles can be used as tumour biomarkers [229,230]. While EVs with specific surface proteins and nucleic acids could be regarded as diagnostic indicators for different kinds of cancer, such as liver cancer, lung cancer and ovarian cancer etc. [231]. In a recent study, the state

Table 3
Representative studies using EV cargos as biomarkers for different diseases.

Disease type	Sample type	EV biomarkers		EV Enrichment technique	Detection technique	Refs
Lung cancer	Plasma	Protein	EpCAM; IGF-1R	Immunomagnetic enrichment in microfluid chip	Chemifluorescence-based immunoassays	[95]
	Plasma	Protein	EGFR T790M	Isolation kit	qPCR	[235]
	Plasma	Protein	CD151, CD171, and tetraspanin 8	Immunoaffinity	Fluorescence microscopy	[236]
Breast cancer	Blood	Protein	CA-125, EpCAM, CD24	Immunomagnetic enrichment in microfluid chip	Fluorescence microscopy	[96]
	Serum	Nucleic acid	miR-375	Thermophoretic accumulation of nanoflare-treated exosomes	Fluorescence microscopy	[147]
	Plasma	Protein	Developmental endothelial locus-1 protein	Differential centrifugation	ELISA	[237]
Prostate cancer	Serum	Nucleic acid	miR-200c, miR-605, miR-135a*, miR-433, miR-106a	Exosome precipitation solution	Scano-miR assay	[238]
	Urine	Protein	Prostate-enriched proteins (ACPP, PSA, PSMA, TGM4)	Ultracentrifugation	LC-MS	[239]
	Urine	Lipid	Phospholipid	Reversed-phase chromatography	Hyphenate microLC-Q-TOF-MS	[234]
Colorectal cancer	Serum	Nucleic acid	miR-19a	Ultracentrifugation	Quantitative real-time RT–PCR	[142]
Gastric cancer	Plasma	Nulceic acid	Long intergenic non-protein-coding RNA 152	Ultracentrifugation	qRT-PCR	[240]
Liver cancer	Serum	Nulceic acid	miR-718	Isolation kit	microarray analysis	[241]
	Serum	Nulceic acid	miR-21	Total Exosome Isolation Reagent	Real-time qRT-PCR	[242]
Ovarian cancer	Ascite	Protein	CD24; EpCAM	Immunocapture in microfluidic chip	Surface plasmon resonance	[190]
	Plasma	Protein	CD24; EpCAM FR	Immunocapture in microfluidic chip	Fluorescence microscopy	[137]
	Serum	Nulceic acid	miR-21, miR-141, miR-184, miR-193b, miR-200a, miR-200c, miR-200b, miR-203, miR-205, miR-214	Modified magnetic activated cell	MicroRNA	[243]
Pancreatic cancer	Serum	Protein	Glypican-1	Ultracentrifugation	ELISA	[244]
	Plasma	Protein	Macrophage migration inhibitory factor	Ultracentrifugation	Immunofluorescence	[245]
	Plasma	Protein	EGFR, EPCAM, MUC1, GPC1, and WNT2	Ultracentrifugation	Nanoplasmonic sensor	[246]
Bladder cancer	Urine	Protein	Apolipoproteins.	Ultracentrifugation	Dot blot and western blot	[247]
		Nucleic acid	miR-146a, miR-194 and let-7c	Ultracentrifugation	Reverse transcription & real-time qPCR	
Glioblastoma multiforme	Serum	Protein	EGFR	Microbead-based enrichment	Flow cytometry analysis	[12]
		Nucleic acid	PTTG1 mRNA, NLGN3 mRNA	Ultracentrifugation	Real-time PCR	
	Serum/Plasma	Nucleic acid	EGFRvIII mutant mRNA	Immunocapture in microfluidic chip	PCR	[91]
Nasopharyngeal carcinoma	Serum	Nucleic acid	hsa-miR-24-3p, hsa-miR-891a, hsa-miR-106a-5p, hsa-miR-20a-5p, and hsa-miR-1908	Ultracentrifugation	microRNA chip array assay	[248]
Alzheimer disease	Cerebrospinal fluid	Protein	AT270	Sucrose gradient fractionation	ELISA	[249]
Parkinson disease	Plasma	Protein	α-synuclein	Immunomagnetic enrichment	Mass spectrometry	[250]
Acute kidney injury	Urine	Protein	Fetuin-A	Differential centrifugation	Mass spectrometry	[251]
	Urine	Protein	Transcription factor 3	Differential centrifugation	Western blot	[252]
Acute heart failure	Serum	Nucleic acid	MiR-92b-5p	Ultracentrifugation	Quantitative reverse-transcript PCR	[253]

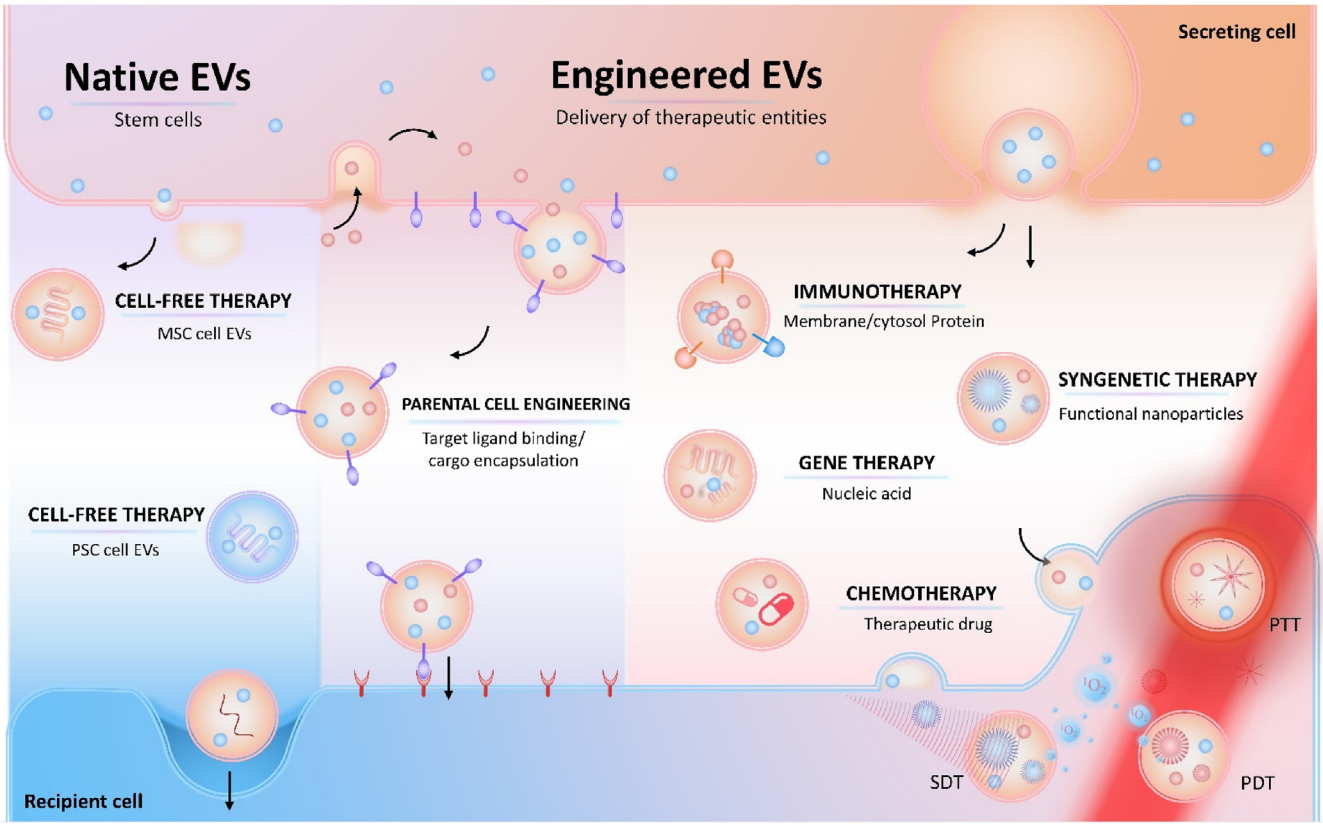

Fig. 15. Overall illustration of the therapeutic used of EVs. Native EVs secreted by stem cells including MSC and PSC exert their ability in cell-free therapy. Engineered EVs are used as the delivery vehicles of various therapeutic entities including proteins, nucleic acids, therapeutic drugs, as well as functional nanoparticles.

of protein phosphorylation could be a key to understanding cellular physiology such as early-stage cancer. Patients diagnosed with breast cancer exhibit significantly higher levels of phosphoproteins in plasma EVs than healthy controls, providing a feasible way for cancer screening and monitoring [232]. Glioma is one of the most common malignant primary brain tumours of the central nervous system. The analysis of EGFR in serum EVs, exhibited a high correlation with the malignancy of glioma. As a result, EGFR was identified as an effective diagnostic marker of glioma [12]. In addition, plasma prostasome microvesicles secreted by prostate acinar cells could be biomarkers of prostate cancer [231].

Several groups have reported on the progress of using EV lipids as biomarkers for diseases [153,233,234]. Research on EVs offers many new opportunities for liquid biopsy which importantly is a minimal invasive diagnostic technology. Therefore, in combination with various advanced technologies, such as microfluidic strategy, "point-of-care" diagnosis of various diseases is achievable [89].

6.2. Therapeutic application

EVs are vehicles that transport functional biomolecules between cells to enable intercellular communication. Therefore, the development of new therapeutic strategies based on EVs has been intensively investigated to help treat diseases. On one hand, therapies that utilize the inherent biological functions of EVs to mimic natural repair processes have been developed, given their innate therapeutic capability in immune modulation and tissue repair. While on another hand, drug delivery methodologies that use EVs as vectors to deliver therapeutic units to the repair site have been extensively investigated [254]. In this regard, both as secreted and engineered EVs are emerging as important therapeutic transporters for drug delivery. EVs are highly versatile for either surface engineering or cargo encapsulation. They are considered to exert therapeutic function towards numerous membrane defect-related diseases, and the entities attached to the vesicle surface can enhance the targeting ability of EV's, exhibit increased expression levels and trigger antigen immunogenicity [5,255]. In general, there are two distinct approaches that can be classified as the direct use of native EVs for therapy and use of engineered EVs for cargo delivery (drug, protein and nucleic acid) to treat diseases and achieve different therapeutic effects [256]. In this section, we will describe emerging EV-based therapeutic applications (Fig. 15), highlighting advances made in the development of state of the art therapeutic EVs.

6.2.1. Native EVs for therapy

It has been well recognized that stem cells hold great promise for treating several diseases. For example, MSC are particularly efficient for the treatment of autoimmune and neurodegenerative diseases. However, MSC-based treatments cannot fully reach their potential as therapeutics due to their large size. Fortunately, EVs generated by these cells have been demonstrated to modulate the immune system and possess therapeutic effect, indicating their ability for the development of cell-free therapeutics. For example, a number of studies have demonstrated that EVs derived from MSC exhibit beneficial paracrine effects in models of kidney injury, myocardial infraction, and skeletal muscle repair. The paracrine effect depends on the transfer of bioactive lipids, proteins, growth factors and genetic materials to recipient cells using EVs and reduces the potential safety concerns related to direct stem cell transplantation [257-260]. These MSC-derived EVs mediate the same functions as their parent cells and exhibit superior bioactive properties. Thus, they have been intensively evaluated for their innate therapeutic application in clinical models [26].

Msc-secreted small EVs contain many potent signalling molecules that play crucial roles in tissue regeneration such as cytokines and microRNA. To improve the low patency rates of vascular grafts in patients a MSC-derived EV-functionalized vascular graft was constructed and applied to an *in vivo* model the system inhibited thrombosis and calcification and enhanced patency of the vascular grafts. The fabrication of vascular grafts with immunomodulatory role could provide an effective approach to improve vascular function and performance vital for cardiovascular regenerative medicine [261]. The treatment of multiple sclerosis which is an inflammatory disease of the central nervous system exosomes both derived from native MSC (Native-Exo) or MSC activated by IFNγ (IFNγ-Exo) have been evaluated in a mouse model. IFNγ, a pleiotropic cytokine involved in the onset orchestration and resolution of adaptive immune and autoimmune responses has been reported to promote the immunosuppressive effects of MSCs. These results indicated that both native-Exo and IFNγ-Exo could ameliorate diseases while IFNγ-Exo exhibited higher effect. RNA sequencing results indicated that IFNγ-Exo contained anti-inflammatory RNAs and harboured multiple anti-inflammatory and neuroprotective proteins facilitating sustained clinical recovery and reduced neuroinflammation in the mouse. Therefore they could serve as cell-free therapies in creating a tolerogenic immune response as therapies for central nervous system and autoimmune disorders [262]. Recently it has been reported that small EVs obtained from human MSCs could prevent group 2 innate lymphoid cell-dominant allergic airway inflammation through delivery of miR-146a-5p as cargo [263]. Gao reported that cell paracrine secretions that bear the functions of microenvironment regulation could be delivered by MSC-secreted exosomes. In combination with a new implantation strategy that uses immobilized exosomes in a peptide -modified adhesive hydrogel the functional vesicle matrix exhibited positive treatment effects on the disease [264].

In addition, another type of stem cell, perivascular stem cells (PSCs) have been highlighted for their therapeutic ability. The vascular wall is a source of progenitor cells that can induce skeletal repair, primarily by the paracrine mechanisms. It has been demonstrated that human PSCs derived EVs possess the same pro-migratory, pro-osteogenic and mitogenic properties of their parent cells, which are dependent on the surface-associated tetraspanins. Therefore, PSC-EVs facilitate the same tissue repair effects of perivascular stem cells and provide an 'off-the-shelf' substitute for bone tissue regeneration [265]. Apart from stem cells, some other cell species can secret EVs with innate therapeutic effect. For instance, EVs derived from human dermal fibroblasts exhibited anti-skin-aging abilities. The vesicles were collected and then introduced to a photoaging mouse model using a needle-free injector. The treatment resulted in a high level of tissue inhibition of metalloproteinases-1, collagen synthesis capability and antiaging effects [266]. In a recent study, lung spheroid cell secreted exosomes (LSC-Exo) were used to treat different models of lung injury and fibrosis. Due to their innate therapeutic capability, LSC-Exo could attenuate lung fibrosis by re-establishing normal alveolar structure and decreased both collagen accumulation and myofibroblast proliferation. Of note, LSC-Exo exhibited superior effects compared to MSC derived exosomes for treatment, indicating the great innate therapeutic potential of these vesicles for lung regeneration [267].

6.2.2. Engineered EVs for cargo delivery

EVs can be engineered either by surface modification or cargo encapsulation, which could improve their function in therapeutic applications [268,269]. In addition, tumour derived EVs can breach the blood – brain barrier (BBB) *in vivo*, and thus facilitates the development of drug delivery approaches for therapeutic cargoes across the BBB for the treatment of a variety of brain diseases [11]. There are two different approaches to develop EV-based delivery systems: transfection of parent cells and exogenous loading of various therapeutic entities. A wide range of exogenous cargos have been encapsulated into EVs such as therapeutic drugs, proteins, RNA and functional NPs, using various methods including surfactant permeabilization, electroporation, sonication, freeze–thaw cycles, hypotonic dialysis, extrusion and cell-mediated packaging [270-272] As such EVs are emerging as potential natural drug delivery vehicles with many advantages in the drug delivery workflow including drug loading, intrinsic cell targeting , ability to cross natural barriers and *in vivo* stability during circulation [229]. The biogenesis of EVs offers unique opportunities for the loading of cargos to secreted vesicles by delivering these therapeutic factors to a cell [254]. Such cargo loaded EVs have exhibited encouraging therapeutic effects in various diseases such as many kinds of cancers [273,274] and neurodegenerative diseases [254]. The most commonly applied strategies for exogenous loading of therapeutic moieties, include direct membrane fusion, encapsulation and engineering of parental cells to obtain EVs containing the desired cargo.

a. Therapeutic drug delivery

Benefiting from their specific structure and intrinsic biochemical properties, EVs can serve as stable drug delivery platforms for chemotherapy. Following from the seminal work by Zhang et al. in 2010, where they reported the enhanced anti-inflammatory effect of using exosomes to deliver curcumin to target inflammatory cells, EVs have been intensively investigated to encapsulate various therapeutic drugs for disease treatment [275]. For instance, exosomes modified by targeting ligands loaded with a chemotherapeutics doxorubicin (DOX) via electroporation exhibited excellent potential for cancer treatments [273,276]. While, a micelle-aided method has been used to efficiently load the low-toxicity anticancer agent imperialine into intact EVs to treat non-small cell lung cancer [277]. Based on the preferential recruitment of macrophages by breast cancer, macrophage-derived exosomes could provide a potential drug delivery platform for breast cancer-targeted therapies. As such, Wu et al., developed optimized docking NPs prepared via nanoprecipitation and composed of a laurate functionalized platinum Pt (IV) prodrug (Pt(lau)), human serum albumin (HSA), and lecithin [278]. The authors isolated the exosomes spontaneously secreted by murine RAW 264.7 cells (Rex) to encapsulate the NPs by sonication and ultracentrifugation (Fig. 16a). When compared with free cisplatin, the nanoassembly NPs/Rex facilitated breast-cancer-targeted Pt delivery due to the tumour-homing ability of the macrophage-secreted exosomes. In addition, NPs/Rex displayed prolonged blood circulation, smart organ tropism, and enhanced biocompatibility, as well as robust Pt chemotherapy for breast cancer cells in orthotopic tumours of fat pads and metastatic nodules in lungs [278]. In another example, Bi_2Se_3 nanodots and DOX co-embedded microparticles (Bi_2Se_3/DOX@MPs) were fabricated using ultraviolet light irradiation-induced budding of parent cells which were preloaded with Bi_2Se_3 nanodots and DOX using electroporation. The drug-loaded microparticles (microvesicles) exhibited dual-modal imaging capacity and outstanding tumour suppression effects due to their excellent photothermal performance and tumour targeting ability [279]. By using cancer-derived exosomes to load and deliver ultrathin palladium catalyst to cells, localized prodrug activation could be achieved. This is anticipated to promote the development of new targeted therapy modality, namely exosome-directed catalyst prodrug therapy for the treatment of cancers [280].

The above studies are based on direct loading of drugs to EVs. For indirect approaches, EVs carrying drugs could be obtained by secretion of parent cells. For instance, RAW macrophages were

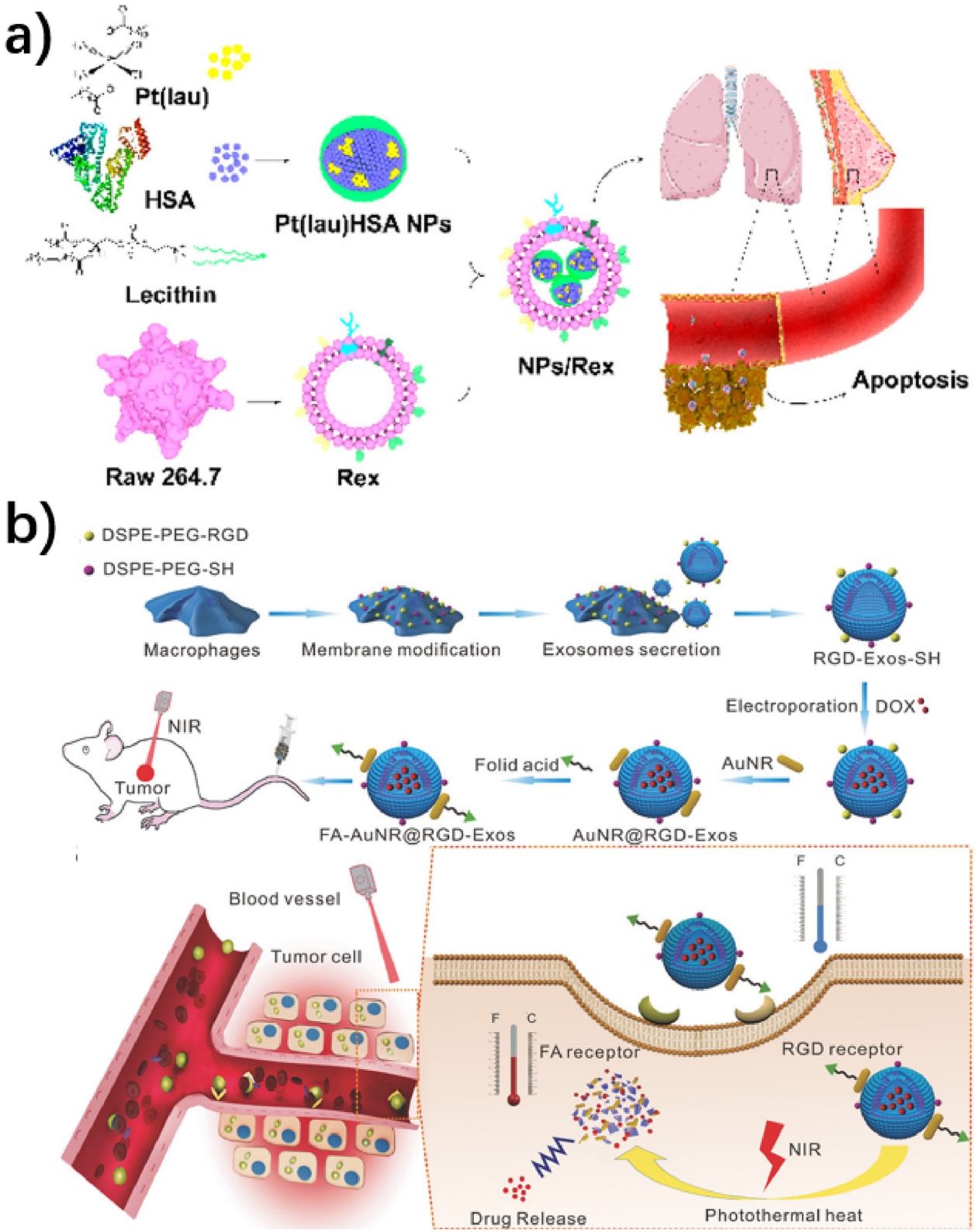

Fig. 16. a) Schematic illustration of the Pt(lau)HSA NP-loaded exosome platform (NPs/Rex) for efficient chemotherapy of breast cancer. Adapted with permission from ref [278]. Copyright 2019 American Chemical Society. b) Schematic of the design of FA-AuNR@RGD-DOX-Exos and their antitumor effect under NIR irradiation. The therapeutic efficiency of FA-AuNR@RGD-DOX-Exos was evaluated in a tumour-bearing mouse model. (Bottom) Schematic of FA-AuNR@RGD-DOX-Exos as an effective nanoplatform for targeted delivery and chemo-photothermal synergistic tumour therapy. Adapted with permission from ref [281]. Copyright 2018 John Wiley and Sons.

incubated with dexamethasone (DEX) and the microvesicles loaded with DEX are isolated from the supernatant by centrifugation. MV-DEX could efficiently deliver dexamethasone to the inflamed kidney and exhibited excellent ability to suppress renal inflammation and fibrosis without apparent glucocorticoid adverse effects [282]. Liu et al. reported the labelling of donor cells with

dual ligands (biotin and avidin) in the phospholipid membrane able to encapsulate drugs in the cytosol in order to obtain secreted exosomes with the desired dual ligands and drugs, which exhibited excellent targeting for tumour cells and efficient receptor-mediated cellular uptake [93]. Using a similar cell labelling strategy, the same group generated exosomes modified with arginyl-glycyl-aspartic acid (RGD) and sulfhydryl group which were encapsulated with DOX and functionalized with Au nanorods. After modifying another tumour-specific targeting ligand (folic acid, FA), the obtained exosomes (FA-AuNR@RGD-Exos) accumulated at the tumour site due to the dual ligand-mediated endocytosis (Fig. 16b). AuNRs could then induce localized hyperthermia under NIR irradiation, resulting in photothermal activity and enhanced drug release by impacting the permeability of the exosome membrane. Therefore, the designed exosome assembly provided a functional platform for the photothermal chemotherapeutic treatment of tumours [281]. In another study, tumour cells incubated with porous silicon NPs (PSiNPs) loaded with DOX were used to generate exosome-sheathed DOX (DOX@E-PSiNPs) by exocytosis of cells. The biocompatible DOX@E-PSiNPs exhibited increased tumour accumulation, extravasation from blood vessels and deep tumour penetration of parenchyma. Moreover, DOX@E-PSiNPs possess significant cellular uptake and cytotoxicity with both cancer stem cells (CSCs) and bulk cancer cells regardless of their origin [283]. In a similar manner, extrussion of cells with DOX, resulted in the enrichment of encapsulated DOX EVs (EVdox), which were then applied for the fabrication of an EV-supported popcorn-like nanostructure using self-grown AuNPs surrounding the EVdox. This nanoplatform retained the photothermal transduction from gold nanoparticle assemblies and cytotoxicity of DOX and exhibited enhanced antitumor efficacy and reduced side effects in tumour-bearing mouse models [284].

b. Therapeutic protein delivery

Over the past several decades, various cell membrane proteins have been studied in preclinical and clinical studies as targets for therapeutic formulations [285]. Such proteins must be expressed and purified in systems close to the native conformation. Therefore, EVs released from most cells are an ideal platform for membrane-associated therapeutic protein delivery [24]. Natural EVs contain a variety of membrane and cytosol proteins, offering a significant number of binding sites for specific targeting/homing ligands in targeted therapy or combined with exogenous therapeutic proteins for efficient protein delivery [16]. In brief, therapeutic proteins can be delivered by membrane fusion or fusogenic EVs to elicit nonimmune and immune responses. Protein cargo loading can be achieved by engineering the EV surface using the fusion of the moiety of interest. Combined with aptamers or chemical antibodies, molecularly targeted exosomes can be as assembled as smart engineered nanovesicles for precision medicine [286]. For instance, based on the natural capability of BBB breaching by EVs, macrophage derived EVs have been used to bind a brain-derived neurotrophic factor on the membrane by electrostatic and polysaccharide interactions to form a BDNF-EV complex. The application of this system to mice models facilitated the successful delivery of proteins using EVs to inflamed brains [287]. The anchoring of a propeptide to the surface of exosomes through fusing the inhibitory domain of myostatin propeptide into the second extracellular loop of CD63, resulted in the targeted delivery of propeptide to damaged muscle, and resulted in a promising approach to accelerated muscle regeneration and growth [288]. In another study, a biomimetic nanoparticle platform was constructed by caging guest proteins in a matrix of metal-organic frameworks (MOFs) and then decorating the NPs onto the EVs by membrane binding (Fig. 17a). This EV-like nanoparticle could protect proteins against protease digestion, evade clearance by the immune system, target homotypic tumour sites and promote tumour cell uptake, followed by autonomous release of the guest protein after internalization. Based on these biomimetic NPs, intracellular delivery of the bioactive therapeutic protein gelonin significantly inhibits tumour growth *in vivo* and increased therapeutic efficacy 14-fold [289]. Recently, Choi et al. reported a new tool for the intracellular delivery of target proteins via optically reversible protein–protein interactions (Fig. 17b). A photoreceptor cryptochrome 2 (CRY2) and CRY-interacting protein (CIBN) bound via blue light-dependent phosphorylation was used in the experiment. Under blue light illumination, the transient docking of CRY2-conjugated cargo proteins binding to CIBN which was conjugated with exosomal CD9 protein, inducing the generation of exosomes with the desired cargo proteins after endogenous biogenesis. Upon removal of the blue light, the cargo proteins are detached from the CD9-conjugated CIBN, enabling release of the exosomes into the intraluminal space and efficient delivery to the cytosolic compartment of targeted cells [290]. This study provided a new method for loading protein cargos through fusion with membrane proteins upon regulation by external physical stimulus. To facilitate diverse surface functionalization of exsomes, an oligonucleotide tethers strategy was developed by Das et al. In their work, an immunomodulatory protein, FasL was used to modify the surface of exosomes, which exhibited spatial induction of apoptosis in tumour cells and suppressed proliferation of alloreactive T cells [291]. Taking advantage of the specific features of the phospholipid bilayers of exosomes to decorate functional moieties, membrane protein engineering could be used to fabricate on-demand nanoplatforms with the desired physicochemical/biological characteristics, such as improved physiological stability, enhanced targeting ability, as well as multifunctionality [16,292].

In addition, fusogenic vesicles provide an efficient approach to control the function of membrane proteins and the effective delivery of membrane proteins, as well as cytosol proteins to target cells [293]. For example, Yang and co-workers have developed a fusogenic exosome platform using the viral fusogen, vascular stomatitis virus (VSV)-G protein which was capable of fusing with the cell membrane at acidic pH. The authors have shown that the fusogenic exosomes could efficiently deliver glucose transporter-4 (GLUT4-GFP) or GFP fused CD63 (CD63-GFP) to cell membranes and mediate the transfer of GLUT4 to mouse muscle membranes *in vitro* and *in vivo*, resulting in an increased glucose uptake for the recipient cells. This study confirmed the potential of using the fusogenic exosome platform for delivering membrane proteins [294].

Other investigations have shown that EVs can induce an immune response by presenting parent cell signalling proteins or tumour antigens to immune cells [276]. In addition, EVs express tumour-specific antigens that display strong antigen immunogenicity and can be used to develop cancer vaccines [295]. For example, dendritic cell derived exosomes bearing membrane protein, MHC-I, complexed with tumour-derived peptides could be used to induce anti-tumour immune responses [296]. In addition, the surface expression of other antigens e.g. ICAM-1 and NKG2D ligand could activate T cells and NK cells, resulting in an immune response [297,298]. While, a well-recognized therapy for haematological and non-haematological malignancies has been developed based on the acute toxic chimeric antigen receptor (CAR) which is expressed by genetically engineered T cells and displays target specificity due to antigen-recognition regions. Similarly, EVs, mostly in the form of exosomes released by CAR-T cells carry CAR on their surface. The CAR-containing exosomes express a high level of cytotoxic molecules (e.g. granzyme B) and can be used in tumour treatments to induce rapid and durable clinical responses. The results of tumour treatment in a preclinical model indicated

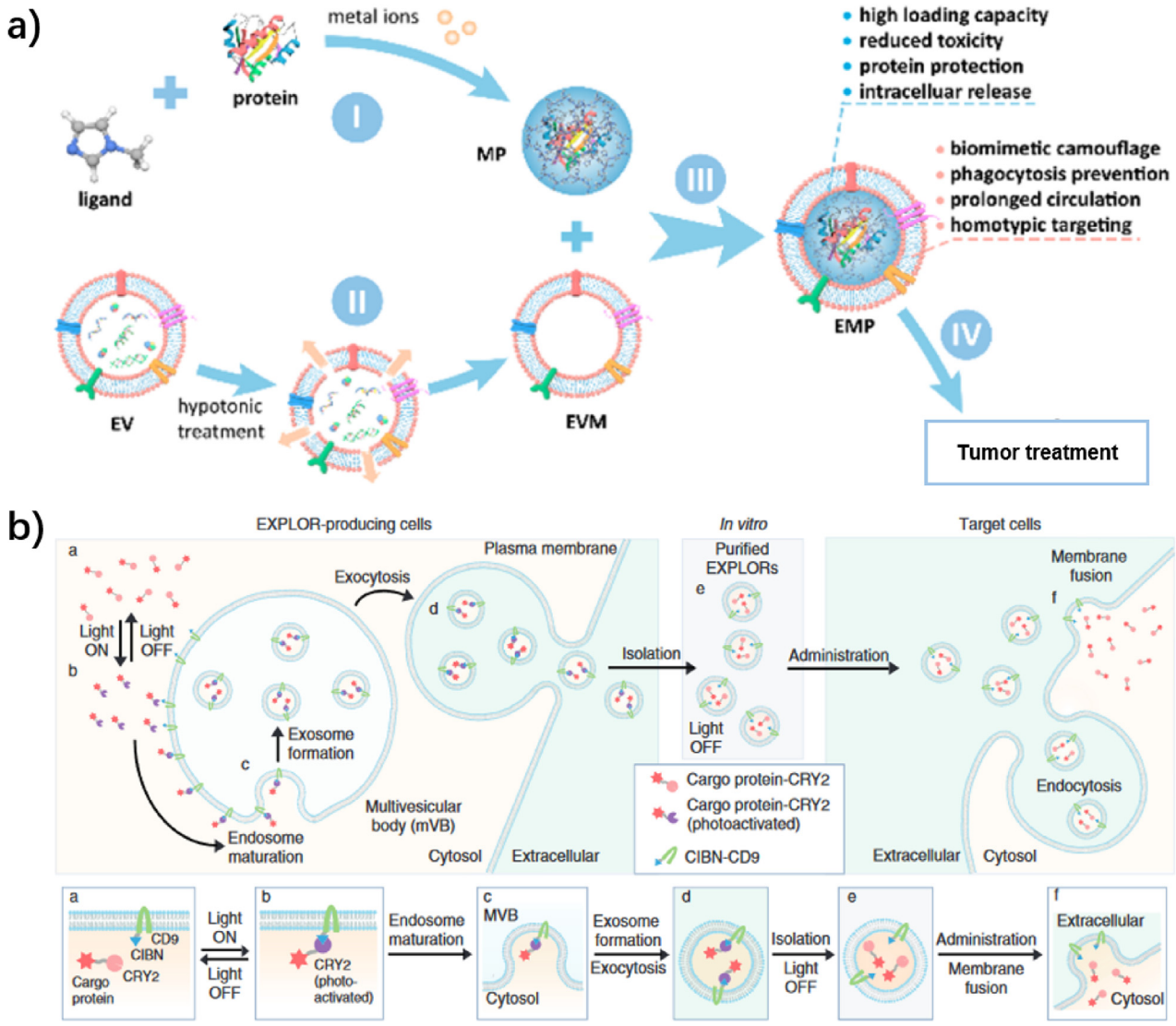

Fig. 17. a) Schematic illustration of the method for preparing biomimetic EMP NPs for homotypic targeting and intracellular delivery of guest proteins. I: Caging protein cargo by self-assembly of blocks of inorganic nodes and organic ligands to synthesize MOF-protein NPs. II: Extraction of extracellular vesicle membrane (EVM) through a hypotonic treatment of EVs. III: Self-assembly of EVM on MP nanoparticle surface by ultrasonication and extrusion to form EVMOF-protein (EMP) NPs. IV: Systemic and intracellular delivery of the guest proteins by EMP NPs. Adapted with permission from ref [289]. Copyright 2018 American Chemical Society. b) Schematic illustration of EXPLOR technology. In EXPLOR-producing donor cells, CRY2 protein was fused to a cargo protein, and CIBN was conjugated with the exosomal surface biomarker, CD9 protein. The reversible PPI between CIBN and CRY2 fusion proteins can be induced by blue light illumination i. Under continuous blue light irradiation, the cargo proteins are guided to the inner surface of the cell membrane or the surface of early endosomes. MVBs then readily release cargo protein-carrying exosomes (EXPLORs) from the cells by membrane fusion with the plasma membrane. After exocytosis, EXPLORs can be easily separated and purified *in vitro*. Purified EXPLORs can be used to deliver the cargo proteins into target cells through membrane fusion or endocytosis. Bottom grey boxes highlight the essential steps from EXPLORs biogenesis to target cell delivery. Adapted with permission from ref [290]. Copyright 2016 Nature Publishing Group.

that EVs exhibited superior antitumor effect but inferior toxicity to CAR-T cells, suggestive of a potential therapeutic approach [299]. For cancer immunotherapy using a tumour antigen vaccination combined with an adjuvant, it is particularly difficult to identify a specific tumour antigen and efficient delivery of the antigen to receipt cells. Takakura et al. proposed an efficient exosome-based tumour antigens-adjuvant co-delivery system using genetically engineered tumour cell-derived exosomes containing endogenous tumour antigens and immunostimulatory CpG DNA. The results demonstrated the efficient delivery of tumour antigens and CpG DNA, which successfully activated DC cells for tumour treatment [300]. Another important consideration in immunotherapy is the targeted delivery of therapeutic proteins with low immunogenicity and system toxicity to achieve optimal tumour treatment. Gaertner et al. developed a new immunotherapeutic approach for adjuvant treatment of chronic lympho-cytic leukaemia (CLL) based on engineered EVs carrying proteins and antigens of human viruses. The results indicated that engineered EVs were able to target patients' malignant cells and render these cells immunogenic to allogeneic and autologous cells, thus providing an attractive tool for the adjuvant treatment of CLL [272].

c. Nucleic acid delivery

RNA-based therapeutics has been recognized as promising in disease treatments. Both *in vitro* and *in vivo* delivery of nucleic acids plays a vital role in emerging gene therapy. Natural EVs are rich in nucleic acids, such as miRNAs, mRNAs and DNA etc. Thus, they are a suitable and rational vehicle for the delivery of nucleic acids. In addition, recent studies have demonstrated that mRNA-

loaded lipid NPs could undergo endocytosis and packaging into EVs, and as such could protect the exogenous mRNA during *in vivo* delivery [301]. A significant amount of research has been devoted towards the engineering of EVs for RNA loading. For instance, Wood et al. reported the pioneering study on the delivery of RNA by EVs. The authors used dendritic cells derived exosomes which were engineered with targeting proteins loaded with exogenous siRNA by electroporation. Intravenous injection of the engineered EVs resulted in the delivery of siRNA to the brain and exhibited the excellent therapeutic potential of exosome-mediated siRNA delivery for brain diseases, e.g. Alzheimer's disease [302]. Through the construction of a fusion protein in which the exosomal membrane protein CD9 was fused with RNA binding protein, Yuan et al. engineered exosomes for RNA loading. The CD9 protein was fused with HuR an RNA binding protein that interacts with miR-155 with a relatively high affinity. Subsequently, exosomes carrying miR-155 were enriched with fused CD9-HuR and then secreted by parental cells and miR-155 was delivered to the receipt cells. This study provided a novel strategy for enhanced RNA cargo encapsulation into engineered exosomes for delivery to recipient cells (Fig. 18a) [303]. Based on the experimental results that MSC-Exo could penetrate the BBB and homed into the injured spinal cord region, Levenberg et al. used MSC derived exosomes loaded with phosphatase and tensin homolog small interfering RNA (ExoPTEN) to treat spinal cord injury. They demonstrated that ExoPTEN could not only promote robust axonal outgrowth of DRG neurons *in vitro*, but also achieve improved neovascularization and therapeutic efficacy in rats with spinal cord injury (Fig. 18b) [304].

In order to improve the efficacy of gene therapy, the loading efficiency of RNAs into EVs needs to be considered. In a recent study, protonation of EVs to create a pH gradient across the EV membrane was shown to enhance vesicle loading of a nucleic acid cargo, specifically small interfering RNA (siRNA), microRNA (miRNA), and single-stranded DNA (ssDNA). Cellular uptake of EVs was not impaired by the loading process, nor was any significant EV-induced toxicity observed in mice [305]. In addition, taking advantage of the development of RNA nanotechnology, the effective reprogramming of native EVs for RNA delivery was possible. For example, the positioning of arrow-shaped RNA was altered to control ligand display on EV membranes for specific cell targeting, or to regulate intracellular trafficking of siRNA or miRNA. The placement of membrane anchoring cholesterol at the tail of the arrow resulted in the display of RNA aptamer or folate on the outer surface of EVs. However, placing the cholesterol at the arrowhead induced the partial loading of RNA nanoparticles into EVs. Using the RNA ligand for specific targeting and extracellular vesicles for efficient membrane fusion, the resulting EVs were able to specifically deliver siRNA to cells, and halt tumour growth in prostate, breast and colorectal cancer models [306].

To generate targeted nucleic acid or enable their targeted delivery, cellular engineering is required. Through transfection of cells with an expression vector, targeted exosomes could be generated with exosomal protein fused with a peptide ligand, which could then be applied for tissue-specific nucleic acid delivery [307]. For instance, Kuroda and co-workers have determined that targeting ability was achieved by engineering the donor cells to express the transmembrane domain of platelet-derived growth factor receptor fused to the GE11 peptide. The modified exosomes derived from cells could then successfully deliver miRNA to EGFR-expressing cancer tissues. In addition, intravenously injected exosomes targeting EGFR were capable of delivering let-7a specifically to xenograft breast cancer cells in a mice model, indicating that the exosomes targeted EGFR-expressing cells could provide a platform for miRNA replacement therapies for the treatment of many cancers [308]. In another study, vesicles carrying suicide gene mRNAs and proteins were obtained from transfected parental cells. The vesicles were then injected into Schwannoma tumours from an orthotropic mouse model. Combined with systemic prodrug treatments, the vesicles resulted in successful tumour treatment [309]. With regards to the RNA loading of exosomes, analytical methods to sort exosomes and their sub-populations, and the influence of exosomal proteins and lipids on the recipient cells need to be further evaluated. Further studies on these aspects of exosome biology will enable advancements of the field and could result in the clinical translation of exosome-based gene therapy [310].

d. Functional nanoparticle delivery

Recently, the following methods have emerged as successful approaches for tumour treatment; photodynamic therapy (PDT) which is based on reactive oxygen species (ROS) produced by photosensitizers under light irradiation [311], photothermal therapy (PTT), which is induced by the photothermal effect of photothermal transduction agents (PTAs) [312] and sonodynamic therapy (SDT), relying on the sonosensitizer triggered generation of ROS via ultrasound [313]. With the growing interest in cancer therapy using PDT, PTT and SDT, the development and efficient transfer of novel nanomaterial-based photosensitizers, PTAs and sonosensitizers have been intensively investigated [314], which has inspired the construction of EV-based nanoplatforms to deliver functional NPs e.g. photosensitizers. Li et al. have developed multifunctional chimeric peptide engineered exosomes (ChiP-Exo) for use as plasma membrane and nucleus targeting photosensitizer delivery. The plasma membrane targeted PDT of Chip-Exo could directly destroy the membrane structure and kill the cells. Combined with dual-stage light strategy, Chip-Exo could be delivered to the cytosol and penetrated the nuclei and generated ROS *in situ* to destroy the nuclei for an improved synergetic PDT, resulting in an improved therapeutic effect on the inhibition of tumour growth with minimized system toxicity [315]. In a recent study, Tang et al. prepared a tumour-exocytosed exosome hybrid using electroporation, which transported photosensitizers with aggregation-induced emission properties to facilitate efficient tumour penetration and PDT [316]. To improve the limited therapeutic efficiency of PTT, small fluorescent vanadium carbide quantum dots (V_2C QDs) were modified with TAT peptides and packaged into exosomes engineered with cell targeting RDG peptide as photothermal agents to obtain cancer cell membrane and nucleus dual-targeting system (V_2C-PEG-TAT@Ex-RGD). Upon laser irradiation at 1064 nm, the resulting NPs could induce cell necrosis at low temperature (Fig. 19a). *In vivo* anticancer treatment proved that the exosome-based NPs exhibited good biocompatibility, long circulation time, and endosomal escape ability, which could target the cell and enter the nucleus to realize low-temperature PTT with advanced tumour destruction efficiency [317]. The development of nanosensitizers with good biosafety and high sono-activatable efficiency is critical for efficient SDT-based cancer therapy. Wang et al. reported a functionalized smart nanosonosensitizer by loading sinoporphyrin sodium (DVDMS), an excellent porphyrin sensitizer with potential therapeutic and imaging applications, onto homotypic tumour cell-derived exosomes. The synthesized EXO-DVDMS was utilized for the controlled ultrasound-responsive release and enhanced SDT. In addition, the exosomal formulation provided a functionalized nanostructure, and aided simultaneous imaging and inhibition of tumour metastasis, which was 3-fold and 10-fold better than that of free form, resulting in a promising nanoplatform for activated cancer theranostics [318].

In order to construct on-demand engineered EVs, microfluidic-based strategies have been developed to readily engineer EVs for any desired application. For instance, a streamlined microfluidic cell culture platform was used to integrate harvesting, antigenic

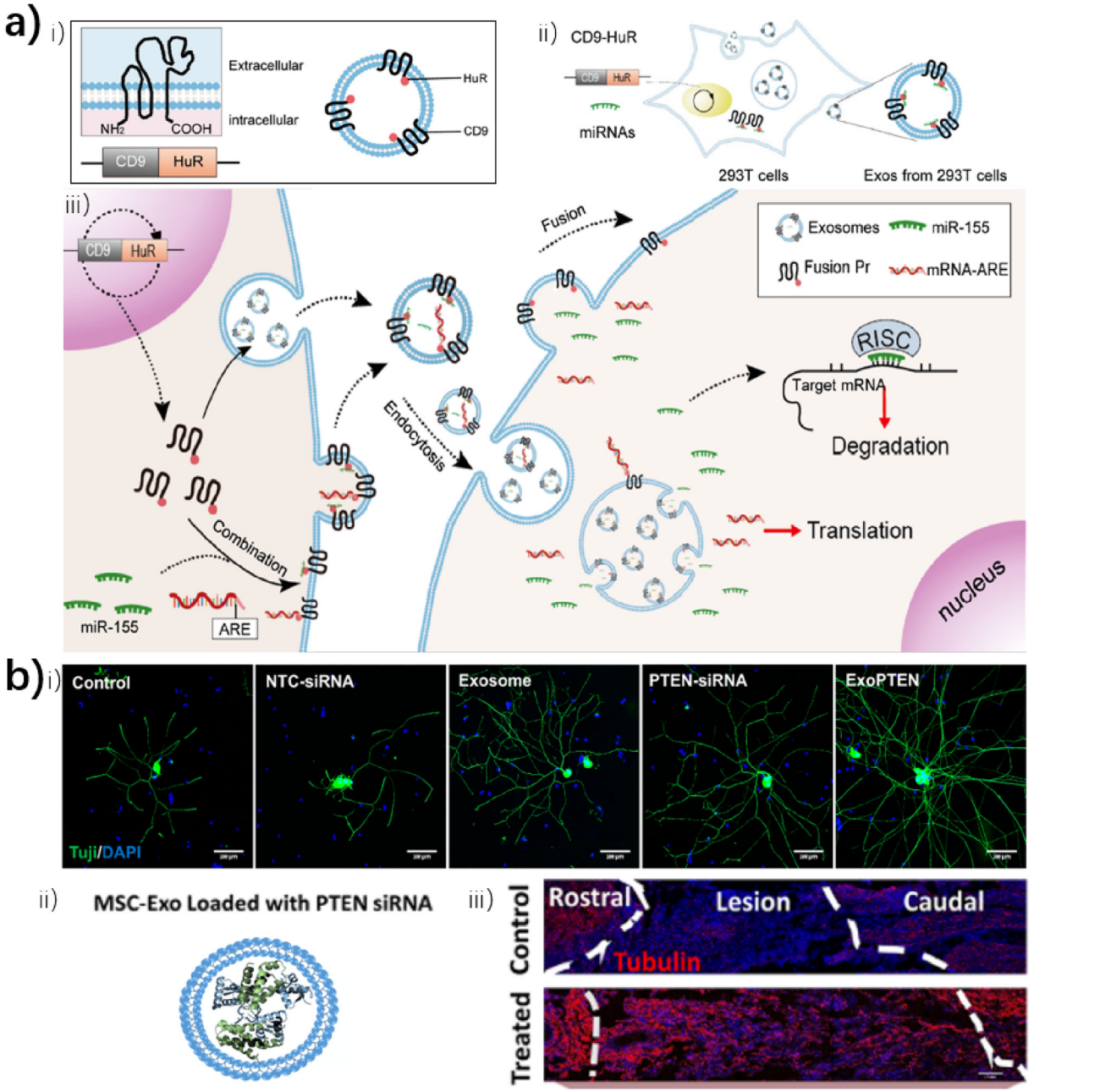

Fig. 18. a) i) Exosome surface functionalization with CD9-HuR fusion protein. ii) Illustration of the procedure how miR-155 or miR-328 was encapsulated by the CD9-HuR fusion protein functionalized exosomes. iii) Schematic illustration of the study. In the packaging cells, CD9-HuR fusion protein recruits the target miRNAs or mRNAs to the exosomes via the RNA-HuR recognition. In the recipient cells, miRNAs or mRNAs of interest are released from the CD9-HuR exosomes and thus act as functional miRNAs or mRNAs. Adapted with permission from ref [303]. Copyright 2019 American Chemical Society. b) i) Representative immunofluorescent staining images of DRG neurons treated with medium, nontargeting control siRNA, MSC-Exo, PTEN-siRNA, or ExoPTEN. Neurons (green), nuclei (blue). Scale bar: 200 μm. ii) Schematic illustration of MSC-Exo loaded with PTEN-siRNA. iii) Immunofluorescent images of control and treated lesion microenvironment. Adapted with permission from ref [304]. Copyright 2019 American Chemical Society.

modifications, and the photo-release of intact, surface engineered exosomes. The surface engineered antigenic exosomes were enriched in real-time from the on-chip culture of leukocytes separated from human blood, resulting in enhanced cellular uptake which have lead to advances in cancer immunotherapy [320]. Sun et al. have reported a microfluidic sonication approach to generate biomimetic NPs such as exosome membrane (EM)-coated poly(lactic-co-glycolic acid) (PLGA) NPs, encapsulated with imaging agents (Fig. 19b). The EM could lower nonspecific uptake and enhance tumour targeting, whereas the PLGA cores loaded with imaging agents could support the rigid core–shell nanostructures. Furthermore, cellular uptake and *in vivo* experiments indicated that the tumour cell-derived EM-coated PLGA NPs consisting of endosomal and plasma membrane proteins exhibited superior homotypic targeting capability. This study provided a controllable microfluidic-based approach for fabricating exosome-based drug delivery system in a facial and efficient manner [319].

6.2.3. Challenges and considerations for EV-based therapy

So far, there have only been a few human clinical trials where the immune cell-derived EVs have been used as cancer vaccines, and in those examples the tumour-specific antigens are carried

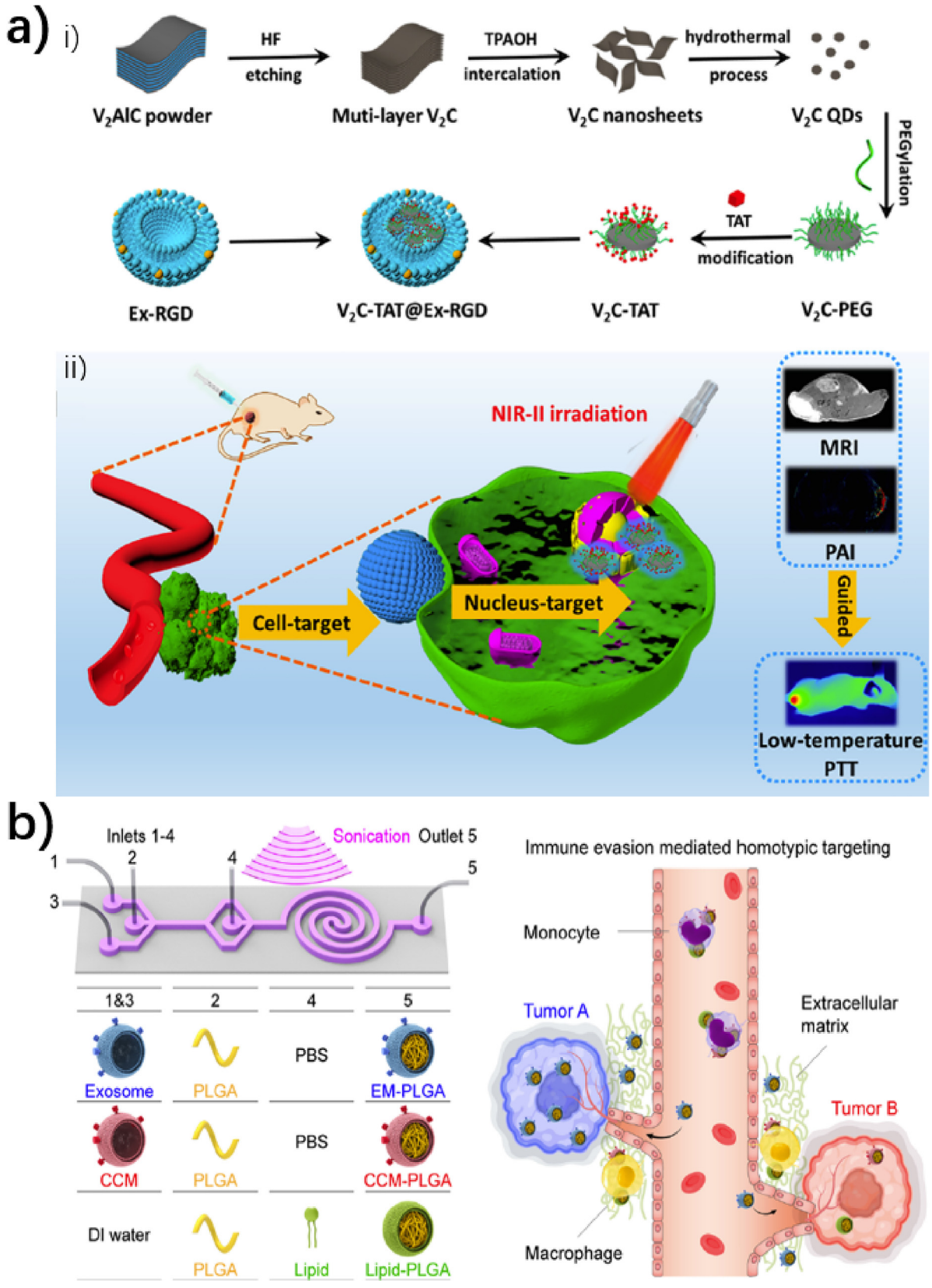

Fig. 19. a) i) Preparation procedure of the V2C-TAT@Ex-RGD. ii) Schematic diagram of cancer cell membrane and nucleus organelle dual-target V2C-TAT@Ex-RGD nano-agent for multimodal imaging-guided PTT in the NIR-II bio-window at low temperature. Adapted with permission from ref [317]. Copyright 2019 American Chemical Society. b) Schematic of the microfluidic sonication approach to assemble biomimetic core – shell NPs for immune evasion-mediated tumour targeting. (Left) One-step microfluidic synthesis of exosome membrane (EM)-, cancer cell membrane (CCM)-, and lipid-coated PLGA NPs via the combined effects of acoustic pulses and hydrodynamic mixing. (Right) EMPLGA NPs indicating reduced uptake by peripheral blood monocytes and extracellular matrix macrophages and superior homotypic targeting, compared to CCM-PLGA NPs and lipid-PLGA NPs. Adapted with permission from ref [319]. Copyright 2019 American Chemical Society.

on the vesicles [229]. To the best of our knowledge, research towards using EVs as state of the art delivery vehicles for therapeutic drugs, nucleic acids and functional nanoparticles etc. have only been reported in advanced preclinical studies using animals as models, e.g. mice [267,279] or rats [304]. Practical therapeutic applications of EVs have been limited due the major challenge of producing EVs of a clinical grade. For drug delivery, there is a lack of methods for scalable EV isolation and efficient drug loading. When translating into practical application, a large quantity of cells is required to generate enough EVs for *in vitro* assays and *in vivo* animal models. Furthermore, when using for clinical treatments in human patients, a scaling up in the production of EVs is required [321]. The function and mechanisms regarding the application of EVs in cancer treatment need to be completely understood. As discussed above, recent research has focused on EVs as natural NPs for therapeutic applications, especially engineered EVs that provide attractive tools for the advancement of novel therapeutic interventions, such as vaccinations, cancer immunotherapies, or targeted drug delivery. Therefore, by engineering the surface and cargo of EVs through chemical and biological approaches, scientists hope to enable the favourable characteristics whilst removing any unfavourable properties. However, the efficient engineering of EVs without negatively impacting their function remains challenging. Manipulating parent cells is complex and time-consuming, whilst direct functionalization of surface proteins of EVs sometimes suffers from low specificity and low efficiency [268]. In addition, the application of such engineered EVs requires the precise evaluation of the interaction of the EVs with cells in order to determine their uptake routes and intracellular routing [322]. In particular, for drug delivery systems, the intrinsic safety and toxicity of EVs are critical. Importantly studies have demonstrated that EVs have minimal hepatotoxicity, which is important since NPs accumulate in the liver [323]. There remains several key biological factors that must be considered when using EVs for *in vivo* drug delivery including the interaction between the EVs and the receipt cell, and a deep understanding of the mode of action for both active and non-active components of the drug loaded EVs *in vivo* from a pharmacological perspective. [254,324]. Therefore, systematic evaluations and optimizations of EV-based therapies are required to improve the translation of engineered EVs into clinical applications as a new class of drug delivery systems [322].

7. Summary and future perspectives

EVs carry diverse cellular constituents (proteins, lipids, genetic agents) from their parent cells and convey information between cells to regulate the phenotype and function of the recipient cells. Due to their physiological and pathological function and the abundance in various body fluids, studies on EVs to enable non-invasive liquid biopsy and disease therapies have grown logarithmically over the past a few years. As reviewed in this article, advanced techniques based on fluorescence, SERS, SPR etc., nanomaterials and microfluidic platforms have been developed for EV analysis. Compared to conventional methods, these techniques exhibited advantages in simplification of production, higher sensitivity for the analysis of EVs and portability in sensing platforms for point-of-care applications. With the progressive insight into EV biogenesis and analysis, EVs are becoming increasingly important in disease diagnosis as non-invasive circulating biomarkers and in disease therapeutics as nanodrug carriers. Despite the growing knowledge of EVs and progress in EV analysis and application, research on EVs is still in its infancy. Based on the research progresses and the remaining challenges in EV-related research, we describe what we consider to be key issues for future development.

Firstly, analysis of a particularly important vesicle component, the lipid, including the composition and function, will lead to new techniques for analysis and application in disease diagnosis. Compared to the available information on proteins and nucleic acids, knowledge on the lipid content is still limited. Yet lipids are essential molecular components of cells, as integral units of the cell membrane bilayers. To date research has shown that the lipid composition of EVs differs from the parental cells, however, the underlining sorting mechanisms is still unknown. In addition, the lipid composition of vesicles could be altered when culturing tumour cells in an acidic environment, mimicking the deep core of tumours. In addition, relationships between the lipid metabolism and central nervous system disorders has been demonstrated [152]. Further research in these areas would be particularly helpful to obtain insight into EV biogenesis and intracellular interactions [18]. Recently, it has been shown that the analysis of EV lipid content as a circulating biomarker could facilitate the diagnosis of diseases, such as blade cancer, Alzheimer's, and Parkinson's disease. Therefore, with the importance of lipids in vesicles starting to emerge, we anticipate an increasing number of studies based on lipid related EVs.

Secondly, emerging research interest have focused on investigating the roles of EVs in prokaryotes including parasites and bacteria. While, several studies have evaluated the biogenesis and types of vesicles related to parasites and bacteria, the area is still largely unexplored. Parasites exist everywhere, with a large number of notorious ones causing diseases in plants, animals and human beings. Scientists have made great effort to study parasites and made progress in understanding the pathological roles of EVs in affecting parasite-host interaction over recent years, which is particularly important in understanding parasite pathogenesis. However, there is still much to be understood including the nature of the cell machinery for the release and uptake of EVs, the mode of EVs transport to the destination, and whether blocking parasitic-EV secretion can influence disease progression etc. [53]. Further investigation on these issues will be helpful for developing novel strategies in diagnostics, intervention and effective control of parasite related diseases. In addition, bacteria can induce infectious diseases in humans and animals, and are harmful to the environment. Therefore, the important physiological roles of membrane vesicles may encourage future research into the ecological role and abundance of different vesicle types in the environment [57]. Recently, the innate immune mechanisms of host cells against the virulence of toxins induced from bacteria was investigated, which raised great interest in evaluating the interaction between bacteria toxin, exosomes and host cells [325]. Therefore, we envision that further insight into bacteria secreted EVs will contribute to the understanding of bacteria-induced diseases and related fields.

Thirdly, advanced techniques are required for single EV analysis due to the heterogeneity of EVs, which would be useful for understanding the heterogeneous biogenesis and molecular composition of different EVs by single EV profiling. To date, several approaches have been proposed for single EV analysis. Studies have demonstrated multiplexed single EV profiling using various strategies, for instance, flow cytometry, Raman tweezers, fluorescence microscopy (e.g. TIRF, confocal fluorescence microscopy) in combination with data processing are efficient in obtaining useful information. In addition, microfluidic systems provide suitable platforms for analysing these nanoscale vesicles. Nevertheless, it is still challenging to easily, rapidly and sensitively analyse single EV for clinical application due to the small size of exosomes and low instrumental sensitivity. The analysis of individual EVs could reveal the unique molecular information of EVs derived from specific cells, which will further promote the potential clinical application of these vesicles, therefore, future research efforts are desired for the develop-

ment of strategies that can meet the requirements for practical applications.

Fourthly, standardization of EV purification and analysis techniques, as well as specimen handling, appropriate normative controls are desired for further research on EV biochemistry and applications. The potential of these vehicles as biomarkers of disease and therapeutic targets have emerged prominently in the field of oncology. However, there remain many unsolved questions regarding EV biochemistry, for instance, the incomplete understanding of EV subtypes, the delivered cargo, and mechanisms of intercellular shuttling. Therefore, apart from the progress achieved in EV research, standardized isolation and analysis methods, and procedures for EVs are required to establish and guide EV-based diagnosis (liquid biopsy) or drug delivery [69].

Finally, combinatorial therapeutics will exert their role in achieving improved therapeutic outcomes. Over the past several decades, tremendous effort has been made towards the EV-based treatment of diseases, whilst more efficient therapy still needs to be developed to improve treatment outcomes. Such as taking advantage of EVs innate cargo loading capability, MSC-derived EVs could be loaded with drugs, which can achieve synergetic effects for specific diseases. In addition, by taking advantage of the rapid developments in nanotechnology, EVs carrying therapeutic drugs could be linked with functional nanoparticles to realize the destruction of tumour cells by chemotherapy, phototherapies, PDT or sonodynamic therapy, resulting in greatly enhanced therapeutic effect on diseases.

Declaration of Competing Interest

The authors declare that they have no known competing financial interests or personal relationships that could have appeared to influence the work reported in this paper.

Acknowledgements

This work was supported by Hainan Key Research and Development Project (Grant ZDYF2019130), National Natural Science Foundation of China (Nos. 21904030, 21775162 and 21864011), Hainan High- Level Talents Project (Grant 2019RC210 and 2019RC220), Hainan Higher Education Research Project (Nos. Hnky2019ZD-29, Hnky2019ZD-30 and Hnky2020-32), CAMS Innovation Fund for Medical Sciences (2019-I2M-5-023), Talent Program of Hainan Medical University (XRC180006, XRC190017, XRC180007 and XRC190025), Hundred-Talent Program of Hainan (2018) and Nanhai Young-Talent Program of Hainan (20202018 and 20202007). TDJ wishes to thank the Royal Society for a Wolfson Research Merit Award.

References

[1] C. Théry, L. Zitvogel, S. Amigorena, Nat. Rev. Immunol. 2 (2002) 569–579.
[2] G. Raposo, W. Stoorvogel, J. Cell. Biol. 200 (2013) 373–383.
[3] T.N. Ellis, M.J. Kuehn, Microbiol. Mol. Biol. Rev. 74 (2010) 81.
[4] G. Raposo, H.W. Nijman, W. Stoorvogel, R. Liejendekker, C.V. Harding, C.J. Melief, H.J. Geuze, J. Exp. Med. 183 (1996) 1161–1172.
[5] C. Théry, M. Ostrowski, E. Segura, Nat. Rev. Immunol. 9 (2009) 581–593.
[6] N. Chaput, C. Théry, Semin. Immunopathol. 33 (2011) 419–440.
[7] L. Balaj, R. Lessard, L. Dai, Y.-J. Cho, S.L. Pomeroy, X.O. Breakefield, J. Skog, Nat. Commun. 2 (2011) 180.
[8] J. Wolfers, A. Lozier, G. Raposo, A. Regnault, C. Théry, C. Masurier, C. Flament, S. Pouzieux, F. Faure, T. Tursz, E. Angevin, S. Amigorena, L. Zitvogel, Nat. Med. 7 (2001) 297–303.
[9] M. Tkach, C. Théry, Cell 164 (2016) 1226–1232.
[10] J. Skog, T. Würdinger, S. van Rijn, D.H. Meijer, L. Gainche, W.T. Curry, B.S. Carter, A.M. Krichevsky, X.O. Breakefield, Nat. Cell Biol. 10 (2008) 1470–1476.
[11] G. Morad, C.V. Carman, E.J. Hagedorn, J.R. Perlin, L.I. Zon, N. Mustafaoglu, T.E. Park, D.E. Ingber, C.C. Daisy, M.A. Moses, ACS Nano 13 (2019) 13853–13865.
[12] H. Wang, D. Jiang, W. Li, X. Xiang, J. Zhao, B. Yu, C. Wang, Z. He, L. Zhu, Y. Yang, Theranostics 9 (2019) 5347–5358.
[13] M. Hosseini, S. Khatamianfar, S.M. Hassanian, R. Nedaeinia, M. Shafiee, M. Maftouh, M. Ghayour-Mobarhan, S. ShahidSales, A. Avan, Curr. Pharm. Des. 23 (2017) 1705–1709.
[14] L. Zitvogel, A. Regnault, A. Lozier, J. Wolfers, C. Flament, D. Tenza, P. Ricciardi-Castagnoli, G. Raposo, S. Amigorena, Nat. Med. 4 (1998) 594–600.
[15] O.P.B. Wiklander, M.Á. Brennan, J. Lötvall, X.O. Breakefield, S. El Andaloussi, Sci. Transl. Med. 11 (2019) eaav8521.
[16] B. Yang, Y. Chen, J. Shi, Adv. Mater. 31 (2019) e1802896.
[17] N. Cheng, D. Du, X. Wang, D. Liu, W. Xu, Y. Luo, Y. Lin, Trends Biotechnol. (2019).
[18] M. Colombo, G. Raposo, C. Théry, Annu. Rev. Cell Dev. Biol. 30 (2014) 255–289.
[19] D.M. Pegtel, S.J. Gould, Annu. Rev. Biochem 88 (2019) 487–514.
[20] M. Mathieu, L. Martin-Jaular, G. Lavieu, C. Théry, Nat. Cell Biol. 21 (2019) 9–17.
[21] J. Kowal, G. Arras, M. Colombo, M. Jouve, J.P. Morath, B. Primdal-Bengtson, F. Dingli, D. Loew, M. Tkach, C. Théry, Proc. Natl. Acad. Sci. U. S. A. 113 (2016) E968.
[22] E. Willms, C. Cabañas, I. Mäger, M.J.A. Wood, P. Vader, Front. Immunol. 9 (2018).
[23] H. Zhang, D. Freitas, H.S. Kim, K. Fabijanic, Z. Li, H. Chen, M.T. Mark, H. Molina, A.B. Martin, L. Bojmar, J. Fang, S. Rampersaud, A. Hoshino, I. Matei, C.M. Kenific, M. Nakajima, A.P. Mutvei, P. Sansone, W. Buehring, H. Wang, J.P. Jimenez, L. Cohen-Gould, N. Paknejad, M. Brendel, K. Manova-Todorova, A. Magalhães, J.A. Ferreira, H. Osório, A.M. Silva, A. Massey, J.R. Cubillos-Ruiz, G. Galletti, P. Giannakakou, A.M. Cuervo, J. Blenis, R. Schwartz, M.S. Brady, H. Peinado, J. Bromberg, H. Matsui, C.A. Reis, D. Lyden, Nat. Cell Biol. 20 (2018) 332–343.
[24] Y. Yang, Y. Hong, E. Cho, G.B. Kim, I.S. Kim, J. Extracell, Vesicles 7 (2018) 1440131.
[25] J. Morhayim, M. Baroncelli, J.P.V. Leeuwen, Arch. Biochem. Biophys. 561 (2014) 38–45.
[26] S. El Andaloussi, I. Mäger, X.O. Breakefield, M.J.A. Wood, Nat. Rev. Drug Discov. 12 (2013) 347.
[27] E. Segura, S. Amigorena, C. Théry, Blood Cells Mol. Dis. 35 (2005) 89–93.
[28] A. Clayton, J.P. Mitchell, J. Court, M.D. Mason, Z. Tabi, Cancer Res. 67 (2007) 7458.
[29] G. Van Niel, G. Raposo, C. Candalh, M. Boussac, R. Hershberg, N. Cerf-Bensussan, M. Heyman, Gastroenterology 121 (2001) 337–349.
[30] V. Budnik, C. Ruiz-Cañada, F. Wendler, Nat. Rev. Neurosci. 17 (2016) 160.
[31] S. Wang, F. Cesca, G. Loers, M. Schweizer, F. Buck, F. Benfenati, M. Schachner, R. Kleene, J. Neurosci. 31 (2011) 7275.
[32] M. Chivet, F. Hemming, K. Pernet-Gallay, S. Fraboulet, R. Sadoul, Front. Physiol. 3 (2012) 145.
[33] L. Bagno, K.E. Hatzistergos, W. Balkan, J.M. Hare, Mol. Ther. 26 (2018) 1610–1623.
[34] Z. Zeng, Y. Li, Y. Pan, X. Lan, F. Song, J. Sun, K. Zhou, X. Liu, X. Ren, F. Wang, J. Hu, X. Zhu, W. Yang, W. Liao, G. Li, Y. Ding, L. Liang, Nat. Commun. 9 (2018) 5395.
[35] J.L. Hood, R.S. San, S.A. Wickline, Cancer Res. 71 (2011) 3792.
[36] R. Chen, X. Xu, Z. Qian, C. Zhang, Y. Niu, Z. Wang, J. Sun, X. Zhang, Y. Yu, Cell. Mol. Life Sci. 76 (2019) 4613–4633.
[37] I. Wortzel, S. Dror, C.M. Kenific, D. Lyden, Dev. Cell 49 (2019) 347–360.
[38] W. Feng, D.C. Dean, F.J. Hornicek, H. Shi, Z. Duan, Mol. Cancer 18 (2019) 124.
[39] H.-G. Zhang, W.E. Grizzle, Clin. Cancer Res. 17 (2011) 959–964.
[40] Z. Cai, F. Yang, L. Yu, Z. Yu, L. Jiang, Q. Wang, Y. Yang, L. Wang, X. Cao, J. Wang, J. Immunol. 188 (2012) 5954.
[41] M. Yang, J. Chen, F. Su, B. Yu, F. Su, L. Lin, Y. Liu, J.-D. Huang, E. Song, Mol. Cancer 10 (2011) 117.
[42] T. Huang, C. Song, L. Zheng, L. Xia, Y. Li, Y. Zhou, Mol. Cancer 18 (2019) 62.
[43] L. Zhang, S. Zhang, J. Yao, F.J. Lowery, Q. Zhang, W.-C. Huang, P. Li, M. Li, X. Wang, C. Zhang, H. Wang, K. Ellis, M. Cheerathodi, J.H. McCarty, D. Palmieri, J. Saunus, S. Lakhani, S. Huang, A.A. Sahin, K.D. Aldape, P.S. Steeg, D. Yu, Nature 527 (2015) 100–104.
[44] E. Emmanouilidou, K. Melachroinou, T. Roumeliotis, S.D. Garbis, M. Ntzouni, L.H. Margaritis, L. Stefanis, K. Vekrellis, J. Neurosci. 30 (2010) 6838–6851.
[45] S. Bellingham, B. Guo, B. Coleman, A. Hill, Front. Physiol. 3 (2012) 124.
[46] N. Perets, O. Betzer, R. Shapira, S. Brenstein, A. Angel, T. Sadan, U. Ashery, R. Popovtzer, D. Offen, Nano Lett. 19 (2019) 3422–3431.
[47] M. Mack, A. Kleinschmidt, H. Brühl, C. Klier, P.J. Nelson, J. Cihak, J. Plachý, M. Stangassinger, V. Erfle, D. Schlöndorff, Nat. Med. 6 (2000) 769–775.
[48] D.M. Pegtel, K. Cosmopoulos, D.A. Thorley-Lawson, M.A.J. van Eijndhoven, E.S. Hopmans, J.L. Lindenberg, T.D. de Gruijl, T. Würdinger, J.M. Middeldorp, Proc. Natl. Acad. Sci. U. S. A. 107 (2010) 6328–6333.
[49] A.H. Buck, G. Coakley, F. Simbari, H.J. McSorley, J.F. Quintana, T. Le Bihan, S. Kumar, C. Abreu-Goodger, M. Lear, Y. Harcus, A. Ceroni, S.A. Babayan, M. Blaxter, A. Ivens, R.M. Maizels, Nat. Commun. 5 (2014) 5488.
[50] A.J. Szempruch, L. Dennison, R. Kieft, J.M. Harrington, S.L. Hajduk, Nat. Rev. Microbiol. 14 (2016) 669.
[51] J. Liu, L. Zhu, J. Wang, L. Qiu, Y. Chen, R.E. Davis, G. Cheng, PLoS Pathog. 15 (2019) e1007817.
[52] E.P. Hansen, B. Fromm, S.D. Andersen, A. Marcilla, K.L. Andersen, A. Borup, A.R. Williams, A.R. Jex, R.B. Gasser, N.D. Young, R.S. Hall, A. Stensballe, V. Ovchinnikov, Y. Yan, M. Fredholm, S.M. Thamsborg, P. Nejsum, J. Extracell, Vesicles 8 (2019) 1578116.
[53] Y. Ofir-Birin, N. Regev-Rudzki, Science 363 (2019) 817.
[54] C. Schwechheimer, M.J. Kuehn, Nat. Rev. Microbiol. 13 (2015) 605–619.

[55] X. Wang, W.J. Eagen, J.C. Lee, Proc. Natl. Acad. Sci. U. S. A. 117 (2020) 3174.
[56] S.J. Biller, F. Schubotz, S.E. Roggensack, A.W. Thompson, R.E. Summons, S.W. Chisholm, Science 343 (2014) 183–186.
[57] M. Toyofuku, N. Nomura, L. Eberl, Nat. Rev. Microbiol. 17 (2019) 13–24.
[58] V. Hyenne, S. Ghoroghi, M. Collot, J. Bons, G. Follain, S. Harlepp, B. Mary, J. Bauer, L. Mercier, I. Busnelli, O. Lefebvre, N. Fekonja, M.J. Garcia-Leon, P. Machado, F. Delalande, A.A. López, S.G. Silva, F.J. Verweij, G. van Niel, F. Djouad, H. Peinado, C. Carapito, A.S. Klymchenko, J.G. Goetz, Dev. Cell 48 (2019) 554–572.e7.
[59] K.E. van der Vos, E.R. Abels, X. Zhang, C. Lai, E. Carrizosa, D. Oakley, S. Prabhakar, O. Mardini, M.H.W. Crommentuijn, J. Skog, A.M. Krichevsky, A. Stemmer-Rachamimov, T.R. Mempel, J. El Khoury, S.E. Hickman, X.O. Breakefield, Neuro Oncol. 18 (2015) 58–69.
[60] H. Cao, Z. Yue, H. Gao, C. Chen, K. Cui, K. Zhang, Y. Cheng, G. Shao, D. Kong, Z. Li, D. Ding, Y. Wang, ACS Nano 13 (2019) 3522–3533.
[61] P. Zhang, B. Dong, E. Zeng, F. Wang, Y. Jiang, D. Li, D. Liu, Anal. Chem. 90 (2018) 11273–11279.
[62] C.P. Lai, E.Y. Kim, C.E. Badr, R. Weissleder, T.R. Mempel, B.A. Tannous, X.O. Breakefield, Nat. Commun. 6 (2015) 7029.
[63] R. White, K. Rose, L. Zon, Nat. Rev. Cancer 13 (2013) 624–636.
[64] F.J. Verweij, V. Hyenne, G. Van Niel, J.G. Goetz, Trends Cell Biol. 29 (2019) 770–776.
[65] F.J. Verweij, C. Revenu, G. Arras, F. Dingli, D. Loew, D.M. Pegtel, G. Follain, G. Allio, J.G. Goetz, P. Zimmermann, P. Herbomel, F. Del Bene, G. Raposo, G. van Niel, Dev. Cell 48 (2019) 573–589.e4.
[66] M. Collot, P. Ashokkumar, H. Anton, E. Boutant, O. Faklaris, T. Galli, Y. Mély, L. Danglot, A.S. Klymchenko, Cell, Chem. Biol. 26 (2019) 600–614.e7.
[67] P. Li, M. Kaslan, S.H. Lee, J. Yao, Z. Gao, Theranostics 7 (2017) 789–804.
[68] M.L. Merchant, I.M. Rood, J.K.J. Deegens, J.B. Klein, Nat. Rev. Nephrol. 13 (2017) 731.
[69] F.A.W. Coumans, A.R. Brisson, E.I. Buzas, F. Dignat-George, E.E.E. Drees, S. El-Andaloussi, C. Emanueli, A. Gasecka, A. Hendrix, A.F. Hill, R. Lacroix, Y. Lee, T. G. van Leeuwen, N. Mackman, I. Mager, J.P. Nolan, E. van der Pol, D.M. Pegtel, S. Sahoo, P.R.M. Siljander, G. Sturk, O. de Wever, R. Nieuwland, Circ. Res. 120 (2017) 1632–1648.
[70] X.-X. Yang, C. Sun, L. Wang, X.-L. Guo, J. Control. Release 308 (2019) 119–129.
[71] C. Gardiner, D.D. Vizio, S. Sahoo, C. Théry, K.W. Witwer, M. Wauben, A.F. Hill, J. Extracell, Vesicles 5 (2016) 32945.
[72] D. Freitas, M. Balmaña, J. Poças, D. Campos, H. Osório, A. Konstantinidi, S.Y. Vakhrushev, A. Magalhães, C.A. Reis, J. Extracell, Vesicles 8 (2019) 1621131.
[73] C. Théry, S. Amigorena, G. Raposo, A. Clayton, Curr. Protoc. Cell Biol., 30 (2006) 3.22.21-3.22.29.
[74] D. Wang, W. Sun, Proteomics 14 (2014) 1922–1932.
[75] W. Mao, Y. Wen, H. Lei, R. Lu, S. Wang, Y. Wang, R. Chen, Y. Gu, L. Zhu, K.K. Abhange, Z.J. Quinn, Y. Chen, F. Xue, M. Zheng, Y. Wan, Anal. Chem. 91 (2019) 13729–13736.
[76] J.Z. Nordin, Y. Lee, P. Vader, I. Mäger, H.J. Johansson, W. Heusermann, O.P.B. Wiklander, M. Hällbrink, Y. Seow, J.J. Bultema, J. Gilthorpe, T. Davies, P.J. Fairchild, S. Gabrielsson, N.C. Meisner-Kober, J. Lehtiö, C.I.E. Smith, M.J.A. Wood, S.E.L. Andaloussi, Nanomed. Nanotechnol. Biol. Med. 11 (2015) 879–883.
[77] J. Chen, Y. Xu, Y. Lu, W. Xing, Anal. Chem. 90 (2018) 14207–14215.
[78] S. Cai, B. Luo, P. Jiang, X. Zhou, F. Lan, Q. Yi, Y. Wu, Nanoscale 10 (2018) 14280–14289.
[79] Š. Sitar, A. Kejžar, D. Pahovnik, K. Kogej, M. Tušek-Žnidarič, M. Lenassi, E. Žagar, Anal. Chem. 87 (2015) 9225–9233.
[80] H. Zhang, D. Lyden, Nat. Protoc. 14 (2019) 1027–1053.
[81] A. Ku, H.C. Lim, M. Evander, H. Lilja, T. Laurell, S. Scheding, Y. Ceder, Anal. Chem. 90 (2018) 8011–8019.
[82] H. Kim, K.H. Lee, S.I. Han, D. Lee, S. Chung, D. Lee, J.H. Lee, Lab Chip 19 (2019) 3917–3921.
[83] H.K. Woo, V. Sunkara, J. Park, T.H. Kim, J.R. Han, C.J. Kim, H.I. Choi, Y.K. Kim, Y. K. Cho, ACS Nano 11 (2017) 1360–1370.
[84] R.T. Davies, J. Kim, S.C. Jang, E.-J. Choi, Y.S. Gho, J. Park, Lab Chip 12 (2012) 5202–5210.
[85] B.H. Wunsch, J.T. Smith, S.M. Gifford, C. Wang, M. Brink, R.L. Bruce, R.H. Austin, G. Stolovitzky, Y. Astier, Nat. Nanotechnol. 11 (2016) 936.
[86] H. Jeong, H. Shin, J. Yi, Y. Park, J. Lee, Y. Gianchandani, J. Park, Lab Chip 19 (2019) 3326–3336.
[87] C. Liu, J. Guo, F. Tian, N. Yang, F. Yan, Y. Ding, J. Wei, G. Hu, G. Nie, J. Sun, ACS Nano 11 (2017) 6968–6976.
[88] M. Wu, Y. Ouyang, Z. Wang, R. Zhang, P.-H. Huang, C. Chen, H. Li, P. Li, D. Quinn, M. Dao, S. Suresh, Y. Sadovsky, T.J. Huang, Proc. Natl. Acad. Sci. U. S. A. 114 (2017) 10584.
[89] J.C. Contreras-Naranjo, H.J. Wu, V.M. Ugaz, Lab Chip 17 (2017) 3558–3577.
[90] H. Xu, C. Liao, P. Zuo, Z. Liu, B.-C. Ye, Anal. Chem. 90 (2018) 13451–13458.
[91] E. Reátegui, K.E. van der Vos, C.P. Lai, M. Zeinali, N.A. Atai, B. Aldikacti, F.P. Floyd, A.H. Khankhel, V. Thapar, F.H. Hochberg, L.V. Sequist, B.V. Nahed, B.S. Carter, M. Toner, L. Balaj, D.T. Ting, X.O. Breakefield, S.L. Stott, Nat. Commun. 9 (2018) 175.
[92] C.L. Hisey, K.D.P. Dorayappan, D.E. Cohn, K. Selvendiran, D.J. Hansford, Lab Chip 18 (2018) 3144–3153.
[93] J. Wang, W. Li, L. Zhang, L. Ban, P. Chen, W. Du, X. Feng, B.-F. Liu, A.C.S. Appl, Mater. & Interfaces 9 (2017) 27441–27452.
[94] J. Dong, R.Y. Zhang, N. Sun, M. Smalley, Z. Wu, A. Zhou, S.-J. Chou, Y.J. Jan, P. Yang, L. Bao, D. Qi, X. Tang, P. Tseng, Y. Hua, D. Xu, R. Kao, M. Meng, X. Zheng, Y. Liu, T. Vagner, X. Chai, D. Zhou, M. Li, S.-H. Chiou, G. Zheng, D. Di Vizio, V.G. Agopian, E. Posadas, S.J. Jonas, S.-P. Ju, P.S. Weiss, M. Zhao, H.-R. Tseng, Y. Zhu, A.C.S. Appl, Mater. & Interfaces 11 (2019) 13973–13983.
[95] M. He, J. Crow, M. Roth, Y. Zeng, A.K. Godwin, Lab Chip 14 (2014) 3773–3780.
[96] Z. Zhao, Y. Yang, Y. Zeng, M. He, Lab Chip 16 (2016) 489–496.
[97] F. Gao, F. Jiao, C. Xia, Y. Zhao, W. Ying, Y. Xie, X. Guan, M. Tao, Y. Zhang, W. Qin, X. Qian, Chem. Sci. 10 (2019) 1579–1588.
[98] A. Liga, A.D.B. Vliegenthart, W. Oosthuyzen, J.W. Dear, M. Kersaudy-Kerhoas, Lab Chip 15 (2015) 2388–2394.
[99] C. Liu, Q. Feng, J. Sun, Adv. Mater. (2018) e1804788.
[100] F. Yang, X. Liao, Y. Tian, G. Li, Biotechnol. J. 12 (2017) 1600699.
[101] Y.S. Chen, Y.D. Ma, C. Chen, S.C. Shiesh, G.B. Lee, Lab Chip 19 (2019) 3305–3315.
[102] Z. Wang, H.-J. Wu, D. Fine, J. Schmulen, Y. Hu, B. Godin, J.X.J. Zhang, X. Liu, Lab Chip 13 (2013) 2879–2882.
[103] X. Dong, J. Chi, L. Zheng, B. Ma, Z. Li, S. Wang, C. Zhao, H. Liu, Lab Chip 19 (2019) 2897–2904.
[104] J. Rho, J. Chung, H. Im, M. Liong, H. Shao, C.M. Castro, R. Weissleder, H. Lee, ACS Nano 7 (2013) 11227–11233.
[105] K. Lee, H. Shao, R. Weissleder, H. Lee, ACS Nano 9 (2015) 2321–2327.
[106] C. Chen, J. Skog, C.-H. Hsu, R.T. Lessard, L. Balaj, T. Wurdinger, B.S. Carter, X.O. Breakefield, M. Toner, D. Irimia, Lab Chip 10 (2010) 505–511.
[107] C. Wang, D. Jin, Y. Yu, L. Tang, Y. Sun, Z. Sun, G.-J. Zhang, Sens. Actuators B Chem. 314 (2020) 128056.
[108] H. Shao, J. Chung, K. Lee, L. Balaj, C. Min, B.S. Carter, F.H. Hochberg, X.O. Breakefield, H. Lee, R. Weissleder, Nat. Commun. 6 (2015) 6999.
[109] Y.-T. Kang, E. Purcell, C. Palacios-Rolston, T.-W. Lo, N. Ramnath, S. Jolly, S. Nagrath, Small 15 (2019) 1903600.
[110] S.D. Ibsen, J. Wright, J.M. Lewis, S. Kim, S.-Y. Ko, J. Ong, S. Manouchehri, A. Vyas, J. Akers, C.C. Chen, B.S. Carter, S.C. Esener, M.J. Heller, ACS Nano 11 (2017) 6641–6651.
[111] K.W. Witwer, E.I. Buzás, L.T. Bemis, A. Bora, C. Lässer, J. Lötvall, E.N. Nolte-'t Hoen, M.G. Piper, S. Sivaraman, J. Skog, C. Théry, M.H. Wauben, F. Hochberg, J. Extracell. Vesicles, 2 (2013) 20360.
[112] V. Sokolova, A.-K. Ludwig, S. Hornung, O. Rotan, P.A. Horn, M. Epple, B. Giebel, Colloids Surf. B. Biointerfaces 87 (2011) 146–150.
[113] H. Shao, J. Chung, L. Balaj, A. Charest, D.D. Bigner, B.S. Carter, F.H. Hochberg, X. O. Breakefield, R. Weissleder, H. Lee, Nat. Med. 18 (2012) 1835–1840.
[114] J. Hakulinen, L. Sankkila, N. Sugiyama, K. Lehti, J. Keski-Oja, J. Cell. Biochem. 105 (2008) 1211–1218.
[115] Y. Yuana, R.I. Koning, M.E. Kuil, P.C.N. Rensen, A.J. Koster, R.M. Bertina, S. Osanto, J. Extracell, Vesicles 2 (2013) 21494.
[116] S. Sharma, H.I. Rasool, V. Palanisamy, C. Mathisen, M. Schmidt, D.T. Wong, J.K. Gimzewski, ACS Nano 4 (2010) 1921–1926.
[117] C. Gardiner, Y.J. Ferreira, R.A. Dragovic, C.W.G. Redman, I.L. Sargent, J. Extracell, Vesicles 2 (2013) 19671.
[118] Z. Varga, Y. Yuana, A.E. Grootemaat, E. van der Pol, C. Gollwitzer, M. Krumrey, R. Nieuwland, J. Extracell, Vesicles 3 (2014) 23298.
[119] M. Gao, F. Yu, C. Lv, J. Choo, L. Chen, Chem. Soc. Rev. 46 (2017) 2237–2271.
[120] Y. Zou, M. Li, Y. Xing, T. Duan, X. Zhou, F. Yu, ACS Sens. 5 (2020) 242–249.
[121] H. Zong, J. Peng, X.-R. Li, M. Liu, Y. Hu, J. Li, Y. Zang, X. Li, T.D. James, Chem. Commun. 56 (2020) 515–518.
[122] M.E. Shirbhate, S. Kwon, A. Song, S. Kim, D. Kim, H. Huang, Y. Kim, H. Lee, S.-J. Kim, M.-H. Baik, J. Yoon, K.M. Kim, J. Am. Chem. Soc. 142 (2020) 4975–4979.
[123] S. Xu, H.-W. Liu, L. Chen, J. Yuan, Y. Liu, L. Teng, S.-Y. Huan, L. Yuan, X.-B. Zhang, W. Tan, J. Am. Chem. Soc. 142 (2020) 2129–2133.
[124] Y. Yoshioka, N. Kosaka, Y. Konishi, H. Ohta, H. Okamoto, H. Sonoda, R. Nonaka, H. Yamamoto, H. Ishii, M. Mori, K. Furuta, T. Nakajima, H. Hayashi, H. Sugisaki, H. Higashimoto, T. Kato, F. Takeshita, T. Ochiya, Nat. Commun. 5 (2014) 3591.
[125] K. Mori, M. Hirase, T. Morishige, E. Takano, H. Sunayama, Y. Kitayama, S. Inubushi, R. Sasaki, M. Yashiro, T. Takeuchi, Angew. Chem. Int. Ed. 58 (2019) 1612–1615.
[126] T. Takeuchi, K. Mori, H. Sunayama, E. Takano, Y. Kitayama, T. Shimizu, Y. Hirose, S. Inubushi, R. Sasaki, H. Tanino, J. Am. Chem. Soc. 142 (2020) 6617–6624.
[127] Y. Ji, D. Qi, L. Li, H. Su, X. Li, Y. Luo, B. Sun, F. Zhang, B. Lin, T. Liu, Y. Lu, Proc. Natl. Acad. Sci. U. S. A. 116 (2019) 5979.
[128] Z. Zhang, C. Tang, L. Zhao, L. Xu, W. Zhou, Z. Dong, Y. Yang, Q. Xie, X. Fang, Nanoscale 11 (2019) 10106–10113.
[129] J. Zhou, J. Rossi, Nat. Rev. Drug Discov. 16 (2017) 181–202.
[130] X. Yu, L. He, M. Pentok, H. Yang, Y. Yang, Z. Li, N. He, Y. Deng, S. Li, T. Liu, X. Chen, H. Luo, Nanoscale 11 (2019) 15589–15595.
[131] C. Liu, J. Zhao, F. Tian, L. Cai, W. Zhang, Q. Feng, J. Chang, F. Wan, Y. Yang, B. Dai, Y. Cong, B. Ding, J. Sun, W. Tan, Nat. Biomed. Eng. 3 (2019) 183–193.
[132] P. Reineck, C.J. Wienken, D. Braun, Electrophoresis 31 (2010) 279–286.
[133] M. Huang, J. Yang, T. Wang, J. Song, J. Xia, L. Wu, W. Wang, Q. Wu, Z. Zhu, Y. Song, C. Yang, Angew. Chem. Int. Ed. 59 (2020) 4800–4805.
[134] Y. Xing, A. Wyss, N. Esser, P.S. Dittrich, Analyst 140 (2015) 7896–7901.
[135] Y. Xing, N. Esser, P.S. Dittrich, J. Mater. Chem. C 4 (2016) 9235–9244.
[136] Y. Xing, G. Sun, E. Speiser, N. Esser, P.S. Dittrich, A.C.S. Appl, Mater. & Interfaces 9 (2017) 17271–17278.
[137] P. Zhang, X. Zhou, M. He, Y. Shang, A.L. Tetlow, A.K. Godwin, Y. Zeng, Nat. Biomed. Eng. 3 (2019) 438–451.
[138] S.S. Kanwar, C.J. Dunlay, D.M. Simeone, S. Nagrath, Lab Chip 14 (2014) 1891–1900.

[139] Z. Wei, A.O. Batagov, S. Schinelli, J. Wang, Y. Wang, R. El Fatimy, R. Rabinovsky, L. Balaj, C.C. Chen, F. Hochberg, B. Carter, X.O. Breakefield, A.M. Krichevsky, Nat. Commun. 8 (2017) 1145.
[140] J.R. Chevillet, Q. Kang, I.K. Ruf, H.A. Briggs, L.N. Vojtech, S.M. Hughes, H.H. Cheng, J.D. Arroyo, E.K. Meredith, E.N. Gallichotte, E.L. Pogosova-Agadjanyan, C. Morrissey, D.L. Stirewalt, F. Hladik, E.Y. Yu, C.S. Higano, M. Tewari, Proc. Natl. Acad. Sci. U. S. A. 111 (2014) 14888–14893.
[141] D.P. Joyce, M.J. Kerin, R.M. Dwyer, Int. J. Cancer 139 (2016) 1443–1448.
[142] T. Matsumura, K. Sugimachi, H. Iinuma, Y. Takahashi, J. Kurashige, G. Sawada, M. Ueda, R. Uchi, H. Ueo, Y. Takano, Y. Shinden, H. Eguchi, H. Yamamoto, Y. Doki, M. Mori, T. Ochiya, K. Mimori, Br. J. Cancer 113 (2015) 275–281.
[143] J. Zhang, L.-L. Wang, M.-F. Hou, Y.-K. Xia, W.-H. He, A. Yan, Y.-P. Weng, L.-P. Zeng, J.-H. Chen, Biosens. Bioelectron. 102 (2018) 33–40.
[144] Y. Xia, L. Wang, J. Li, X. Chen, J. Lan, A. Yan, Y. Lei, S. Yang, H. Yang, J. Chen, Anal. Chem. 90 (2018) 8969–8976.
[145] X. Gao, S. Li, F. Ding, H. Fan, L. Shi, L. Zhu, J. Li, J. Feng, X. Zhu, C. Zhang, Angew. Chem. Int. Ed. 58 (2019) 8719–8723.
[146] H.J. Oh, J. Kim, H. Park, S. Chung, D.W. Hwang, D.S. Lee, Biosens. Bioelectron. 126 (2019) 647–656.
[147] J. Zhao, C. Liu, Y. Li, Y. Ma, J. Deng, L. Li, J. Sun, J. Am. Chem. Soc. 142 (2020) 4996–5001.
[148] S. Cho, H.C. Yang, W.J. Rhee, Biosens. Bioelectron. 146 (2019) 111749.
[149] A. Llorente, T. Skotland, T. Sylvänne, D. Kauhanen, T. Róg, A. Orłowski, I. Vattulainen, K. Ekroos, K. Sandvig, Biochim. Biophys. Acta 1831 (2013) 1302–1309.
[150] T. Skotland, K. Sandvig, A. Llorente, Prog. Lipid Res. 66 (2017) 30–41.
[151] I. Parolini, C. Federici, C. Raggi, L. Lugini, S. Palleschi, A.D. Milito, C. Coscia, E. Iessi, M. Logozzi, A. Molinari, M. Colone, M. Tatti, M. Sargiacomo and S. Fais, J. Biol. Chem., 284 (2009) 34211-34222.
[152] S. Vanherle, M. Haidar, J. Irobi, J.F.J. Bogie, J.J.A. Hendriks, Adv. Drug Del. Rev. (2020), https://doi.org/10.1016/j.addr.2020.1004.1011.
[153] T. Skotland, K. Sagini, K. Sandvig, A. Llorente, Adv. Drug Del. Rev. (2020), https://doi.org/10.1016/j.addr.2020.1003.1002.
[154] E. Sezgin, T. Sadowski, K. Simons, Langmuir 30 (2014) 8160–8166.
[155] R. Subiros-Funosas, L. Mendive-Tapia, J. Sot, J.D. Pound, N. Barth, Y. Varela, F. M. Goñi, M. Paterson, C.D. Gregory, F. Albericio, I. Dransfield, R. Lavilla, M. Vendrell, Chem. Commun. 53 (2017) 945–948.
[156] D. Gill, R.G. Kilponen, L. Rimai, Nature 227 (1970) 743–744.
[157] Y. Zhang, X. Mi, X. Tan, R. Xiang, Theranostics 9 (2019) 491–525.
[158] F. Lavialle, S. Deshayes, F. Gonnet, E. Larquet, S.G. Kruglik, N. Boisset, R. Daniel, A. Alfsen, I. Tatischeff, Int. J. Pharm. 380 (2009) 206–215.
[159] I. Tatischeff, E. Larquet, J.M. Falcón-Pérez, P.Y. Turpin, S.G. Kruglik, J. Extracell, Vesicles 1 (2012) 19179.
[160] A. Gualerzi, S. Niada, C. Giannasi, S. Picciolini, C. Morasso, R. Vanna, V. Rossella, M. Masserini, M. Bedoni, F. Ciceri, M.E. Bernardo, A.T. Brini, F. Gramatica, Sci. Rep. 7 (2017) 9820.
[161] A. Gualerzi, S.A.A. Kooijmans, S. Niada, S. Picciolini, A.T. Brini, G. Camussi, M. Bedoni, J. Extracell, Vesicles 8 (2019) 1568780.
[162] W. Lee, A. Nanou, L. Rikkert, F.A.W. Coumans, H.L. Offerhaus, Anal. Chem. 90 (2018) 11290–11296.
[163] M. Roman, A. Kamińska, A. Drożdż, M. Platt, M. Kuźniewski, M.T. Małecki, W. M. Kwiatek, C. Paluszkiewicz, E.Ł. Stępień, Nanomed. Nanotechnol. Biol. Med. 17 (2019) 137–149.
[164] J. Langer, D. Jimenez de Aberasturi, J. Aizpurua, R.A. Alvarez-Puebla, B. Auguié, J.J. Baumberg, G.C. Bazan, S.E.J. Bell, A. Boisen, A.G. Brolo, J. Choo, D. Cialla-May, V. Deckert, L. Fabris, K. Faulds, F.J. García de Abajo, R. Goodacre, D. Graham, A.J. Haes, C.L. Haynes, C. Huck, T. Itoh, M. Käll, J. Kneipp, N.A. Kotov, H. Kuang, E.C. Le Ru, H.K. Lee, J.-F. Li, X.Y. Ling, S.A. Maier, T. Mayerhöfer, M. Moskovits, K. Murakoshi, J.-M. Nam, S. Nie, Y. Ozaki, I. Pastoriza-Santos, J. Perez-Juste, J. Popp, A. Pucci, S. Reich, B. Ren, G.C. Schatz, T. Shegai, S. Schlücker, L.-L. Tay, K.G. Thomas, Z.-Q. Tian, R.P. Van Duyne, T. Vo-Dinh, Y. Wang, K.A. Willets, C. Xu, H. Xu, Y. Xu, Y.S. Yamamoto, B. Zhao, L.M. Liz-Marzán, ACS Nano 14 (2020) 28–117.
[165] L. Tirinato, F. Gentile, D. Di Mascolo, M.L. Coluccio, G. Das, C. Liberale, S.A. Pullano, G. Perozziello, M. Francardi, A. Accardo, F. De Angelis, P. Candeloro, E. Di Fabrizio, Microelectron. Eng. 97 (2012) 337–340.
[166] C. Lee, R.P. Carney, S. Hazari, Z.J. Smith, A. Knudson, C.S. Robertson, K.S. Lam, S. Wachsmann-Hogiu, Nanoscale 7 (2015) 9290–9297.
[167] C. Lee, R. Carney, K. Lam, J.W. Chan, J. Raman Spectrosc. 48 (2017) 1771–1776.
[168] M. Avella-Oliver, R. Puchades, S. Wachsmann-Hogiu, A. Maquieira, Sens. Actuators B Chem. 252 (2017) 657–662.
[169] J. Park, M. Hwang, B. Choi, H. Jeong, J.H. Jung, H.K. Kim, S. Hong, J.H. Park, Y. Choi, Anal. Chem. 89 (2017) 6695–6701.
[170] H. Shin, H. Jeong, J. Park, S. Hong, Y. Choi, ACS Sens. 3 (2018) 2637–2643.
[171] H. Shin, S. Oh, S. Hong, M. Kang, D. Kang, Y.-G. Ji, B.H. Choi, K.-W. Kang, H. Jeong, Y. Park, S. Hong, H.K. Kim, Y. Choi, ACS Nano 14 (2020) 5435–5444.
[172] J. Carmicheal, C. Hayashi, X. Huang, L. Liu, Y. Lu, A. Krasnoslobodtsev, A. Lushnikov, P.G. Kshirsagar, A. Patel, M. Jain, Y.L. Lyubchenko, Y. Lu, S.K. Batra, S. Kaur, Nanomedicine 16 (2019) 88–96.
[173] Y. Wang, B. Yan, L. Chen, Chem. Rev. 113 (2013) 1391–1428.
[174] G. McNay, D. Eustace, W.E. Smith, K. Faulds, D. Graham, Appl. Spectrosc. 65 (2011) 825–837.
[175] M.D. Porter, R.J. Lipert, L.M. Siperko, G. Wang, R. Narayanan, Chem. Soc. Rev. 37 (2008) 1001–1011.
[176] S. Zong, L. Wang, C. Chen, J. Lu, D. Zhu, Y. Zhang, Z. Wang, Y. Cui, Anal. Methods 8 (2016) 5001–5008.
[177] Y. Pang, J. Shi, X. Yang, C. Wang, Z. Sun, R. Xiao, Biosens. Bioelectron. 148 (2020) 111800.
[178] E.A. Kwizera, R. O'Connor, V. Vinduska, M. Williams, E.R. Butch, S.E. Snyder, X. Chen, X. Huang, Theranostics 8 (2018) 2722–2738.
[179] T.-D. Li, R. Zhang, H. Chen, Z.-P. Huang, X. Ye, H. Wang, A.-M. Deng, J.-L. Kong, Chem. Sci. 9 (2018) 5372–5382.
[180] L. Qi, M. Xiao, X. Wang, C. Wang, L. Wang, S. Song, X. Qu, L. Li, J. Shi, H. Pei, Anal. Chem. 89 (2017) 9850–9856.
[181] D. Ma, C. Huang, J. Zheng, J. Tang, J. Li, J. Yang, R. Yang, Biosens. Bioelectron. 101 (2018) 167–173.
[182] W. Zhou, Y.-F. Tian, B.-C. Yin, B.-C. Ye, Anal. Chem. 89 (2017) 6120–6128.
[183] Y. Wu, Y. He, X. Yang, R. Yuan, Y. Chai, Sensors Actuators B: Chem. 275 (2018) 260–266.
[184] J.U. Lee, W.H. Kim, H.S. Lee, K.H. Park, S.J. Sim, Small 15 (2019) 1804968.
[185] Y. Pang, C. Wang, L. Lu, C. Wang, Z. Sun, R. Xiao, Biosens. Bioelectron. 130 (2019) 204–213.
[186] J. Homola, Chem. Rev. 108 (2008) 462–493.
[187] L. Zhu, K. Wang, J. Cui, H. Liu, X. Bu, H. Ma, W. Wang, H. Gong, C. Lausted, L. Hood, G. Yang, Z. Hu, Anal. Chem. 86 (2014) 8857–8864.
[188] S. Picciolini, A. Gualerzi, R. Vanna, A. Sguassero, F. Gramatica, M. Bedoni, M. Masserini, C. Morasso, Anal. Chem. 90 (2018) 8873–8880.
[189] Q. Wang, L. Zou, X. Yang, X. Liu, W. Nie, Y. Zheng, Q. Cheng, K. Wang, Biosens. Bioelectron. 135 (2019) 129–136.
[190] H. Im, H. Shao, Y.I. Park, V.M. Peterson, C.M. Castro, R. Weissleder, H. Lee, Nat. Biotechnol. 32 (2014) 490–495.
[191] G. Qiu, A. Thakur, C. Xu, S.-P. Ng, Y. Lee, C.-M.L. Wu, Adv. Funct. Mater. 29 (2019) 1806761.
[192] S. Jeong, J. Park, D. Pathania, C.M. Castro, R. Weissleder, H. Lee, ACS Nano 10 (2016) 1802–1809.
[193] R. Huang, L. He, Y. Xia, H. Xu, C. Liu, H. Xie, S. Wang, L. Peng, Y. Liu, Y. Liu, N. He, Z. Li, Small 15 (2019) 1900735.
[194] Y. Yu, Y.T. Li, D. Jin, F. Yang, D. Wu, M.M. Xiao, H. Zhang, Z.Y. Zhang, G.J. Zhang, Anal. Chem. 91 (2019) 10679–10686.
[195] H. Zhang, Z. Wang, F. Wang, Y. Zhang, H. Wang, Y. Liu, Anal. Chem. 92 (2020) 5546–5553.
[196] J. Park, H.-Y. Lin, J.P. Assaker, S. Jeong, C.-H. Huang, A. Kurdi, K. Lee, K. Fraser, C. Min, S. Eskandari, S. Routray, B. Tannous, R. Abdi, L. Riella, A. Chandraker, C. M. Castro, R. Weissleder, H. Lee, J.R. Azzi, ACS Nano 11 (2017) 11041–11046.
[197] X. Yin, T. Hou, B. Huang, L. Yang, F. Li, Chem. Commun. 55 (2019) 13705–13708.
[198] Y. An, T. Jin, Y. Zhu, F. Zhang, P. He, Biosens. Bioelectron. 142 (2019) 111503.
[199] Y. Cao, L. Li, B. Han, Y. Wang, Y. Dai, J. Zhao, Biosens. Bioelectron. 141 (2019) 111397.
[200] Z. Chen, S.-B. Cheng, P. Cao, Q.-F. Qiu, Y. Chen, M. Xie, Y. Xu, W.-H. Huang, Biosens. Bioelectron. 122 (2018) 211–216.
[201] X. Chen, J. Lan, Y. Liu, L. Li, L. Yan, Y. Xia, F. Wu, C. Li, S. Li, J. Chen, Biosens. Bioelectron. 102 (2018) 582–588.
[202] F. Zhu, D. Li, Q. Ding, C. Lei, L. Ren, X. Ding, X. Sun, Biosens. Bioelectron. 147 (2019) 111787.
[203] H.-Q. Nguyen, D. Lee, Y. Kim, M. Paek, M. Kim, K.-S. Jang, J. Oh, Y.-S. Lee, J.E. Yeon, D.M. Lubman, J. Kim, Anal. Chem. 91 (2019) 13297–13305.
[204] A. Gyuris, J. Navarrete-Perea, A. Jo, S. Cristea, S. Zhou, K. Fraser, Z. Wei, A.M. Krichevsky, R. Weissleder, H. Lee, S.P. Gygi, A. Charest, Cell Rep. 27 (2019) 3972–3987.e6.
[205] E.J. van der Vlist, E.N.M. Nolte-'t Hoen, W. Stoorvogel, G.J.A. Arkesteijn, M.H. M. Wauben, Nat. Protoc., 7 (2012) 1311.
[206] E.N.M.N.-t. Hoen, E.J. van der Vlist, M. Aalberts, H.C.H. Mertens, B.J. Bosch, W. Bartelink, E. Mastrobattista, E.V.B. van Gaal, W. Stoorvogel, G.J.A. Arkesteijn, M.H.M. Wauben, Nanomed. Nanotechnol. Biol. Med., 8 (2012) 712-720.
[207] A. Görgens, M. Bremer, R. Ferrer-Tur, F. Murke, T. Tertel, P.A. Horn, S. Thalmann, J.A. Welsh, C. Probst, C. Guerin, C.M. Boulanger, J.C. Jones, H. Hanenberg, U. Erdbrügger, J. Lannigan, F.L. Ricklefs, S. El-Andaloussi, B. Giebel, J. Extracell, Vesicles 8 (2019) 1587567.
[208] F.L. Ricklefs, C.L. Maire, R. Reimer, L. Duhrsen, K. Kolbe, M. Holz, E. Schneider, A. Rissiek, A. Babayan, C. Hille, K. Pantel, S. Krasemann, M. Glatzel, D.H. Heiland, J. Flitsch, T. Martens, N.O. Schmidt, S. Peine, X.O. Breakefield, S. Lawler, E.A. Chiocca, B. Fehse, B. Giebel, A. Gorgens, M. Westphal, K. Lamszus, J. Extracell, Vesicles 8 (2019) 1588555.
[209] D. Choi, L. Montermini, H. Jeong, S. Sharma, B. Meehan, J. Rak, ACS Nano 13 (2019) 10499–10511.
[210] C. Chen, S. Zong, Y. Liu, Z. Wang, Y. Zhang, B. Chen, Y. Cui, Small (2019) e1901014.
[211] K. Lee, K. Fraser, B. Ghaddar, K. Yang, E. Kim, L. Balaj, E.A. Chiocca, X.O. Breakefield, H. Lee, R. Weissleder, ACS Nano 12 (2018) 494–503.
[212] C. Liu, X. Xu, B. Li, B. Situ, W. Pan, Y. Hu, T. An, S. Yao, L. Zheng, Nano Lett. 18 (2018) 4226–4232.
[213] S.-L. Ho, H.-M. Chan, A.W.-Y. Ha, R.N.-S. Wong, H.-W. Li, Anal. Chem. 86 (2014) 9880–9886.
[214] D. He, H. Wang, S.L. Ho, H.N. Chan, L. Hai, X. He, K. Wang, H.W. Li, Theranostics 9 (2019) 4494–4507.
[215] C. Liu, J. Zhao, F. Tian, J. Chang, W. Zhang, J. Sun, J. Am. Chem. Soc. 141 (2019) 3817–3821.
[216] S.G. Kruglik, F. Royo, J.M. Guigner, L. Palomo, O. Seksek, P.Y. Turpin, I. Tatischeff, J.M. Falcon-Perez, Nanoscale 11 (2019) 1661–1679.

[217] Z.J. Smith, C. Lee, T. Rojalin, R.P. Carney, S. Hazari, A. Knudson, K. Lam, H. Saari, E.L. Ibañez, T. Viitala, T. Laaksonen, M. Yliperttula, S. Wachsmann-Hogiu, J. Extracell, Vesicles 4 (2015) 28533.
[218] P. Beekman, A. Enciso-Martinez, H.S. Rho, S.P. Pujari, A. Lenferink, H. Zuilhof, L.W.M.M. Terstappen, C. Otto, S. Le Gac, Lab Chip 19 (2019) 2526–2536.
[219] S. Stremersch, M. Marro, B.-E. Pinchasik, P. Baatsen, A. Hendrix, S.C. De Smedt, P. Loza-Alvarez, A.G. Skirtach, K. Raemdonck, K. Braeckmans, Small 12 (2016) 3292–3301.
[220] Y. Yang, G. Shen, H. Wang, H. Li, T. Zhang, N. Tao, X. Ding, H. Yu, Proc. Natl. Acad. Sci. U. S. A. 115 (2018) 10275–10280.
[221] R.P. Carney, S. Hazari, M. Colquhoun, D. Tran, B. Hwang, M.S. Mulligan, J.D. Bryers, E. Girda, G.S. Leiserowitz, Z.J. Smith, K.S. Lam, Anal. Chem. 89 (2017) 5357–5363.
[222] S.Y. Kim, D. Khanal, B. Kalionis, W. Chrzanowski, Nat. Protoc. 14 (2019) 576–593.
[223] D. Wu, J. Yan, X. Shen, Y. Sun, M. Thulin, Y. Cai, L. Wik, Q. Shen, J. Oelrich, X. Qian, K.L. Dubois, K.G. Ronquist, M. Nilsson, U. Landegren, M. Kamali-Moghaddam, Nat. Commun. 10 (2019) 3854.
[224] Y. Li, J. Zhao, S. Yu, Z. Wang, X. He, Y. Su, T. Guo, H. Sheng, J. Chen, Q. Zheng, Y. Li, W. Guo, X. Cai, G. Shi, J. Wu, L. Wang, P. Wang, X. He, S. Huang, Clin. Chem. 65 (2019) 798–808.
[225] P. Vader, X.O. Breakefield, M.J.A. Wood, Trends Mol. Med. 20 (2014) 385–393.
[226] S. Fais, L. O'Driscoll, F.E. Borras, E. Buzas, G. Camussi, F. Cappello, J. Carvalho, A. Cordeiro da Silva, H. Del Portillo, S. El Andaloussi, T. Ficko Trček, R. Furlan, A. Hendrix, I. Gursel, V. Kralj-Iglic, B. Kaeffer, M. Kosanovic, M.E. Lekka, G. Lipps, M. Logozzi, A. Marcilla, M. Sammar, A. Llorente, I. Nazarenko, C. Oliveira, G. Pocsfalvi, L. Rajendran, G. Raposo, E. Rohde, P. Siljander, G. van Niel, M.H. Vasconcelos, M. Yáñez-Mó, M.L. Yliperttula, N. Zarovni, A.B. Zavec, B. Giebel, ACS Nano 10 (2016) 3886–3899.
[227] B.W.M. van Balkom, T. Pisitkun, M.C. Verhaar, M.A. Knepper, Kidney Int. 80 (2011) 1138–1145.
[228] Z. Tang, J. Huang, H. He, C. Ma, K. Wang, Coord. Chem. Rev. 415 (2020) 213317.
[229] D. Zocco, P. Ferruzzi, F. Cappello, W.P. Kuo, S. Fais, Front. Oncol. 4 (2014) 267.
[230] X. Li, C. Li, L. Zhang, M. Wu, K. Cao, F. Jiang, D. Chen, N. Li, W. Li, Mol. Cancer 19 (2020) 1–11.
[231] S. Kourembanas, Annu. Rev. Physiol. 77 (2015) 13–27.
[232] I.H. Chen, L. Xue, C.-C. Hsu, J.S.P. Paez, L. Pan, H. Andaluz, M.K. Wendt, A.B. Iliuk, J.-K. Zhu, W.A. Tao, Proc. Natl. Acad. Sci. U. S. A. 114 (2017) 3175–3180.
[233] P. Del Boccio, F. Raimondo, D. Pieragostino, L. Morosi, G. Cozzi, P. Sacchetta, F. Magni, M. Pitto, A. Urbani, Electrophoresis 33 (2012) 689–696.
[234] H.K. Min, S. Lim, B.C. Chung, M.H. Moon, Anal. Bioanal. Chem. 399 (2011) 823–830.
[235] E. Castellanos-Rizaldos, D.G. Grimm, V. Tadigotla, J. Hurley, J. Healy, P.L. Neal, M. Sher, R. Venkatesan, C. Karlovich, M. Raponi, A. Krug, M. Noerholm, J. Tannous, B.A. Tannous, L.E. Raez, J.K. Skog, Clin. Cancer Res. 24 (2018) 2944.
[236] B. Sandfeld-Paulsen, K.R. Jakobsen, R. Bæk, B.H. Folkersen, T.R. Rasmussen, P. Meldgaard, K. Varming, M.M. Jørgensen, B.S. Sorensen, J. Thorac. Oncol. 11 (2016) 1701–1710.
[237] P.-G. Moon, J.-E. Lee, Y.-E. Cho, S.J. Lee, J.H. Jung, Y.S. Chae, H.-I. Bae, Y.-B. Kim, I.-S. Kim, H.Y. Park, M.-C. Baek, Clin. Cancer Res. 22 (2016) 1757–1766.
[238] A.H. Alhasan, A.W. Scott, J.J. Wu, G. Feng, J.J. Meeks, C.S. Thaxton, C.A. Mirkin, Proc. Natl. Acad. Sci. U. S. A. 113 (2016) 10655.
[239] S. Principe, E.E. Jones, Y. Kim, A. Sinha, J.O. Nyalwidhe, J. Brooks, O.J. Semmes, D.A. Troyer, R.S. Lance, T. Kislinger, R.R. Drake, Proteomics 13 (2013) 1667–1671.
[240] Q. Li, Y. Shao, X. Zhang, T. Zheng, M. Miao, L. Qin, B. Wang, G. Ye, B. Xiao, J. Guo, Tumor Biol. 36 (2015) 2007–2012.
[241] K. Sugimachi, T. Matsumura, H. Hirata, R. Uchi, M. Ueda, H. Ueo, Y. Shinden, T. Iguchi, H. Eguchi, K. Shirabe, T. Ochiya, Y. Maehara, K. Mimori, Br. J. Cancer 112 (2015) 532–538.
[242] H. Wang, L. Hou, A. Li, Y. Duan, H. Gao, X. Song, Biomed Res. Int. 2014 (2014) 864894.
[243] D.D. Taylor, C. Gercel-Taylor, Gynecol. Oncol. 110 (2008) 13–21.
[244] S.A. Melo, L.B. Luecke, C. Kahlert, A.F. Fernandez, S.T. Gammon, J. Kaye, V.S. LeBleu, E.A. Mittendorf, J. Weitz, N. Rahbari, C. Reissfelder, C. Pilarsky, M.F. Fraga, D. Piwnica-Worms, R. Kalluri, Nature 523 (2015) 177–182.
[245] B. Costa-Silva, N.M. Aiello, A.J. Ocean, S. Singh, H. Zhang, Basant K. Thakur, A. Becker, A. Hoshino, M.T. Mark, H. Molina, J. Xiang, T. Zhang, T.-M. Theilen, G. García-Santos, C. Williams, Y. Ararso, Y. Huang, G. Rodrigues, T.-L. Shen, K.J. Labori, I.M.B. Lothe, E.H. Kure, J. Hernandez, A. Doussot, S.H. Ebbesen, Paul M. Grandgenett, Michael A. Hollingsworth, M. Jain, K. Mallya, S.K. Batra, William R. Jarnagin, Robert E. Schwartz, I. Matei, H. Peinado, B.Z. Stanger, J. Bromberg, D. Lyden, Nat. Cell Biol. 17 (2015) 816–826.
[246] K.S. Yang, H. Im, S. Hong, I. Pergolini, A.F. del Castillo, R. Wang, S. Clardy, C.-H. Huang, C. Pille, S. Ferrone, R. Yang, C.M. Castro, H. Lee, C.F. del Castillo, R. Weissleder, Sci. Transl. Med., 9 (2017) eaal3226.
[247] Z. Andreu, R. Otta Oshiro, A. Redruello, S. López-Martín, C. Gutiérrez-Vázquez, E. Morato, A.I. Marina, C. Olivier Gómez, M. Yáñez-Mó, Eur. J. Pharm. Sci. 98 (2017) 70–79.
[248] S.B. Ye, Z.L. Li, D.H. Luo, B.J. Huang, Y.S. Chen, X.S. Zhang, J. Cui, Y.X. Zeng, J. Li, Oncotarget 5 (2014) 5439–5452.
[249] S. Saman, W. Kim, M. Raya, Y. Visnick, S. Miro, S. Saman, B. Jackson, A.C. McKee, V.E. Alvarez, N.C.Y. Lee, G.F. Hall, J. Biol. Chem. 287 (2012) 3842–3849.
[250] M. Shi, C. Liu, T.J. Cook, K.M. Bullock, Y. Zhao, C. Ginghina, Y. Li, P. Aro, R. Dator, C. He, M.J. Hipp, C.P. Zabetian, E.R. Peskind, S.-C. Hu, J.F. Quinn, D.R. Galasko, W.A. Banks, J. Zhang, Acta Neuropathol. 128 (2014) 639–650.
[251] H. Zhou, T. Pisitkun, A. Aponte, P.S.T. Yuen, J.D. Hoffert, H. Yasuda, X. Hu, L. Chawla, R.F. Shen, M.A. Knepper, R.A. Star, Kidney Int. 70 (2006) 1847–1857.
[252] H. Zhou, A. Cheruvanky, X. Hu, T. Matsumoto, N. Hiramatsu, M.E. Cho, A. Berger, A. Leelahavanichkul, K. Doi, L.S. Chawla, G.G. Illei, J.B. Kopp, J.E. Balow, H.A. Austin III, P.S.T. Yuen, R.A. Star, Kidney Int. 74 (2008) 613–621.
[253] T. Wu, Y. Chen, Y. Du, J. Tao, Z. Zhou, Z. Yang, Cell. Physiol. Biochem. 46 (2018) 1939–1950.
[254] J.P.K. Armstrong, M.M. Stevens, Adv. Drug Deliv. Rev. 130 (2018) 12–16.
[255] J. Ren, W. He, L. Zheng, H. Duan, Biomater. Sci. 4 (2016) 910–921.
[256] S. Stremersch, S.C. De Smedt, K. Raemdonck, J. Control. Release 244 (2016) 167–183.
[257] S. Rani, A.E. Ryan, M.D. Griffin, T. Ritter, Mol. Ther. 23 (2015) 812–823.
[258] T. Katsuda, N. Kosaka, F. Takeshita, T. Ochiya, Proteomics 13 (2013) 1637–1653.
[259] R.W.Y. Yeo, R.C. Lai, B. Zhang, S.S. Tan, Y. Yin, B.J. Teh, S.K. Lim, Adv. Drug Del. Rev. 65 (2013) 336–341.
[260] C. Akyurekli, Y. Le, R.B. Richardson, D. Fergusson, J. Tay, D.S. Allan, Stem Cell Rev. Rep. 11 (2015) 150–160.
[261] Y. Wei, Y. Wu, R. Zhao, K. Zhang, A.C. Midgley, D. Kong, Z. Li, Q. Zhao, Biomaterials 204 (2019) 13–24.
[262] M. Riazifar, M.R. Mohammadi, E.J. Pone, A. Yeri, C. Lässer, A.I. Segaliny, L.L. McIntyre, G.V. Shelke, E. Hutchins, A. Hamamoto, E.N. Calle, R. Crescitelli, W. Liao, V. Pham, Y. Yin, J. Jayaraman, J.R.T. Lakey, C.M. Walsh, K. Van Keuren-Jensen, J. Lotvall, W. Zhao, ACS Nano 13 (2019) 6670–6688.
[263] S.-B. Fang, H.-Y. Zhang, C. Wang, B.-X. He, X.-Q. Liu, X.-C. Meng, Y.-Q. Peng, Z.-B. Xu, X.-L. Fan, Z.-J. Wu, D. Chen, L. Zheng, S.G. Zheng, Q.-L. Fu, J. Extracell, Vesicles 9 (2020) 1723260.
[264] L. Li, Y. Zhang, J. Mu, J. Chen, C. Zhang, H. Cao, J. Gao, Nano Lett., (2020).
[265] J. Xu, Y. Wang, C.Y. Hsu, Y. Gao, C.A. Meyers, L. Chang, L. Zhang, K. Broderick, C. Ding, B. Peault, K. Witwer, A.W. James, Elife 8 (2019) e48191.
[266] S. Hu, Z. Li, J. Cores, K. Huang, T. Su, P.U. Dinh, K. Cheng, ACS Nano, (2019).
[267] P.-U.C. Dinh, D. Paudel, H. Brochu, K.D. Popowski, M.C. Gracieux, J. Cores, K. Huang, M.T. Hensley, E. Harrell, A.C. Vandergriff, A.K. George, R.T. Barrio, S. Hu, T.A. Allen, K. Blackburn, T.G. Caranasos, X. Peng, L.V. Schnabel, K.B. Adler, L.J. Lobo, M.B. Goshe, K. Cheng, Nat. Commun. 11 (2020) 1064.
[268] P. Vader, E.A. Mol, G. Pasterkamp, R.M. Schiffelers, Adv. Drug Deliv. Rev. 106 (2016) 148–156.
[269] O.M. Elsharkasy, J.Z. Nordin, D.W. Hagey, O.G. de Jong, R.M. Schiffelers, S.E.L. Andaloussi, P. Vader, Adv. Drug Del. Rev. (2020), https://doi.org/10.1016/j.addr.2020.1004.1004.
[270] G. Fuhrmann, A. Serio, M. Mazo, R. Nair, M.M. Stevens, J. Control. Release 205 (2015) 35–44.
[271] J.P.K. Armstrong, M.N. Holme, M.M. Stevens, ACS Nano 11 (2017) 69–83.
[272] K. Gärtner, M. Luckner, G. Wanner, R. Zeidler, J. Extracell, Vesicles 8 (2019) 1573051.
[273] Y.H. Tian, S.P. Li, J. Song, T.J. Ji, M.T. Zhu, G.J. Anderson, J.Y. Wei, G.J. Nie, Biomaterials 35 (2014) 2383–2390.
[274] S. Kamerkar, V.S. LeBleu, H. Sugimoto, S. Yang, C.F. Ruivo, S.A. Melo, J.J. Lee, R. Kalluri, Nature 546 (2017) 498–503.
[275] D. Sun, X. Zhuang, X. Xiang, Y. Liu, S. Zhang, C. Liu, S. Barnes, W. Grizzle, D. Miller, H.-G. Zhang, Mol. Ther. 18 (2010) 1606–1614.
[276] Z. Fan, K. Xiao, J. Lin, Y. Liao, X. Huang, Small (2019) e1903761.
[277] Q. Lin, M. Qu, B. Zhou, H.K. Patra, Z. Sun, Q. Luo, W. Yang, Y. Wu, Y. Zhang, L. Li, L. Deng, L. Wang, T. Gong, Q. He, L. Zhang, X. Sun, Z. Zhang, J. Control. Release 311–312 (2019) 104–116.
[278] F. Xiong, X. Ling, X. Chen, J. Chen, J. Tan, W. Cao, L. Ge, M. Ma, J. Wu, Nano Lett. 19 (2019) 3256–3266.
[279] D. Wang, Y. Yao, J. He, X. Zhong, B. Li, S. Rao, H. Yu, S. He, X. Feng, T. Xu, B. Yang, T. Yong, L. Gan, J. Hu, X. Yang, Adv. Sci. 7 (2020) 1901293.
[280] M. Sancho-Albero, B. Rubio-Ruiz, A.M. Pérez-López, V. Sebastián, P. Martín-Duque, M. Arruebo, J. Santamaría, A. Unciti-Broceta, Nat. Catal. 2 (2019) 864–872.
[281] J. Wang, Y. Dong, Y. Li, W. Li, K. Cheng, Y. Qian, G. Xu, X. Zhang, L. Hu, P. Chen, W. Du, X. Feng, Y.-D. Zhao, Z. Zhang, B.-F. Liu, Adv. Funct. Mater. 28 (2018) 1707360.
[282] T.T. Tang, L.L. Lv, B. Wang, J.Y. Cao, Y. Feng, Z.L. Li, M. Wu, F.M. Wang, Y. Wen, L.T. Zhou, H.F. Ni, P.S. Chen, N. Gu, S.D. Crowley, B.C. Liu, Theranostics 9 (2019) 4740–4755.
[283] T. Yong, X. Zhang, N. Bie, H. Zhang, X. Zhang, F. Li, A. Hakeem, J. Hu, L. Gan, H. A. Santos, X. Yang, Nat. Commun. 10 (2019) 3838.
[284] D. Zhang, X. Qin, T. Wu, Q. Qiao, Q. Song, Z. Zhang, Biomaterials 197 (2019) 220–228.
[285] S. Lee, T.C. Pham, C. Bae, Y. Choi, Y.K. Kim, J. Yoon, Coord. Chem. Rev. 412 (2020) 213258.
[286] P.H.L. Tran, D. Xiang, T.T.D. Tran, W. Yin, Y. Zhang, L. Kong, K. Chen, M. Sun, Y. Li, Y. Hou, Y. Zhu, W. Duan, Adv. Mater. 32 (2019) 1904040.
[287] D. Yuan, Y. Zhao, W.A. Banks, K.M. Bullock, M. Haney, E. Batrakova, A.V. Kabanov, Biomaterials 142 (2017) 1–12.
[288] N. Ran, X. Gao, X. Dong, J. Li, C. Lin, M. Geng, H. Yin, Biomaterials 236 (2020) 119826.
[289] G. Cheng, W. Li, L. Ha, X. Han, S. Hao, Y. Wan, Z. Wang, F. Dong, X. Zou, Y. Mao, S.-Y. Zheng, J. Am. Chem. Soc. 140 (2018) 7282–7291.

[290] N. Yim, S.-W. Ryu, K. Choi, K.R. Lee, S. Lee, H. Choi, J. Kim, M.R. Shaker, W. Sun, J.-H. Park, D. Kim, W.D. Heo, C. Choi, Nat. Commun. 7 (2016) 12277.
[291] S.S. Yerneni, S. Lathwal, P. Shrestha, H. Shirwan, K. Matyjaszewski, L. Weiss, E. S. Yolcu, P.G. Campbell, S.R. Das, ACS Nano 13 (2019) 10555–10565.
[292] J. Wang, W. Li, Z. Lu, L. Zhang, Y. Hu, Q. Li, W. Du, X. Feng, H. Jia, B.-F. Liu, Nanoscale 9 (2017) 15598–15605.
[293] P.-E. Mangeot, S. Dollet, M. Girard, C. Ciancia, S. Joly, M. Peschanski, V. Lotteau, Mol. Ther. 19 (2011) 1656–1666.
[294] Y. Yang, Y. Hong, G.-H. Nam, J.H. Chung, E. Koh, I.-S. Kim, Adv. Mater. 29 (2017) 1605604.
[295] Z.C. Hartman, J. Wei, O.K. Glass, H. Guo, G. Lei, X.-Y. Yang, T. Osada, A. Hobeika, A. Delcayre, J.-B. Le Pecq, M.A. Morse, T.M. Clay, H.K. Lyerly, Vaccine 29 (2011) 9361–9367.
[296] G.G. Romagnoli, B.B. Zelante, P.A. Toniolo, I.K. Migliori, J.A.M. Barbuto, Front. Immunol. 5 (2014) 692.
[297] E. Segura, C. Nicco, B.r.r. Lombard, P. Véron, G.a. Raposo, F.d.r. Batteux, S. Amigorena, C. Théry, Blood, 106 (2005) 216-223.
[298] S. Munich, A. Sobo-Vujanovic, W.J. Buchser, D. Beer-Stolz, N.L. Vujanovic, OncoImmunology 1 (2012) 1074–1083.
[299] W. Fu, C. Lei, S. Liu, Y. Cui, C. Wang, K. Qian, T. Li, Y. Shen, X. Fan, F. Lin, M. Ding, M. Pan, X. Ye, Y. Yang, S. Hu, Nat. Commun. 10 (2019) 4355.
[300] M. Morishita, Y. Takahashi, A. Matsumoto, M. Nishikawa, Y. Takakura, Biomaterials 111 (2016) 55–65.
[301] M. Maugeri, M. Nawaz, A. Papadimitriou, A. Angerfors, A. Camponeschi, M. Na, M. Hölttä, P. Skantze, S. Johansson, M. Sundqvist, J. Lindquist, T. Kjellman, I.-L. Mårtensson, T. Jin, P. Sunnerhagen, S. Östman, L. Lindfors, H. Valadi, Nat. Commun. 10 (2019) 4333.
[302] L. Alvarez-Erviti, Y. Seow, H. Yin, C. Betts, S. Lakhal, M.J.A. Wood, Nat. Biotechnol. 29 (2011) 341–345.
[303] Z. Li, X. Zhou, M. Wei, X. Gao, L. Zhao, R. Shi, W. Sun, Y. Duan, G. Yang, L. Yuan, Nano Lett. 19 (2019) 19–28.
[304] S. Guo, N. Perets, O. Betzer, S. Ben-Shaul, A. Sheinin, I. Michaelevski, R. Popovtzer, D. Offen, S. Levenberg, ACS Nano 13 (2019) 10015–10028.
[305] A. Jeyaram, T.N. Lamichhane, S. Wang, L. Zou, E. Dahal, S.M. Kronstadt, D. Levy, B. Parajuli, D.R. Knudsen, W. Chao, S.M. Jay, Mol. Ther. 28 (2020) 975–985.
[306] F. Pi, D.W. Binzel, T.J. Lee, Z. Li, M. Sun, P. Rychahou, H. Li, F. Haque, S. Wang, C.M. Croce, B. Guo, B.M. Evers, P. Guo, Nat. Nanotechnol. 13 (2018) 82–89.
[307] S. El-Andaloussi, Y. Lee, S. Lakhal-Littleton, J. Li, Y. Seow, C. Gardiner, L. Alvarez-Erviti, I.L. Sargent, M.J.A. Wood, Nat. Protoc. 7 (2012) 2112–2126.
[308] S.I. Ohno, M. Takanashi, K. Sudo, S. Ueda, A. Ishikawa, N. Matsuyama, K. Fujita, T. Mizutani, T. Ohgi, T. Ochiya, Mol. Ther. 21 (2012) 185–191.
[309] A. Mizrak, M.F. Bolukbasi, G.B. Ozdener, G.J. Brenner, S. Madlener, E.P. Erkan, T. Ströbel, X.O. Breakefield, O. Saydam, Mol. Ther. 21 (2013) 101–108.
[310] S.W. Ferguson, J. Nguyen, J. Control. Release 228 (2016) 179–190.
[311] L. Cheng, C. Wang, L. Feng, K. Yang, Z. Liu, Chem. Rev. 114 (2014) 10869–10939.
[312] J.J. Hu, Y.J. Cheng, X.Z. Zhang, Nanoscale 10 (2018) 22657–22672.
[313] P. Zhu, Y. Chen, J. Shi, ACS Nano 12 (2018) 3780–3795.
[314] X. Li, S. Yu, Y. Lee, T. Guo, N. Kwon, D. Lee, S.C. Yeom, Y. Cho, G. Kim, J.-D. Huang, S. Choi, K.T. Nam, J. Yoon, J. Am. Chem. Soc. 141 (2019) 1366–1372.
[315] H. Cheng, J.-H. Fan, L.-P. Zhao, G.-L. Fan, R.-R. Zheng, X.-Z. Qiu, X.-Y. Yu, S.-Y. Li, X.-Z. Zhang, Biomaterials 211 (2019) 14–24.
[316] D. Zhu, Y. Duo, M. Suo, Y. Zhao, L. Xia, Z. Zheng, Y. Li, B.Z. Tang, Angew. Chem. Int. Ed. (2020), https://doi.org/10.1002/anie.202003672.
[317] Y. Cao, T. Wu, K. Zhang, X. Meng, W. Dai, D. Wang, H. Dong, X. Zhang, ACS Nano 13 (2019) 1499–1510.
[318] Y. Liu, L. Bai, K. Guo, Y. Jia, K. Zhang, Q. Liu, P. Wang, X. Wang, Theranostics 9 (2019) 5261–5281.
[319] C. Liu, W. Zhang, Y. Li, J. Chang, F. Tian, F. Zhao, Y. Ma, J. Sun, Nano Lett. 19 (2019) 7836–7844.
[320] Z. Zhao, J. McGill, P. Gamero-Kubota, M. He, Lab Chip 19 (2019) 1877–1886.
[321] D. Ingato, J.U. Lee, S.J. Sim, Y.J. Kwon, J. Control. Release 241 (2016) 174–185.
[322] O.G. de Jong, S.A.A. Kooijmans, D.E. Murphy, L. Jiang, M.J.W. Evers, J.P.G. Sluijter, P. Vader, R.M. Schiffelers, Acc. Chem. Res. 52 (2019) 1761–1770.
[323] A.F. Saleh, E. Lazaro-Ibanez, M.A. Forsgard, O. Shatnyeva, X. Osteikoetxea, F. Karlsson, N. Heath, M. Ingelsten, J. Rose, J. Harris, M. Mairesse, S.M. Bates, M. Clausen, D. Etal, E. Leonard, M.D. Fellows, N. Dekker, N. Edmunds, Nanoscale 11 (2019) 6990–7001.
[324] T. Lener, M. Gimona, L. Aigner, V. Börger, E. Buzas, G. Camussi, N. Chaput, D. Chatterjee, F.A. Court, H.A. Del Portillo, L. O'Driscoll, S. Fais, J.M. Falcon-Perez, U. Felderhoff-Mueser, L. Fraile, Y.S. Gho, A. Görgens, R.C. Gupta, A. Hendrix, D. M. Hermann, A.F. Hill, F. Hochberg, P.A. Horn, D. de Kleijn, L. Kordelas, B.W. Kramer, E.-M. Krämer-Albers, S. Laner-Plamberger, S. Laitinen, T. Leonardi, M. J. Lorenowicz, S.K. Lim, J. Lötvall, C.A. Maguire, A. Marcilla, I. Nazarenko, T. Ochiya, T. Patel, S. Pedersen, G. Pocsfalvi, S. Pluchino, P. Quesenberry, I.G. Reischl, F.J. Rivera, R. Sanzenbacher, K. Schallmoser, I. Slaper-Cortenbach, D. Strunk, T. Tonn, P. Vader, B.W.M. van Balkom, M. Wauben, S.E. Andaloussi, C. Théry, E. Rohde, B. Giebel, J. Extracell. Vesicles, 4 (2015) 30087.
[325] M.D. Keller, K.L. Ching, F.-X. Liang, A. Dhabaria, K. Tam, B.M. Ueberheide, D. Unutmaz, V.J. Torres, K. Cadwell, Nature 579 (2020) 260–264.